ABSTRACT

OPTIMAL TRAIN CONTROL ON VARIOUS TRACK ALIGNMENTS CONSIDERING SPEED AND SCHEDULE ADHERENCE CONSTRAINTS

by
Kitae Kim

The methodology discussed in this dissertation contributes to the field of transit operational control to reduce energy consumption. Due to the recent increase in gasoline cost, a significant number of travelers are shifting from highway modes to public transit, which also induces higher transit energy consumption expenses.

This study presents an approach to optimize train motion regimes for various track alignments, which minimizes total energy consumption subject to allowable travel time, maximum operating speed, and maximum acceleration/deceleration rates. The research problem is structured into four cases which consist of the combinations of track alignments (e.g., single vertical alignment and mixed vertical alignment) and the variation of maximum operating speeds (e.g., constant and variable). The Simulated Annealing (SA) approach is employed to search for the optimal train control, called "golden run".

To accurately estimate energy consumption and travel time, a Train Performance Simulation (TPS) is developed, which replicates train movements determined by a set of dynamic variables (e.g., duration of acceleration and cruising, coasting position, braking position, etc.) as well as operational constraints (e.g., track alignment, speed limit, minimum travel time, etc.)

The applicability of the developed methodology is demonstrated with geographic data of two real world rail line segments of The New Haven Line of the Metro North

Railroad: Harrison to Rye Stations and East Norwalk to Westport Stations. The results of optimal solutions and sensitivity analyses are presented. The sensitivity analyses enable a transit operator to quantify the impact of the coasting position, travel time constraint, vertical dip of the track alignment, maximum operating speed, and the load and weight of the train to energy consumption.

The developed models can assist future rail system with Automatic Train Control (ATC), Automatic Train Operation (ATO) and Positive Train Control (PTC), or conventional railroad systems to improve the planning and operation of signal systems. The optimal train speed profile derived in this study can be considered by the existing signal system for determining train operating speeds over a route.

OPTIMAL TRAIN CONTROL ON VARIOUS TRACK ALIGNMENTS CONSIDERING SPEED AND SCHEDULE ADHERENCE CONSTRAINTS

by
Kitae Kim

A Dissertation
Submitted to the Faculty of
New Jersey Institute of Technology
In Partial Fulfillment of the Requirements for the Degree of
Doctor of Philosophy in Civil Engineering

Department of Civil and Environmental Engineering

January 2010

BIOGRAPHICAL SKETCH

Author: Kitae Kim

Degree: Doctor of Philosophy

Date: January 2010

Undergraduate and Graduate Education:

- Doctor of Philosophy in Civil and Environmental Engineering, New Jersey Institute of Technology, Newark, NJ, 2010
- Master of Science in Civil and Environmental Engineering, New Jersey Institute of Technology, Newark, NJ, 2005
- Master of Science in Transportation Planning and Engineering, Polytechnic University, Brooklyn, NY, 2002
- Bachelor of Science in Civil Engineering, Chung-Ang University, Seoul, Korea, 1999

Major: Transportation Engineering

Presentations and Publications:

Kitae Kim and Steven Chien, "Optimal Train Operation for Minimum Energy Consumption Considering Schedule Adherence", Transportation Research Board 89th Annual Meeting, January 2010 (Forthcoming)

Kitae Kim and Steven Chien, "Simulation Analysis of Energy Consumption for Various Train Controls and Alignment", Transportation Research Board 88th Annual Meeting, January 2009

Steven Chien, Sunil Kumar Daripally, and **Kitae Kim**, "Development of a Probabilistic Model to Disseminate Bus Arrival Time", Journal of Advanced Transportation, Vol. 41, No. 2, 2007

Steven Chien, **Kitae Kim**, and Janice Daniel, "Cost and Benefit Analysis for Optimized Signal Timing Case Study: New Jersey Route 23", ITE Journal, Vol. 76, No. 10, 2006

APPROVAL PAGE

OPTIMAL TRAIN CONTROL ON VARIOUS TRACK ALIGNMENTS CONSIDERING SPEED AND SCHEDULE ADHERENCE CONSTRAINTS

Kitae Kim

Dr. Steven I-Jy Chien, Dissertation Advisor — Date
Professor of Civil and Environmental Engineering, NJIT

Dr. Lazar Spasovic, Committee Member — Date
Professor of Civil and Environmental Engineering, NJIT

Dr. Athanassios Bladikas, Committee Member — Date
Associate Professor of Mechanical and Industrial Engineering, NJIT

Dr. Janice R. Daniel, Committee Member — Date
Associate Professor of Civil and Environmental Engineering, NJIT

Dr. Jerome Lutin, Committee Member — Date
Distinguished Research Professor, Office of the Dean, NCE, NJIT

I would like to dedicate this dissertation to

My beloved wife, Dongwook Oh, who showed me her love, sacrifice, and encouragement throughout;

My parents, Il-Rang Kim and Heeja Ha, who motivated me to study abroad and made all the sacrifices and my brother Su-young Kim, who gave me encouragement ; and

My mentor, Sun-gak, who always gave me help and advice during my study.

ACKNOWLEDGEMENT

I do greatly appreciate my dissertation advisor, Dr. Steven I-Jy Chien, who constantly supported, inspired and encouraged me with his insight, dedication and understanding during my Ph.D. study. Special thanks are given to Dr. Jerome Lutin, Dr. Lazar Spasovic, Dr. Athanassios Bladikas, and Dr. Janice Daniel for serving as committee members and providing me with precious suggestions on research and industrial practice. I also express my appreciation to Mr. Anthony Pincherri at NJ TRANSIT, who provided me with valuable data for my dissertation.

My fellow graduate students, Dr. Feng-Ming Tsai, Dr. Sungmin Maeng, Dr. Mingzheng Cao, Mr. Yavuz Ulusoy, Ms. Patricia DiJoseph, and Mr. Jinuk Ha, are deserving recognition for their support.

I also appreciate all projects sponsored by the New Jersey Department of Transportation, New Jersey Transit, the National Center for Transportation and Industrial Productivity, New Jersey Institute of Technology, and the International Road Federation (IRF) Fellowship Program, which supported my tuition and other financial needs.

TABLE OF CONTENTS

TABLE OF CONTENTS
(Continued)

Chapter **Page**

TABLE OF CONTENTS
(Continued)

Chapter **Page**

LIST OF TABLES

LIST OF FIGURES

LIST OF FIGURES
(Continued)

Figures **Page**

LIST OF FIGURES
(Continued)

Figures **Page**

LIST OF SYMBOLS

a^t	Acceleration rate at time t	ft/sec^2
a_{max}	Maximum acceleration rate	ft/sec^2
$\bar{a}$	Average speed change rate of acceleration	ft/sec^2
b^t	Deceleration rate at time t	ft/sec^2
b_{max}	Maximum deceleration rate	ft/sec^2
$\bar{b}$	Average speed change rate of deceleration	ft/sec^2
$\overline{c_1}$	Average speed change rate of 1st coasting	ft/sec^2
$\overline{c_2}$	Average speed change rate of 2nd coasting	ft/sec^2
C_0	Initial control parameter	-
D^t	Track curvature at time t	degree
d_i	Damping constant	$lb \cdot sec/ft$
Δe^t	Energy consumption rate at time t	kWh
E	Total energy consumption	kWh
ΔE	Energy change	kWh
$E(S'_\omega)$	Energy at current state	kWh
$E(S'_{\omega+1})$	Energy at subsequent state	kWh
F_a^t	Adhesive force at time t	lb_f
F_{max}^t	Maximum tractive effort at time t	lb_f
F_p^t	Propulsive force at time t	lb_f

$F^t_{B(max)}$	Maximum braking force	lb_f
F^t_{ba}	Adhesion-limited braking force	lb_f
F^t_{bc}	Comfort-limited braking force	lb_f
F^t_i	Tractive effort of the i^{th} car at time t	
g	Gravitational acceleration (=32.2)	ft/sec^2
G^t	Track grade where the train is running at time t	degree
i	Index of car in train	-
I_P	Inflection point	-
j	Index of track segment	
J	Number of time steps for traveling from one station to another	-
k_i	Spring constant	lb/ft
k_B	Boltzmann constant	-
K	Aerodynamic coefficient	-
L	Horizontal track length	ft
m	Train mass	lb_m
M_O	Motion regime	-
M_a	Acceleration regime	-
M_b	Braking regime	-
M_{c1}	1^{st} coasting regime	-
M_{c2}	2^{nd} coasting regime	-

M_v	Cruising regime	-
N	Number of cars per train	cars/train
n	Number of axles per car	axels/car
O	Index of motion regime	-
P	Boltzmann probability	-
P^t	Engine horse power at time t	hp
q	Total number of vertical segment with different grade	segments
R_T^t	Total train resistance	lb_f
R_U^t	Unit resistance per axle	lb_f/ton
S	Station spacing	ft
S_a	Travel distance during accelerating	ft
S_b	Travel distance during braking	ft
S_{c1}	Travel distance during 1st coasting	ft
S_v	Travel distance during cruising	ft
S_{c2}	Travel distance during 2nd coasting	ft
S_b	Travel distance during braking	ft
S′	Neighbor solution in SA	kWh
t_a	Acceleration time	sec
t_{c1}	1st coasting time	sec
t_v	Cruising time	sec

t_{c_2}	2nd coasting time	sec
t_b	Braking time	sec
T	Total travel time	sec
T^{temp}	Temperature in SA	-
u	Index of maximum operating speed	-
v^t	Train speed at time t	ft/sec
Δv^t	Increment of train speed from t to t+1	ft/sec
V^t	Train speed at time t	mph
V_{c_1}	Speed at 1st coasting starts	mph
V_b	Critical speed	mph
V_r^t	Relative speed at time t	mph
V_{M_u}	Maximum operating speed	mph
V_{wd}^t	Wind speed at time t	mph
W	Train weight	ton
x^t	Traveled distance at time t	ft
$y_j(x^t)$	Vertical track alignment where x^t traveled at time t on segment j	ft
δ	Vertical dip/height	ft
γ	Track transition rate in grade in 100 ft	-
η	Transmission efficiency	-
μ^t	Adhesion coefficient at time t	-

θ_i^t	Track angle to the horizontal	degree
θ_{wd}^t	Angle between the directions of wind and train movement	degree
ρ	Rotating mass coefficient	-
λ	Penalty factor	-
ω	Index of iteration number in SA	-

CHAPTER 1

INTRODUCTION

1.1 Background

As a major public transportation mode, rail transit (e.g., light rail and heavy rail systems) has been widely used in many metropolitan areas in the U.S. Over the years, the total consumed transit energy increased as the total line haul distance and passengers train miles of travel increased. It was found that the annual energy usage increased 1.6 percent for rail freight service and 1.7 percent for rail passenger service from 1995 to 2005. In 2005, 571.4 trillion and 87.6 trillion British Thermal Units (BTU) were respectively consumed by rail-freight and rail-passenger services. Due to recent increases of gasoline and other energy costs, many people are expected to shift from highway modes to transit for their daily travel. This might drastically increase energy expenses to rail transit suppliers.

According to a report prepared by the US Energy Information Administration (EIA, 2006), it is expected that transportation energy consumption and energy prices will continue to increase until 2030. Concerned about rising energy costs, rail transit operators have implemented energy conservation strategies to maintain sustainability of rail operations. To improve overall energy efficiency, the San Francisco Bay Area Rapid Transit District (BART) and the Metropolitan Atlanta Rapid Transit Authority (MARTA) incorporated regenerative braking energy into their rail system in order to improve overall energy efficiency. The New York City Transit Authority (NYCTA) has tested several energy efficient strategies, including coasting, regenerative in-vehicle storage, and substation battery energy storage (Uher at al., 1984). Train operations may become

more efficient by using new technology-oriented improvements such as automatic train control (ATC), automatic train operation (ATO), and positive train control (PTC), which, however, are expensive. Moreover, it could be a burden for suppliers to adopt up-and-coming technologies without assurance of success. Thus, train control can be one viable approach to reduce expensive energy bills for transit operators.

For most transit operations, train control for stations-to-station movement is affected by five motion regimes: acceleration, cruising, coasting, braking, and standing. However, the train control (i.e., driving strategy) used most in rail transit is either for a flat-out run (e.g., shortest time) or for a single coasting run at a fixed point to achieve train schedule regulation (Mellitt et al., 1987; Wong and Ho, 2003). Therefore, it is desirable to develop a dynamic passenger train control model that can reduce energy consumption considering schedule adherence.

1.2 Problem Statement

Previous studies (Chang and Sim, 1997; Hwang, 1998; Franke et al., 2000; Albecht, 2004) that minimize train energy consumption have been conducted by using different approaches such as coast control, automatic train operation (ATO), train speed trajectories, equi-block track system, etc. However, few of them discussed the impact of vertical or horizontal track alignment on kinematic train forces (e.g., propulsive force, resistance, adhesion, and acceleration, etc.) and considered alignment as a constant value.

In particular, considering the effect of track alignment variation in optimizing train energy consumption is very important because the tractive effort (i.e., propulsive force or TE) and train resistances are a function of the geometry of the track alignment. The vertical track alignment may be composed of a series of curves with different radii,

which provide a gradual transition from one level to another for smooth riding. There are two types of parabolic curves used in track alignment design: convex and concave. The benefits of a convex (vertically dipped) curve that reduces energy consumption and travel time were discussed by Kim and Schonfeld (1998), while a concave curve favors coasting operations (Howlett and Pudney, 1995).

A number of previous studies developed optimal train control to reduce energy consumption, but only a few studies considered the effect of track alignment on train performance and energy consumption. Furthermore, some approaches for optimizing energy consumption were developed without considering the effect of track alignment on TE and resistance, which resulted in the misrepresentation of performance by the models.

It is desirable to develop a sound train control model, which can minimize energy consumption considering the effect of varying track alignment and train operational characteristics, such as propulsive force, resistance, and acceleration and deceleration rates. In addition, the proposed model should be also capable of dealing with a speed limit, which significantly affects the application of motion regimes (e.g., acceleration, cruising, coasting, and deceleration). A train speed profile along a route is directly affected by the speed limit, because of the geometry of track alignment and/or operational purpose, and by travel time constraints because of scheduled arrival times at downstream stations, which should be considered while optimizing train control.

1.3 Objective and Work Scope

The objective of this study is to develop an analytical model that optimizes train control to reduce train energy consumption by considering the effect of vertical track alignments, schedule adherence, and maximum operating speed, which directly affect the incurred TE and resistances of a train.

While developing an optimal train control, a time-based train performance simulation (TPS) model will also be developed for demonstrating energy consumption and travel time induced by a new train control. Therefore, the TPS must accurately replicate train movements determined by dynamic variables (e.g., duration of acceleration and cruising, coasting position, braking position, etc.) as well as the primary static constraints (e.g., track alignment, speed limit, minimum travel time, etc.).

The Maximum Operating Speed (MOS) used in this study is largely divided into two categories: fixed and variable. The fixed MOS represents a single speed regulating train speed between two stations, while a variable MOS limit consists of multiple operating speeds due to track alignment and operational strategy. To develop an optimal train control by considering the joint impact of track alignment and MOS, four cases are investigated in this study. The optimal train control is investigated for four cases as shown in Table 1.1.

Table 1.1 Proposed Work Scope

		Track Alignment			
		Single Vertical Alignment (SVA)			Mixed Vertical Alignment (MVA)
		Level	Convex	Concave	
Maximum Allowable Operating Speed	Constant	Case I			Case III
	Variable	Case II			Case IV

- Case I: Model I is developed to optimize train control for minimum energy consumption for each of three vertical alignments (e.g., level, convex, and concave) and fixed maximum operating speed.
- Case II: Model II is enhanced from Model I by considering the impact of a variable maximum operating speed on energy consumption, which is commonly used in most rail lines.
- Case III: Model III is enhanced from Model I by considering the joint impact of a mixed vertical alignment (i.e., several curves) and a constant maximum operating speed.
- Case IV: Model IV is developed by integrating Models II and III and considering the impact of mixed vertical alignments and a variable maximum operating speed.

1.4 Dissertation Organization

This dissertation is organized into seven chapters. Chapter 1 introduced the background of the energy consumption problem for the railroad industry and presents the research objective and work scope. Chapter 2 summarizes the efforts of previous studies related to sustainable rail operations, various TPS models, kinematic models for train movement, and optimal train control for energy savings. Chapter 3 presents the development of the proposed TPS model, consisting of three modules for handling dynamic train movement on a continuously varying track with designated motion regimes. Chapter 4 discusses the development of analytical models used to optimize train control. Chapter 5 introduces the Simulated Annealing approach to optimize the research problems defined in Cases I through IV. Chapter 6 presents a numerical example, which demonstrates the applicability of the developed TPS model in estimating station-to-station travel time and energy consumption under various train controls and track alignments. Finally, conclusions and suggestions for future studies are presented in Chapter 7.

CHAPTER 2

LITERATURE REVIEW

This chapter summarizes the literature review, including sustainable rail operations, train performance simulation, and methods to search for optimal train control. This chapter is organized into six sections: Section 2.1 discusses railway energy consumption as a sustainability indicator; Section 2.2 discusses the review of previous TPS models; Section 2.3 reviews essential kinematic train equations for developing a simulation model; Section 2.4 discusses the effect of train control on energy consumption; Section 2.5 discuss previous studies of optimizing train energy consumption; Section 2.6 reviews optimization algorithms and heuristic search methods; and Section 2.7 summarizes the literature review and establishes the rationale for the model developed by this research.

2.1 Sustainable Train Operation

The sustainability of the transportation system has been receiving a great level of attention worldwide. In 1987, the United Nations' Brundtland Commission defined sustainability in the following way: "A sustainable condition for this planet is one in which there is stability for both social and physical systems, achieved through meeting the needs of the present without compromising the ability of future generations to meet their own needs" (United Nations, 1987). The early view of transportation sustainability focused on fuel use and environmental concerns. More recently, people have been concerned not only with fuel use and the environment, but also congestion, mobility, and safety as conditions of sustainability (Richardson, 2000). To assess the sustainability of an urban transportation system, various indicators were identified (Sinha, 2003). The

indicators used in his study of transportation sustainability evaluation were developed based on decennial data (1960 to 1990) from 46 cities in the U.S., Australia, Canada, Europe, and Asia, which had been established in the study conducted by Kenworthy and Laube (1999).

Major initiatives in North America and Europe in characterizing the definition and measurement of transportation sustainability were discussed (Black et al., 2002; Jeon and Amekudzi, 2005), in which the impact on the economy, environment, safety, transportation-related, and social well-being were focused and summarized in Table 2.1.

Table 2.1 Indicators of Sustainable Transportation Systems

	US DOT	US EPA	Trans Canada	EC[1]	NRTEE[2]	ORTEE[3]	TAC[4]	VTPI[5]	CST[6]	OECD[7]	World Bank	EEA[8]
Economy												
Population Density						■	■					
Economic Efficiency						■						
Employment						■	■					
GDP per unit of energy use											■	
Transportation related												
Length of railways and road								■	■	■		
Passenger-km (by mode)				■					■		■	■
Freight ton-km (by mode)									■		■	■
Total Miles Traveled (TMV)	■	■	■	■			■		■			
Public transit and auto use				■			■	■				
Environmental												
CO_2 emission		■	■	■		■	■			■	■	
Green house gas emission	■			■	■							
Fuel consumption				■			■		■	■		
Per-capita use of transportation energy	■				■		■	■	■			
Emission of air pollutants	■	■							■		■	
Safety												
Death and injury						■	■	■	■	■		
Accident										■	■	■
Social well-being												
exposure to airport noise	■	■										■
Ave. access distance								■		■		■
Accessibility						■				■	■	

■ : included by agency □ : not included

1: Environmental Canada (1991)
2: National Round Table on Environment and Economy (2003)
3: Ontario Round Table on Environment and Economy (1995)
4: Transportation Association of Canada (1999)
5: Victoria Transport Policy Institute (2003)
6: Center for Sustainable Transportation Canada (2003)
7: Organization for Economic Co-operation and Development (1999)
8: European Environmental Agency (2002)
Source: Jeon and Amekudzi (2005)

As a major indicator of sustainable transportation systems, energy consumption by the railway industry has been given attention in several previous studies. O'Toole (2008) investigated energy consumption and emissions by the U.S. railway industry. The energy consumption and greenhouse gas (CO_2) emission rate of 63 urban railway systems were assessed. A study of the energy intensity (BTU per passenger mile) of four transportation modes, including passenger cars, light trucks, bus transit, and rail trains over the last 30 years, as shown in Figure 2.1, found that the energy efficiency of light trucks (e.g., all two-axle four-tire truck) has been steadily improved, while the other modes had no noticeable improvement.

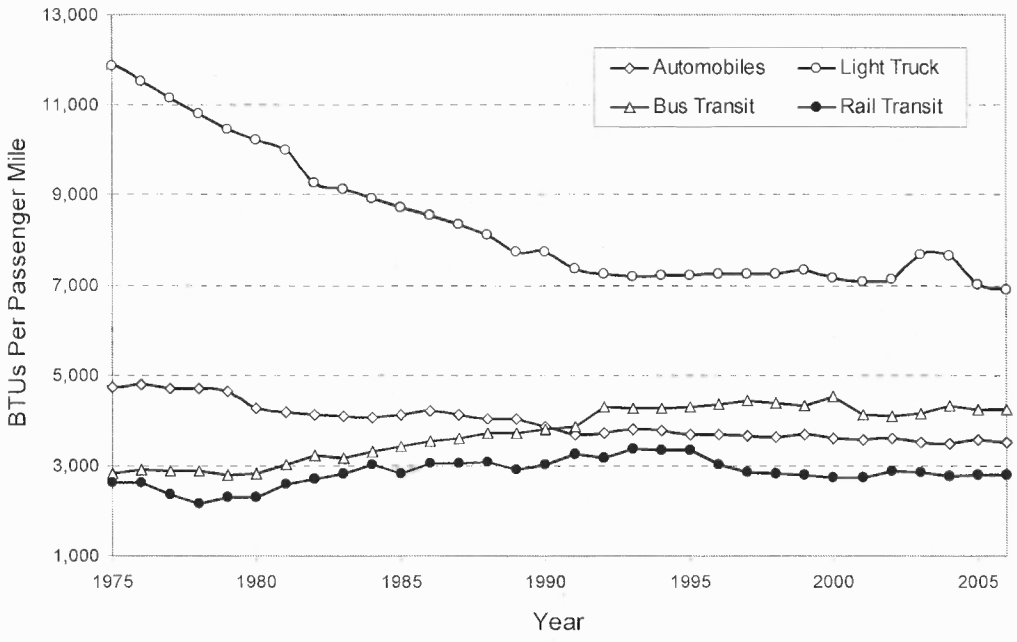

Figure 2.1 Energy intensities of various transportation modes.

Source: Davis et al. (2008), Transportation Energy Data Book (Oak Ridge National Laboratory).

The United Kingdom (UK) railway industry has focused on developing various energy saving programs for many years. Peckham (2007) indicated four possible areas where energy can be saved, which include reducing unnecessary load on trains, running shorter trains in the off-peak period, improving energy efficiency through optimal train controls and operational regulation, and reducing engine idling. It was estimated that the annual potential saving from these opportunities is approximately 740,000 megawatt-hours (MWh) of electricity (26% of the total electricity consumption by UK railways) and 70 million liters of diesel (10% of the total diesel consumption by UK railway). In financial terms, it was worth around 70 million pounds (£, 2005-2006 year value), and if converted into emission rates, more than 500 million kilograms of CO_2.

An energy cost reduction study was conducted by using data provided by the Washington Metropolitan Area Transit Authority (WMATA) (Uher et al., 1984), whose objective was to classify the usage of primary energy and identify energy conservation methods for reducing the electric bill. In addition to analyzing energy costs, this study also developed and evaluated cost-effective energy saving strategies, and recommended suitable plans for implementation. The suggested energy conservation methods included coasting operations, passenger load factor improvement (i.e., running shorter train during the off-peak period), catch-up operation (e.g., results of train delays during the peak periods), and regenerative braking energy. With these methods, WMATA was able to save $ 0.63-1.35 million energy bill per year (1982) by modifying the speed regulation of the transit lines by implementation of coasting operations, reduce 3.82 million annual car-mile by running shorter trains during the off-peak periods, and save $ 2.5 million from energy saving by using of the energy regeneration brake system.

2.2 Train Performance Simulation (TPS) Models

In early 1950, the rail freight market share in the U.S. declined from 56% to 38% because of increased competition from other transportation modes such as trucks, pipelines, and inland waterways. Consequently, their profits significantly decreased. Hence, the Class I railroad companies (defined as the operating revenue greater than $1 million) commenced to investigate train performance measures, including fuel savings, service reliability, line capacity increase, and efficient use of locomotives (Railroad Facts, 1986). A number of technologies [e.g., Advanced Train Controller (ATC), High Productivity Integral Train, etc.] were proposed to improve railroad productivity, yet a large cost was also incurred for field testing and applications. Therefore, a computer-based simulation model which can evaluate the effectiveness of these technologies was desired (Levine, 1985).

The US Federal Railroad Administration (FRA) initiated a study (1978) to develop TPS technology (e.g., in data collection, resistance modeling, power system modeling, brake system modeling, output data, model validation, etc.), which triggered the railroad industry's attention to developing TPS models. The characteristics and features of the developed TPS models that accommodate various predominant areas (e.g., fuel and energy usage, safety, and train operation studies) were evaluated by Howard et al. (1983). The sources of energy consumption in rail transit were classified into three categories, including train handling, engineering modification, and train makeup. Train handling represents the way to control (i.e., drive) a train under various conditions, such as station spacing, track alignment, and speed limit. Engineering modification handles

detailed components of the propulsion system. Train makeup that specifies types of train car by car impacts on aerodynamic and mechanical resistance modeling.

The applications of train simulation models were discussed by Martin (1999), which were classified into three categories: (1) assessing the mechanical and kinematic train performance, such as energy consumption, position of the throttle, TE and resistance as well as travel time and speed over a given infrastructure; (2) assessing rail signal systems to achieve a service goal; and (3) evaluating timetables and the interaction between trains meeting at complex junctions or major terminals. The applications of early category were demonstrated by two types of train simulation model (i.e., single-train and multi-train), which are determined based on project purpose and train network size.

To simulate train control on a rail line, Uher and Disk (1987) developed an energy management model consisting of two major components: Train Performance Simulator and Electric Network Simulator. The Train Performance Simulator was designed to mimic the operation of a single train, while the Electric Network Simulator calculated characteristics of electrical energy such as power flows, voltages, currents and losses. A method, calculating the forward and backward train speed profiles subject to speed limits, was developed to ensure appropriate train speeds at any location along the line. With this method, for example, the intersection of two speed profiles (i.e., backward and forward) was found for starting either the coasting or braking regime according to speed regulation.

Kikuchi (1991) developed a train simulation model for analyzing the operation of rail rapid transit, in which the acceleration/deceleration rate, speed limit profile, and station locations are required inputs. The movement of a train along a rail line operated by the Southeastern Pennsylvania Transportation Authority (SEPTA) was simulated, and

the relationship among travel time, travel distance, and travel speed was investigated. A comparison of travel times between the actual and simulated runs was made. However, the TE and the resistance affected by track alignment were not considered, and the train speed profile was determined by pre-specified, constant acceleration and deceleration rates and the maximum operating speed. The train speed profile was developed on the basis of a series of short, consecutive segments (every 0.02 miles), while the speed of each segment was assumed constant.

Minciardi et al. (1994) adopted a discrete, event based simulation approach to analyze rail transit system performance. Two simulators were used to estimate energy consumption, which includes a stochastic event-driven simulator for analyzing train performance under a given schedule, and an integrated system simulator for analyzing network electricity usage. Since the simulator was purely based on discrete-events, such as train arrival at the beginning of a track circuit, train arrival at a station, train departure from a station, and door closing, the kinematics of train movement affected by track alignment were not considered.

Kim and Schonfeld (1997) developed a deterministic simulation model for analyzing propulsive and braking energy consumption under simplified track alignments (level and convex) connecting two stations. It was found that operating trains on a vertical dipped track alignment can reduce energy consumption and travel time considerably more than on a flat tangent alignment, which indicated that the effect of track alignment is essential in developing an optimization model for train control. Sensitivity analyses were conducted by varying the dip percentage of the studied track

alignment, station spacing and the power of the locomotive, subject to constant acceleration and deceleration rates and maximum operating speed.

Chang et al. (1998) developed a simulation program for evaluating automated train operations, called Inter-station Train Movement Simulation (ITMS). An Automatic Train Control (ATC) strategy using a fuzzy Automatic Train Operation (ATO) and Automatic Train Protection (ATP) was embedded in ITMS. While simulating train movement, an object-oriented approach was used to manage the simulation clock, which generated time driven objects corresponding to train movement (i.e., train coasting, train braking), and event driven objects corresponding to train operation (i.e., train door open, train door close, train arrival at station, and train departure from station). The system performance indicators (e.g., speed, headway, and dwell time) of a rapid transit system under different signal controls for both steady-state and disturbed (i.e., a disturbance occurred due to station dwell time delay) headway conditions were analyzed. With a developed fuzzy algorithm, ITMS was able to determine the optimal dwell time of the trains at stations to ease passenger congestion conditions during the peak period. Simulation results demonstrated that signal control, dwell time, and speed limit significantly affect service headway regularity.

Gordon et al. (1998) evaluated a Train Control Simulator (TCS) developed by the Bay Area Rapid Transit (BART) System in San Francisco. The objective was to test and improve Advanced Automatic Train Control (AATC) for handling short headway operations and assisting coordinated train control and energy management. TCS consists of a train control simulator and a train power simulator. The train control simulator was designed to handle the motion of a train traveling in both directions on a single-track rail

system and to predict the state of the power system at any given moment. On the other hand, the train power simulator was designed to evaluate the severity of voltage sags and the usage of regenerated traction power for the steady state power consumption. It was found that TCS can be utilized to enhance AATC as well as compute speeds and acceleration rates of every train within a control zone.

Zou et al. (1999) developed a train simulation model using a moving block signaling system as a platform for Automatic Train Control (ATC). The structure of the simulation model consists of kinematic, geographical, and dynamic control modules which calculate acceleration/speed/position of a train, determine track layout, and ensure that the train speed does not exceed the maximum operating speed, respectively. Note that the dynamic control module could reduce unnecessary speed changes in the train running profile, which results in considerable energy saving.

Jong and Chang (2005) developed a train simulator, called TrainSim, using object-oriented programming concepts; where two algorithms were embedded to generate speed profiles complying with the equation of motion, and physical constraints of train and track alignment. The speed profiles were developed based on the shortest and normal (i.e., the one shown on the timetable) travel times. The speed profile of the shortest travel time simulated by TrainSim was compared to that generated by the trains operated by the Taiwan Railway Administration (TRA). It was found that the difference between average travel times estimated by TrainSim and under TRA real-world operations was quite small (less than 0.12%).

Unlike previous TPS models, Kim and Chien (2009) developed a dynamic time-based TPS model consisting of a train traction module (TTM), a track alignment module (TAM), and a train control module (TCM), for emulating train travel time and energy consumption considering various control regimes under different vertical track alignments. The developed TPS can generate various train performance indicators (e.g., travel time, train speed, energy consumption, acceleration/deceleration rate, travel distance, etc.), which can be utilized to assess the performance of train control and the accuracy of service schedules. The relationship between train control and track alignment was investigated, and the alignments affecting travel time and energy consumption were analyzed. Particularly, it was found that the train operation on a convex rail alignment significantly reduces consumed energy, which offers greater flexibility to justify train control to meet scheduled service.

After reviewing major features of TPS models, the results of comparative analysis are summarized in Table 2.2, where six major features were identified, including movement calculation, traction power system, energy consumption, tract alignment, train control, and signaling system. However, none of the TPS models was equipped with all the features. It is desired to develop a TPS model that can emulate various components of railway systems to calculate accurately the energy consumption and travel time associated with various track alignments. Thus, the optimal train control alternatives may be determined and evaluated.

Table 2.2 Review of TPS Models

		Features					
		Movement Calculation	Traction Power System	Energy Consumption	Track Alignment	Train Control	Train Signaling System
Simulation Model	Uher & Disk (1987)	Time-based		√			
	Kikuchi (1991)	Event-based					
	Minciardi et al. (1994)	Event-based		√			
	Kim & Schonfeld (1997)	Time-based		√	√		
	Gordon et al. (1998)	Time-based	√	√		√	√
	Chang et al. (1998)	Event-based					
	Zou et al. (1999)	Event-based				√	√
	Jong & Chang (2005)	Time-based		√			
	Kim & Chien (2008)	Time-based		√	√	√	

√: identified features

2.3 Kinematic Models for Train Movement

Moving a train along a route involves many force components, including the TE, resistance, braking force and train weight. While the TE provides a necessary force to move a train, resistance, known as drag, and consisting of the forces acting on the wheels and externally on the train body, opposes the movement and speed of a train. To accelerate or decelerate a train, the TE must be transferred between wheels and the running surface of the rail through a friction force, called adhesion (Vuchic, 1982). A comprehensive review related to TE, adhesion, and resistance was conducted and it is discussed next.

2.3.1 Tractive Effort (TE) and Adhesion

The tractive effort can be computed by equating the work done at the rim of the driving wheel with that performed by the torque or turning effort of the engine or motor (Lipetz, 1935). In general, the engine power consumed for the TE is limited not to exceed the adhesion between wheel and track; otherwise wheel slip will occur and the locomotive will lose traction. Adhesion is a function of the friction at the point of wheel-rail contact. The adhesion coefficient is often taken as 0.25, which represents the percentage of locomotive weight that is available as effective TE (Hay, 1982)

Since the adhesion coefficient, denoted as μ , of a train has non-linear characteristics to its corresponding speed, denoted as v , it is difficult to derive mathematically, but it can be obtained mainly through field tests (Shirai, 1977; Isaev and Golubenko, 1989). Sjokvist (1988) compared adhesion coefficient curves utilized in several European countries (e.g., Germany, Austria, Switzerland, and France), and the result is illustrated in Figure 2.2. Note that Curve A, employed in Germany, Austria, and

Switzerland, was obtained based on running a German Class 19 electric locomotive up to 160 km/h in 1943.

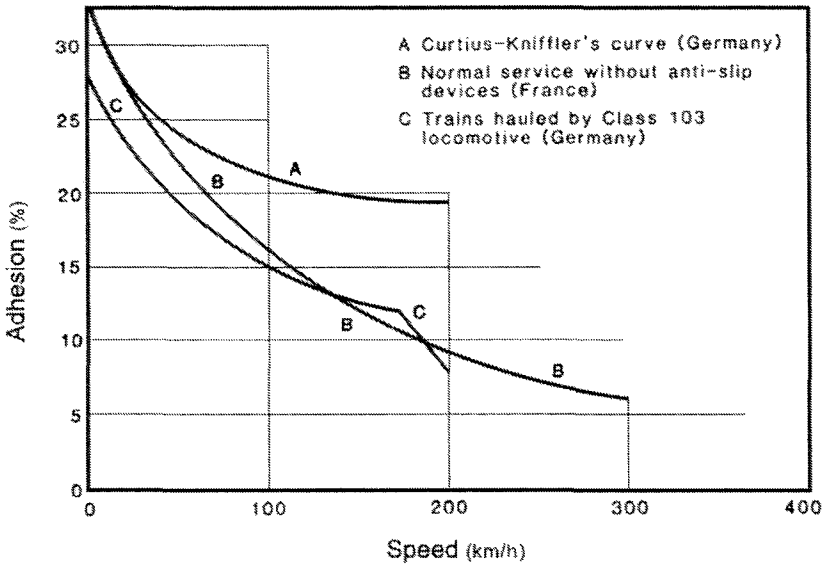

Figure 2.2 Comparison of adhesion coefficients.

Source: Sjokvist (1988)

Later, Curve A, representing the relationship between μ and v in units of kilometer per hour (kph), was formulated by Curtius and Kniffler (1950) as

$$\mu = \frac{7.5}{v + 44} + 0.16 \qquad \left| \frac{\mu}{\%} \right| \frac{v}{\text{kph}} \tag{2.1}$$

which has been widely used in estimating adhesion coefficients at any given speed in Germany (Filipovic, 1995). Unlike Curve A, Curve B represents μ obtained by running an electric locomotive in France in the 1960s (Nouvion, 1968), which was formulated by the French National Railways (SNCF) as

$$\mu = 0.24\frac{8+0.1v}{8+0.2v} \qquad \left|\frac{\mu}{\%}\right|\left|\frac{v}{\text{kph}}\right| \tag{2.2}$$

In addition, Curve C was derived from experiments in Germany by running a train which was hauled by the first German electric locomotive geared for 200 kph.

The Japan National Railways (JNR) conducted an adhesion test using a Shinkansen 200 locomotive for estimating the adhesion coefficient, under wet conditions, on a test bed and in actual service at speeds up to about 250 kph as shown in Figure 2.3. The adhesion for high-speed trains on the Shinkansen network was derived by Maeda et al. (1984) as

$$\mu = \frac{136}{v+85} \qquad \left|\frac{\mu}{\%}\right|\left|\frac{v}{\text{kph}}\right| \tag{2.3}$$

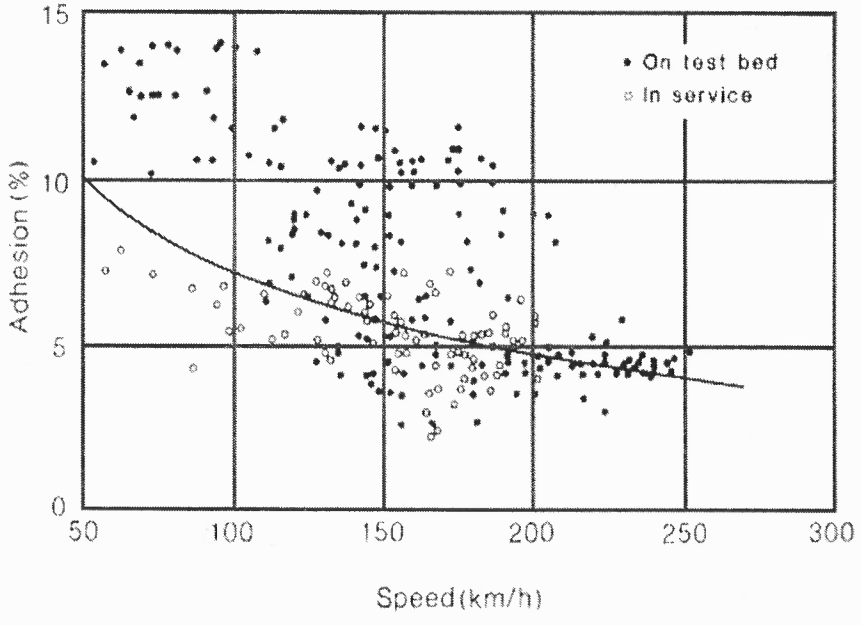

Figure 2.3 Adhesion under wet conditions -Shinkansen 200.

Source: Maeda et al. (1984)

Vuchic (2007) investigated the effect of the surface conditions of highway and rail to determine adhesion coefficients (μ). Under dry conditions, it was found that μ was approximately between 0.52 and 0.8 and between 0.15 and 0.35 for vehicle speeds between 10 kph and 80 kph on highway and rail, respectively. However, μ significantly decreased when the surface condition became wet. For an extreme case, μ of highway vehicles is as low as 0.05 under snow/ice, while μ of rail vehicles is approximately 0.1 under wet conditions. The summary of adhesion coefficients for highway and rail vehicles is shown in Table 2.3.

Table 2.3 Summary of Adhesion Coefficients for Various Weather Conditions

			Surface Conditions					
			Dry		Wet		Snow/Ice	
		Speed (kph)	10	80	10	80	10	80
Modes	Highway	MAX	0.8	0.72	0.6	0.45	0.2	0.05
		MIN	0.66	0.52	0.42	0.27	0.36	0.18
	Rail	MAX	0.35	0.29	0.25	0.17	-	-
		MIN	0.27	0.15	0.19	0.1	-	-

Source: Vuchic (2007)

2.3.2 Train Resistances

To determine whether the propulsion system of a train is able to operate with speed (V), the total resistance, denoted as R, must be known. Schmidt (1910) developed a series of equations for calculating resistances, based on empirical data obtained from the Illinois Central Railroad. On a level track alignment without wind effect, it was found that the total resistance can be expressed by a quadratic equation formulated as

$$R = C_1 + C_2 V + C_3 V^2 \qquad \left|\frac{R}{lb_f}\right|\left|\frac{C_1}{-}\right|\left|\frac{C_2}{-}\right|\left|\frac{C_3}{-}\right|\left|\frac{V}{mph}\right| \tag{2.4}$$

where the coefficients C_1, C_2, and C_3 are dependent on axle load, number of axles, cross section of the train, and shape of the train.

An evaluation of the coefficients of train resistance for Swedish conventional passenger trains, high-speed trains, and freight trains was conducted by Lukaszewicz (2007). After reviewing the comparison study (Rochard and Schmid, 2000) results of three train resistance measurement methods such as tractive effort method, coasting energy method, and dynamometer or drawbar method, the coasting energy method that calculates the changes in kinematic and potential energy of a train when it is coasting between two successive measurement positions was selected for its accuracy. The impact of variables such as speed, number of axles, track type (i.e., surface condition), and train length on resistance coefficients was also analyzed. It was found that C_1 varies with the number of axles, axle load, and track type, and increases linearly with the number of axles, while C_2 and C_3 varying with train length and the front or rear area of the train, respectively.

The train resistance equations developed by Schmidt (1916) vary with the weight and speed of a train, which led Davis (1926) to formulate an empirical equation for unit resistance (see Equation 2.5), consisting of rolling, journal, flange, and air resistances. Equation 2.5, also called the Davis equation, was developed and validated by the data from the Pennsylvania and Burlington Railroads.

$$r = 1.3 + \frac{29}{w} + bV + \frac{CAV^2}{wn} \qquad \left|\frac{r}{lb_f/ton}\right|\frac{w}{ton}\left|\frac{V}{mph}\right|\frac{n}{-}\left|\frac{C}{-}\right|\frac{A}{ft^2}\left| \qquad (2.5)$$

where r is unit resistance in pounds per ton; w is weight per axle in tons; b is an experimental coefficient based on flange friction, shock, sway, and concussion. C is the drag coefficient based on the shape of the front end of the car or locomotive; and A is the cross-sectional area in square feet of the car or locomotive. Later, the modified Davis equation (see Equation 2.6) was developed in 1970 by Committee 16 of the American Railway Engineering Association (AREA). Its intent was to recognize changes in resistance factors, increased train operating speed, and improved track conditions over the earlier days (AREA, 1981). The modified Davis equation is thus developed and formulated as

$$r = 0.6 + \frac{20}{w} + 0.01 \cdot V + \frac{K \cdot V^2}{w \cdot n} \qquad \left|\frac{r}{lb_f/ton}\right|\left|\frac{w}{ton}\right|\left|\frac{V}{mph}\right|\left|\frac{K}{-}\right|\left|\frac{n}{-}\right| \tag{2.6}$$

where K, the air resistance coefficient, is 0.07 for cars, 0.0935 for containers, and 0.16 for trailers on flatcars. Both the Davis and the modified Davis equations were derived for calculating unit resistance of a train, which considered weight per axle, number of axles per car, and the degree of aerodynamic and drag effects.

Hay (1982) discussed the effect of vertical and horizontal track alignments on estimating train resistances. Grade resistance is proportional to the angle (in degree) of the inclined track and can be directly derived from the relationship between train weight and the track grade. It was found that the grade resistance was 20 lb/ton per track grade (in percentage). On the other hand, the resistance associated with a horizontal track curvature was determined by field tests and experiments (the Pennsylvania Railroad, 1907). It was found that the resistance due to horizontal curvature was 0.8 lb/ton per track curvature (in degrees). While evaluating train resistances, Hay (1982) found that the total

resistance is the sum of all resistive forces acting on the train, which are measured in pounds per ton. The evaluated resistive forces and their components are summarized in Table 2.4.

Table 2.4 Characteristics of Train Resistances

Resistive Forces	**Resistance Components**	**Features**
Load weight related	Rolling Resistance	• Results from friction between the wheel tread and the head of the rail • Function of the coefficient of rolling friction • Types of metal in wheel and rail • Condition of wheel and rail surfaces
	Track Resistance	• Results from deflection and reverse bending of the track due to the loading and stiffness of the track structure
	Journal Resistance	• Results from the friction between the journals at the ends of each axle and brasses
Velocity related	Air Resistance	• Varies approximately with the square of the speed and directly as the cross-sectional are • Air resistance $=CAV^2$ o where C: experimental coefficient o A: cross-sectional area (ft^2) o V: velocity (mph)
Curvature related	Curve Resistance	• Friction between the flanges and treads of the wheels • The head and gage corner of the rails due to track curve
Grade related	Grade Resistance	• Major impact on the number of trains, locomotive units, and horse power to move given tonnage

Source: Hay (1982)

Bernsteen et al. (1983) studied the problem of train rolling resistance as an energy consumption end use. Two types of freight train cars (e.g., 120-ton cars and 40-ton cars) were tested to measure the rolling resistance and its effect on energy consumption for various tracks classes [Track Classes 3, 4, 5, and 6 (a system of classification for track quality has been developed by the FRA and each track class has its own speed limit as shown in Table 2.5)]. It was found that the accuracy of the modified Davis equation

decreased when axle load is extremely low, which had an impact on rolling resistance. It was also found that since the rolling resistance strongly depends on class of track, the surface of track alignment should be improved to achieve better energy efficiency.

Table 2.5 Track Class and Train Speed Limit

	Speed Limit (mph)	
Track Type	**Freight Train**	**Passenger Train**
Excepted[1]	< 10	Not allowed
Class 1	10	15
Class 2	25	30
Class 3	40	60
Class 4[2]	60	80
Class 5[3]	80	90
Class 6	110	
Class 7[4]	125	
Class 8[5]	160	
Class 9[6]	200	

1. Only freight trains are allowed to operate on Excepted track and they may only run at speeds up to 10 mph (16 km/h). Passenger trains of any type are prohibited.
2. Mainline track owned by major railroad company
3. Burlington Northern Santa Fe (BNSF) railway & Amtrack's Southwest Chief
4. Most of Amtrack's Northeast Corridor
5. Portion of the Northeast Corridor
6. Currently no Class 9 Track

Source: Federal Railroad Administration Track Safety Standards Compliance Manual (2007)

2.4 Train Control Regimes

Energy consumption and travel time on fully controlled systems are exclusively affected by train control and less interfered by external factors such as traffic, signals, and pedestrians (Vuchic, 1982). Therefore, a number of studies (Hopkins, 1978; Yasukawa, 1987; Howlett and Pudney, 1995; Duarte and Sotomayor, 1999) focused on optimal train control for minimum energy consumption. In general, train control for most transit operations represents a cycle of different motion regimes, including acceleration, cruising, coasting, and braking. For analyzing station-to-station travel time and distance profile, it

is essential to comprehend the description of the motion regimes and their mathematical expressions, which will be discussed in Chapter 3.

Four basic train controls and their motion regimes discussed by Vuchic (1982) are shown in Figure 2.4:

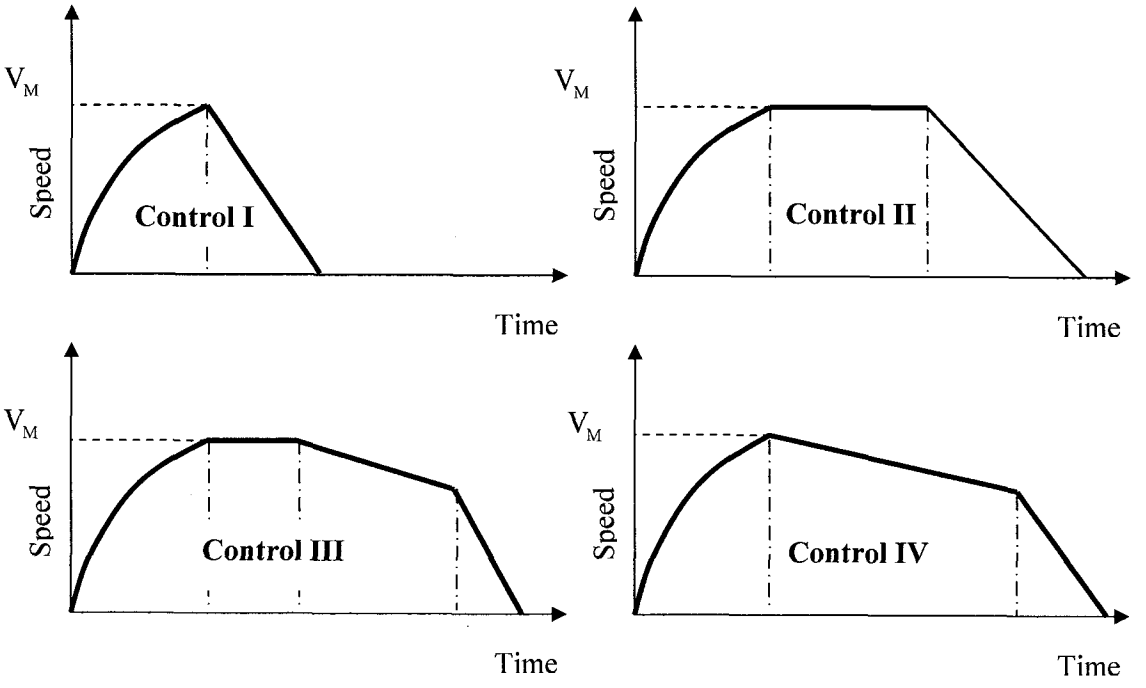

Figure 2.4 Four cases of inter-station train control regimes.

- Control I: Acceleration, then braking must apply;
- Control II: Acceleration, cruising, then braking must apply;
- Control III: Acceleration, cruising, coasting, then braking must apply; and
- Control IV: Acceleration, coasting, then braking must apply.

Each case contains a set of motion regimes (e.g., acceleration, cruising, coasting, and braking) affected by station spacing, acceleration/deceleration rates, and maximum operating speed, denoted as V_M. Controls I and II are used to achieve the least travel time for station spacing, denoted as S, is less and greater than the critical station spacing,

denoted as S_c, respectively. In addition, Controls II, III, and IV are all used for $S>S_c$. In Control II, a train accelerates until V_M is reached, and then V_M is maintained until a brake must be applied to stop at the next station. It is obvious that Control II operation drives shorter travel time but consumes more energy, compared to those in Controls III and IV. Control III operation is commonly used for reducing energy consumption, which consists of an acceleration interval to reach V_M, cruising at that speed, coasting, and then braking. By using Control IV operation, the consumed energy can be further reduced, albeit the longest travel time.

Hopkins et al. (1978) measured train energy consumption for various rail services such as branch line freight, inter-city freight, high speed passenger, and commuter considering train speed, size (weight and length), power to weight ratio, and track profile. It was found that a continuously varying speed profile could consume an additional energy of 5 - 15% than that of a constant speed profile (i.e., cruising), although both yielded the same average speed, which indicated that a train operated with frequent acceleration and braking consumes more energy.

Yasukawa et al. (1987) investigated several energy-efficient train controls for the Tohoku Shinkansen electric motor trains by employing a simulation approach. Four different train controls were simulated on the rail segment between Ohmiya and Oyama stations. As illustrated in Figure 2.5, the proposed train controls used the same acceleration rate until the train speed reaches V_M, then the following motion alternatives will take place:

- Control 1: cruising with V_M, decreasing speed with automatic train control (ATC) brake, cruising again, and then braking ;

- Control 2: coasting, decreasing speed with ATC brake, cruising, and then braking;
- Control 3: cruising, speed decreasing using ATC brake, coasting, and then braking; and
- Control 4: coasting, speed decreasing using ATC brake, coasting again, and then braking.

It was found that Control 4 is the most energy-efficient for which approximately 10% energy can be saved, compared to other controls.

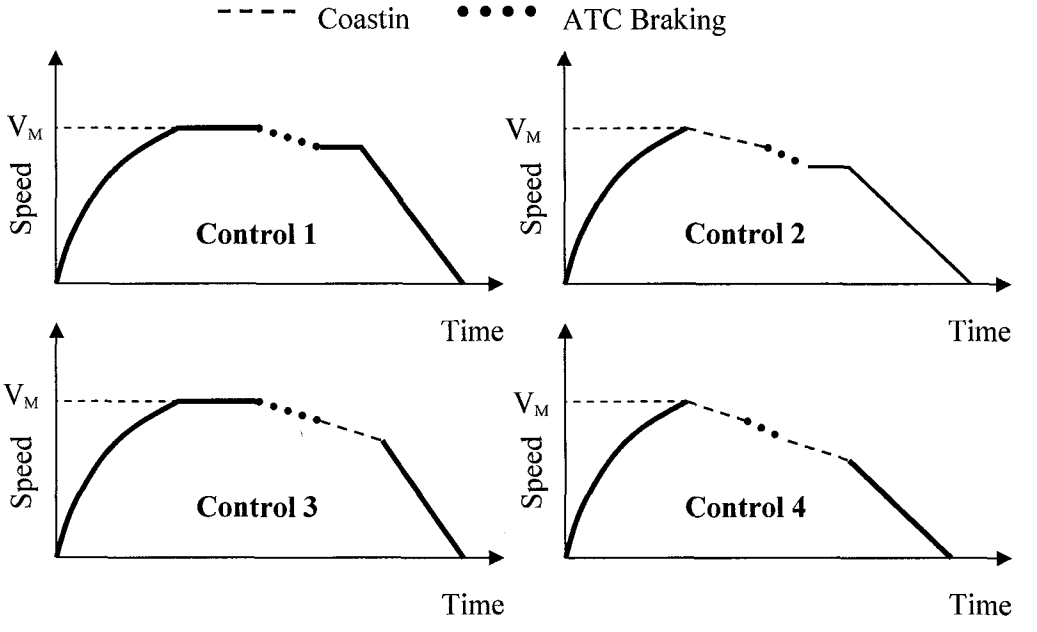

Figure 2.5 Train controls of the Tohoku Shinkansen.

Duarte and Sotomayor (1999) determined train speed trajectories with an optimal control of a train in subway systems. The objective function of the study was minimizing the total energy consumption for a round trip. Several constraints such as speed limit, maximum slope of track alignment, maximum acceleration/deceleration rate, and maximum electrical force were considered. The Gradient-Restoration method developed by Miele et al. (1974) was employed to design an optimal train control used at a subway

system in Santiago, Brazil. An average of 18 % energy saving per train was achieved after executing the optimal train speed profile.

Hiraguri et al. (2004) proposed a train control method based on the prediction of train movement and data communication. The control method intended to avoid unexpected train movement, such as an abrupt deceleration or stopping due to the delay of the preceding train. The concept of the control method was to calculate the predicted time when the preceding train leaves the station and transmit the predicted time to the approaching train, and then the speed profile of the approaching train was controlled to avoid an unexpected stopping. The proposed method was verified in computer simulation and the performance of recovery from traffic disruption was evaluated. The simulation results showed that the proposed method reduced stopping delay between stations and related energy consumption.

Dongen and Schuit (1989) investigated several energy efficient driving strategies of an electric railway system connecting Zandvoort-Maastricht and Heerlen in the Netherlands. They analyzed energy savings, considering energy efficient acceleration, optimized constant speed, and coasting. The energy saving test was conducted in co-operation with the traffic center and train drivers were informed of the optimal control. The test results of driving strategies consisting of optimized acceleration rate, constant speed, and coasting revealed that approximately 25% of the energy consumption under ideal train service circumstances (i.e., undisturbed condition) was saved, while 15% of the energy under unexpected situations (i.e., temporary speed restriction, signal checking, etc.) was saved.

2.5 Minimization of Energy Consumption for Train Operation

A number of studies related to minimizing train energy consumption have been researched by using classical numerical optimization methods such as dynamic programming (Franke et al., 2000; Albrecht, 2004) and the maximum principle (Horn, 1971; Golovitcher, 2001) as well as modern heuristic optimization algorithms such as the Genetic Algorithm (GA) (Chang and Sim, 1997; Wong and Ho, 2003; Bocharnikov et al., 2007), and fuzzy logic combined with GA (Hwang, 1998).

Previous studies on train energy consumption minimization used to over simplify train movement (Horn, 1971) and ignored the effect of track alignment, which considerably influences train resistances and tractive effort (Albrecht, 2004; Hwang, 1998).

Franke et al. (2000) used discrete dynamic programming to minimize train energy consumption by considering the non-linear aspect of train control. Energy was set as a dynamic state variable to minimize energy consumption on a level (without grade and curvature) track alignment. An equation for train motion was formulated in the form of a piecewise function, which was tested on the Zurich-Luzern line of the Swiss Federal Railways (SBB) and achieved 10-30% reduction of traction energy.

Albrecht (2004) investigated the possibilities of train running time modification to reduce power peaks and energy consumption under a given headway. The problem of adjusting train running was regarded as a multi-level decision problem because it has to be decided at each station and solved using dynamic programming. A case study has been conducted for one line of the Berlin S-Bahn network consisting of a track of 18 kilometers (km) with 14 stations. Given that an optimal combination of headway and

synchronization time are known, it was sufficient to use a controller based on the minimization of a single train's energy consumption using dynamic programming. The optimized train running time could lead to energy savings of 4%.

Horn (1971) discussed that a number of studies on energy efficient train control analytically approached a simplified linear train model by using the Maximum principle in the late 1960s. Most optimal controls achieved by the Maximum principle were based on the assumption that an inter-station train movement is composed of four motion regimes: maximum acceleration, cruising, coasting, and maximum deceleration. The application of optimal control was possible when this assumption was met.

Golovitcher (2001) developed an analytical method to achieve optimal train control for minimum energy consumption in rail or other fixed path vehicles. To decrease on-board computational time, he used a Hamiltonian formulation and the maximum principle to determine the set of optimal controls. Based on the results obtained by solving the Hamiltonian, a set of motion regimes (e.g., full tracking, full braking, coasting, cruising, partial tracking and partial braking) was established. The results of the conjugate function of the Hamiltonian, traction effort equation, and braking power equation set up criteria for using motion regimes. In a case study, the optimal control could save 3% of the energy consumption.

Hwang (1998) developed a fuzzy control model which determines an economical (i.e., the most energy efficient) train running profile considering the trade-off between travel time and energy consumption. A speed triplet set (coasting speed, economical speed, and maximum speed) was prepared through simulation runs and was optimized by a proposed GA hybrid method (GA combined with a fuzzy model), but track alignments

were not considered. The studied GA hybrid method was used to a high-speed rail system from Seoul to Busan in Korea. It was found that when the increase of travel time is less than 7%, more than 5% of the energy consumption was saved.

, GA was used to search for the appropriate coasting control in a mass rapid transit (MRT) system. Chang and Sim (1997) developed a dynamic train coasting regime controller and a coasting control table by using GA to determine the timing for coasting and to resume acceleration. Each coasting table was encoded into variable lengths of chromosomes with each gene representing the relative position between stations where coasting should be initiated or terminated. It was found that the use of GA to obtain optimized coast control strategies is successful in improving energy consumption. Later, a similar but enhanced study was conducted by Wong and Ho (2004). They used GA to identify the best coasting locations, and the possible improvement on the fitness of genes was investigated. Single and multiple coasting control with GA were developed and their corresponding train movement was examined. Further, a Hierarchical Genetic Algorithm (HGA) was adopted to identify the number of coasting locations required according to the traffic conditions, and Minimum-Allele-Reserve-Keeper (MARK), a fast and effective mutation scheme for GA, was used to a genetic operator to achieve fitter solutions.

Bocharnikov et al. (2007) used GA to find an optimal coasting strategy combined with varying acceleration and deceleration rates. They derived a fitness function consisting of energy consumption and running time. Fuzzy sets were implemented and optimal control sought which minimized energy consumption within the defined

timetable constraints. It was found that on a 8.53 km track, up to 31.27% of traction energy was saved while travel time increased by 12.5%.

Kim and Chien (2010) developed an optimization model for rail transit to minimize energy consumption used for an inter-station run. The model optimizes the duration of train motion regimes used for train control by considering track geometry, speed limit, and scheduled travel time using the Simulated Annealing algorithm (SA). The model was used in a real case study of the Metro-North Commuter Railroad. The most energy efficient train control, or called "golden run", associated with speed limits, track geometry, and schedule adherence was identified. It was found that the optimal train control saved 30.4 % of the energy consumption in a commuter rail system compared with flat-out run, while travel time increased by 7 %.

Energy minimization for rail public transit systems was discussed by Danziger (1975) from the viewpoint of an integrated systems approach. The approach considered the interaction of all the major subsystems of a rapid transit system rather than each subsystem independently. Some of the major subsystems examined included vehicles and their major propulsion, braking and auxiliary systems, train operations, environmental control facilities, and civil and structural facilities. The major factors that may significantly affect an overall energy evaluation were identified, and the ways in which each of these factors can be controlled to affect overall maximum efficiency of energy use were discussed. Energy evaluation techniques include a new strain performance simulation computer program developed by Parsons, Brinckerhoff, Quade and Douglas, Inc., as part of a 4-year subway environmental research project. It was found that the procedures for evaluation on a total system-wide basis are applicable for any rail transit

system and can be used to extend or modify existing rail transit systems and the design of new ones.

2.6 Optimization Algorithms and Heuristic Methods

The studied optimal train control problem is a large combinatorial optimization problem where the solution space consists of combinations of multiple decision variables, including motion regimes, locations of motion regime changes, and the acceleration rate. Thus, a robust searching algorithm, such as Simulated Annealing and other intelligent optimization techniques, is desired to find a near optimum solution efficiently in the enormous solution space. Several optimization techniques, such as Simulated Annealing (SA), Tabu Search (TS), and Genetic Algorithm (GA) are suitable to solve a combinatorial problem, and are discussed below.

The simulated annealing (SA) algorithm derived from statistical mechanics was developed by Kirkpatrick et al. (1983) based on the strong analogy between the physical annealing process of solids and the problem solving of large combinatorial optimization problems. The states of solid represent the feasible solutions of optimization problems, in which the energy associated with each state corresponds to the value of the objective function of each feasible solution. Accordingly, the minimum energy of a crystal state corresponds to the optimal solution while rapid quenching can be considered as a local optimization. A standard simulated annealing algorithm includes four portions (i.e., solution representation, objective function, generation mechanism of neighbor solutions and has been cooling schedule). SA has been proven effective for fine-tuning a local optimal search, and utilized to solve many optimization problems in transportation related fields, such as transit network optimization (Zhao and Zeng, 2006), robust estimation

(Baselga, 2007), vehicle routing problem (Ting and Chen, 2007), road network design (Kim and Schonfeld, 2008). However, a good initial solution and cooling schedule are very critical in finding the optimal solution.

Busetti (2003) presented an overview of SA by discussing and comparing its features with other optimization methods. The strengths of SA identified in his paper are as follows:

- SA can handle highly non-linear models, chaotic and noisy data, and many constraints.
- SA is flexible and able to find global optimality.
- SA is versatile and does not rely on any restrictive properties of the model.
- SA can be easily tuned. For any reasonably difficult non-linear or stochastic system, a given optimization algorithm can be tuned to enhance its performance and since it takes time and effort to become familiar with a given code, the ability to tune a given algorithm for use in more than one problem should be considered an important feature of an algorithm.

He also made a direct comparison between Adaptive Simulated Annealing (ASA) and GA, using a test suite already adapted and adopted for GA. The result showed that in each case, ASA outperformed the GA problem. He mentioned that GA is a class of algorithms that are interesting in their own right; GA was not originally developed as an optimization algorithm, and basic GA does not offer any statistical guarantee of global convergence to an optimal point.

Zhao and Zeng (2006) presented a stochastic methodology for transit route network (TRN) optimization. Their study goal was to provide an effective computation

tool for the optimization of a large-scale transit network to minimize transfers with reasonable route directness while maximizing service coverage. The methodology includes the representation of a transit route network solution search spaces, representation of the transit route and network constraints, and a stochastic search scheme based on an integrated SA and GA search method. The feasibility of the proposed method has been tested through previously published results and a practical TRN optimization problem of a realistic size. Numerical results showed that the methodology was capable of tackling large-scale transit network design optimization problems.

Baselga (2007) proposed a methodology for robust estimation that has proven to be a valuable approach to adjust surveying network when there are systematic or gross errors in the observations or systematic errors in the functional model. He computed robust estimation with SA and an Iteratively Reweighed Least-Squares (IRLS) process, and compared the results of two methods. In his study, he mentioned that SA is one of the most suitable heuristic methods for large-scale optimization problems, especially when there is a global optimum, which is to be determined among many other local optima.

Ting and Chen (2007) developed a methodology to find the optimal solution of a vehicle routing problem (VRP) which is an important management problem in the field of physical distribution and logistics. The study proposed a multiple ant colony system (MACS) to solve the multi-depot vehicle routing problem with time windows (MDVRPTW). Moreover, two hybrid algorithms, which combine the strengths of the MACS and the SA, were developed to improve the solution quality. The numerical analysis demonstrated that the combination of MACS and SA can improve the solution quality significantly.

Kim and Schonfeld (2008) extended the network design problem (NDP) to the proposed road space allocation problem (RSAP), which finds the optimal lane configuration on each link in a road network that minimizes total system cost. The RSAP was formulated as a bi-level programming problem with an upper-level problem that optimally allocates road space and a lower-level problem that evaluates travelers' mode and route choices in response to each alternative. The demand model employs a multi-class, multi-modal network equilibrium model to efficiently evaluate road space allocation alternatives. A heuristic based on simulated annealing was presented to solve the combinatorial optimization problem. It was found that when toll lanes are provided in the network, in most cases, lower-income users have the longer average travel time than higher-income users. With a lower allowable equity measure, a more equitable solution was reached.

The literature review revealed that existing algorithms have different strengths in solving particular optimization problems. For example, GA was found to outperform SA and TS in solving traveling salesman problems (Pham and Karaboga, 2000). However, in solving large-scale machine-grouping problems, Zolfaghari and Liang (2002) indicated that SA outperforms both GA and TS, and GA is slightly better than TS.

2.7 Summary

Energy consumption is deemed to be a very important indicator for sustainable train operation due to increased energy usage and cost. A number of studies have been conducted to minimize energy consumption for train operations, but some of them required the purchase of new equipment (e.g., kinetic energy storage system, variable voltage variable frequency (VVVF) inverter, gate turn off (GTO) thyristor, etc.) that are

quite expensive. Therefore, implementing optimal train control subject to existing track alignment and regulated speed setting may bring a significant benefit in comparison with alternatives using costly technologies. Most of the previous studies shown in Table 2.6 have been focusing on developing optimal train control models to reduce energy consumption, but those either disregarded the joint effect of varying vertical alignment and horizontal curvature on TE and resistance or neglected the restriction of travel time for schedule adherence. Instead, most of the train control studies were focusing on the effect of train speed control or coasting regime on energy consumption and travel time. This research develops methodologies that optimize train control by considering various aspects (e.g., track alignment, maximum operating speed, schedule adherence, etc.) of train operations.

Table 2.6 Minimum Energy Consumption for Train Operation Studies

Authors (Year)	Methodology	Limitation
Horn (1971)	• Train control model assumed linear • Optimized using Maximum Principle	• Over simplified train movement
Chang and Sim (1997)	• Developed dynamic coasting regime controller by applying GA	• Proposed method was demonstrated for inter-station train movement
Hwang (1998)	• Developed most energy efficient train running profile using a fuzzy control model	• Effect of track alignment was not considered
Franke et al. (2000)	• Employed discrete dynamic programming to minimize train energy consumption	• Studied on only level alignment
Golovitcher (2001)	• Developed analytical method for optimal train control by using maximum principle	• Only four sets of train control are considered
Albrecht (2004)	• Adjusted train running time using dynamic programming	• Effect of track alignment was not considered
Wong and Ho (2004)	• Determined best coasting locations with GA • Identified the number of coasting using MARK	• Proposed method is not applicable for a multiple inter-station run
Bocharnikov et al. (2007)	• Investigated an optimal coasting strategy using GA	• Proposed method is appropriate only for inter-station train movement

CHAPTER 3

DEVELOPMENT OF TRAIN PERFORMANCE SIMULATION (TPS) MODEL

A time-driven TPS model which consists of three key modules: Train Traction Module (TTM), Track Alignment Module (TAM), and Train Control Module (TCM), is developed to simulate passenger train operations, which can be used to evaluate various performance indicators, including travel time and energy consumption for any train control and track alignment. Dynamic information, such as the TE, resistances, the rate of acceleration/deceleration, and speed, will be generated corresponding to the location of a train and the geometry of the track alignment. The development of each module is discussed below.

3.1 Train Traction Module (TTM)

The responsibility of the train traction module (TTM) is to compute the TE needed to move a train along a rail line, considering the speed, the rate of acceleration (or deceleration), and the location of the train at any point in time. TTM calculates the TE based on projected resistances so that the rates of acceleration/deceleration and the target speed for the next interval operation can be obtained. The input parameters of TTM include static information (e.g., locomotive power, number of cars per train, number of axles per car, train weight, cross-section area), dynamic information (e.g., train location, travel time, speed, rates of acceleration/deceleration), track alignment condition (e.g., convex, concave, level), and operational constraints (e.g., speed limit, station spacing, and train schedule, etc.). An iterative computation process is performed based on a user-

specified time interval (e.g., 1 second), in which the needed TE to move the train to the desired location over time can be determined.

The calculated TE with TTM can be used with different types of locomotives (e.g., diesel-electric and electric motors) for estimating consumed energy by justifying the ratio of energy consumption per unit of TE. Note that the function of TE is calculated based on the effective power to move tonnage up on the track alignment (e.g., level, convex, and concave). The developed TTM computes TE and resistances of cars and locomotives of the train by considering the train as a string of masses interconnected by springs and damping as shown in Figure 3.1.

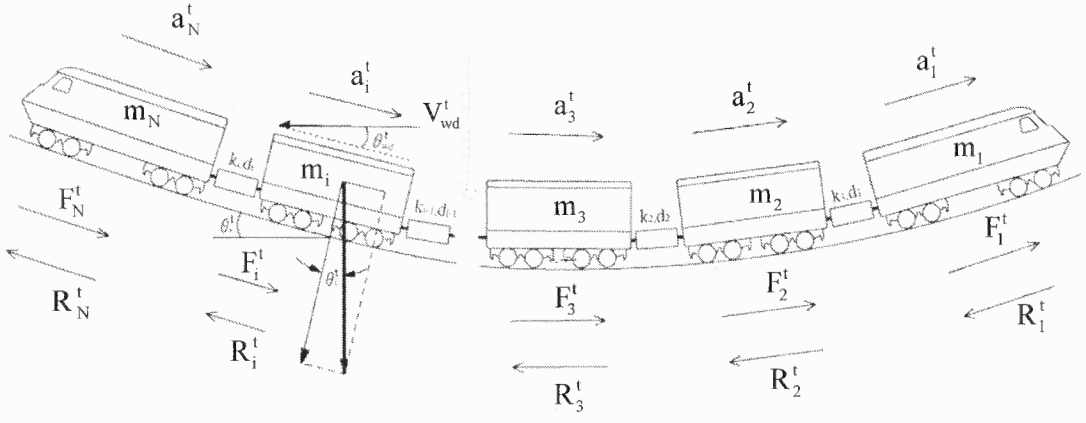

Figure 3.1 Longitudinal train forces on a continuously varying track.

The net force to move each car of the train is equivalent to the differences between TE, denoted as F, the sum of resistances (e.g., bearing, rolling, air, and grade resistance), denoted as R, coupler forces determined by a damper constant (d) and spring constant (k). Considering that locomotives of a train can be placed in any position, the equation of motion for the i^{th} car in a train, at time t, can be determined by Equation 3.1 discussed by Cole (1998).

$$m_i \cdot a_i^t = F_i^t - R_i^t - d_{i-1}(v_i^t - v_{i-1}^t) - d_i(v_i^t - v_{i+1}^t) - k_{i-1}(x_i^t - x_{i-1}^t) - k_i(x_i^t - x_{i+1}^t) \qquad (3.1)$$

$$\left|\frac{m_i}{lb}\right|\frac{a_i^t}{ft/sec^2}\left|\frac{F_i^t}{lb_f}\right|\frac{R_i^t}{lb_f}\left|\frac{d_i}{lb \cdot sec/ft}\right|\frac{k_i}{lb/ft}\left|\frac{v_i^t}{ft/sec^2}\right|\frac{x_i^t}{ft}\right|$$

where m_i is car mass, a_i^t is acceleration of the i^{th} car at time t, d_i is damping constant, k_i is spring constant, v_i^t is speed of the i^{th} car at time t, x_i^t is longitudinal position of the i^{th} car at time t.

To avoid slippage of the wheel on the track, the maximum TE at time t for the i^{th} car, denoted as $F_{max(i)}^t$, is the minimum value of available propulsive force, denoted as $F_{p(i)}^t$, and adhesive force, denoted as $F_{a(i)}^t$. Thus,

$$F_{max(i)}^t = \min(F_{p(i)}^t, F_{a(i)}^t) \qquad \left|\frac{F_{max(i)}^t}{lb_f}\right|\frac{F_{p(i)}^t}{lb_f}\left|\frac{F_{a(i)}^t}{lb_f}\right| \qquad (3.2)$$

As indicated in Eq. 3.2, $F_{P(i)}^t$ represents a needed force for the wheel to overcome the resistance is the product of locomotive's horse power for the i^{th} car, denoted as P_i^t, and energy transmission efficiency, denoted as η, divided by speed of the i^{th} car, denoted as V_i^t, at time t. Thus,

$$F_{P(i)}^t = \frac{375 \cdot \eta \cdot P_i^t}{V_i^t} \qquad \left|\frac{F_{P(i)}^t}{lb_f}\right|\frac{\eta}{-}\left|\frac{P_i^t}{hp}\right|\frac{V_i^t}{mph}\right| \qquad (3.3)$$

where 375 is a parameter to convert the unit rate of work in foot-pounds/second into mile-pounds/hour. Note that Equation 3.3 is derived based on a function discussed by Hay (1982) in which the transmission efficiency (η) is a coefficient of energy loss

between the engine and the wheels. η varies with the type of gears and is usually between 0.78 and 0.85, depending on train speed and track condition.

On the other hand, $F^t_{a(i)}$ represents a friction force caused by the contact between the wheel of the i^{th} car and track surface and is dependent on the car weight, denoted as W_i, and adhesive coefficient, denoted as μ_i^t. The determination of μ_i^t is based on the train speed shown in Figure 3.2 (Vuchic, 2007), which ranges between 0.28 and 0.38 for a speed of 10 kilometers per hour (kph) and between 0.17 and 0.28 for a speed of 80 kilometers per hour (kph) under dry rail and wheel conditions. In the developed TPS, μ_i^t is assumed linearly decreasing as the train speed increases from 0 to 80 kph. Thus,

$$\mu_i^t = 0.33 - 0.002 \cdot V_i^t \quad \left| \frac{\mu_i^t}{-} \right| \left| \frac{V_i^t}{\text{mph}} \right| \tag{3.4}$$

Note that μ_i^t was found non-linearly decreasing with an increasing V_i^t (Candee, 1940), which can be adapted by the developed TPS.

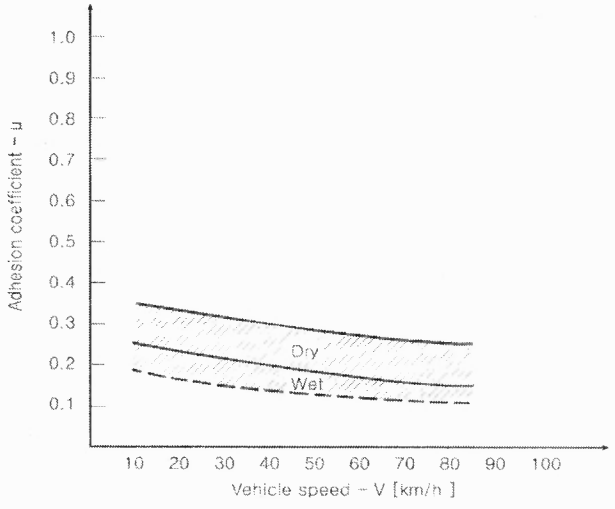

Figure 3.2 Adhesion coefficient vs. speed under different rail and wheel conditions.

The kinematics of the i^{th} car movement at time t inclined at an angle θ_i^t to the horizontal are determined by a couple of force components including TE, resistance and train weight, denoted as F_i^t, R_i^t, and W_i, respectively (See Figure 3.1). Therefore, the adhesive force $F_{a(i)}^t$ for steel wheels on the rail, generated by the car weight component perpendicular to the surface of the track, can be estimated by Equation 3.5 as

$$F_{a(i)}^t = \mu_i^t W_i \cos\theta_i^t \qquad \left|\frac{F_{a(i)}^t}{lb_f}\right|\left|\frac{\mu_i^t}{-}\right|\left|\frac{W_i}{lb}\right|\left|\frac{\theta_i^t}{degree}\right| \tag{3.5}$$

The resistances of a train consists of three principal components, including bearing resistance, rolling resistance, and aerodynamic resistance. The first two resistances purely depend upon the speed and weight of the train, while the third one is affected by the direction and speed of wind as well as the size, shape, and speed of the train. The unit resistance of the i^{th} car at time t, denoted as $R_{u(i)}^t$, can be obtained by the following modified Davis equation as:

$$R_{u(i)}^t = 0.6 + \frac{20}{w_i} + 0.01 \cdot V_i^t + \frac{K_i \cdot (V_r^t)^2}{w_i \cdot n_i} + 20 \cdot G_i^t + 0.8 \cdot D_i^t \tag{3.6}$$

$$\left|\frac{R_{u(i)}^t}{lb_f / ton}\right|\left|\frac{w_i}{ton}\right|\left|\frac{V_i^t}{mph}\right|\left|\frac{V_r^t}{mph}\right|\left|\frac{K_i}{-}\right|\left|\frac{G_i^t}{degree}\right|\left|\frac{D_i^t}{degree}\right|$$

where w_i represents car weight per axle; G_i^t represents grade percentage; D_i^t represents track curvature; and K_i and n_i are the aerodynamic coefficient and the number of axles per car, respectively. Note that V_r^t represents relative train speed based on the direction of wind speed (V_{wd}^t) as shown in Figure 3.1. Thus,

$$V_{r(i)}^t = V_i^t + \cos\theta_{wd(i)}^t \cdot V_{wd(i)}^t \tag{3.7}$$

where $\theta_{wd(i)}^t$ is the angle between the directions of wind and car movement.

The resistance of the i^{th} car at time t, denoted as R_i^t, is the product of unit resistance ($R_{u(i)}^t$), car weight per axle (w_i), number of axles per car (n_i), and number of cars per train (N). Thus,

$$R_i^t = R_{u(i)}^t \cdot w_i \cdot n_i \cdot N \qquad \left|\frac{R_i^t}{lb_f}\right|\left|\frac{R_{u(i)}^t}{lb_f/ton}\right|\left|\frac{w_i}{ton}\right|\left|\frac{n_i}{-}\right|\left|\frac{N}{-}\right| \tag{3.8}$$

The net force to move a car in a train was formulated in Equation 3.1, and is equal to the TE minus the resistance combined with forces resulting from damping and springs. Note that the net force of the i^{th} car at time t divided by the train mass represents acceleration, denoted as a_i^t. Thus,

$$a_i^t = \frac{\left[F_i^t - R_i^t - d_{i-1}(v_i^t - v_{i-1}^t) - d_i(v_i^t - v_{i+1}^t) - k_{i-1}(x_i^t - x_{i-1}^t) - k_i(x_i^t - x_{i+1}^t)\right] \cdot g}{\rho \cdot W_i} \tag{3.9}$$

$$\left|\frac{a_i^t}{ft/sec^2}\right|\left|\frac{W_i}{ton}\right|\left|\frac{F_i^t}{lb_f}\right|\left|\frac{R_i^t}{lb_f}\right|\left|\frac{d_i}{lb\cdot sec/ft}\right|\left|\frac{k_i}{lb/ft}\right|\left|\frac{v_i^t}{ft/sec^2}\right|\left|\frac{x_i^t}{ft}\right|\left|\frac{\rho}{-}\right|\left|\frac{g}{ft/sec^2}\right|$$

where W_i represents the i^{th} car weight, while ρ and g are the coefficients of rotating mass and gravitational acceleration, respectively. The process of calculating train deceleration is similar to that for calculating acceleration, which is determined by actual braking force,

denoted as $F^t_{b(i)}$, the maximum value of comfort-limited braking force, denoted as F_{bc}, and adhesion-limited braking force, denoted as F_{ba}. Thus,

$$F^t_{B[max(i)]} = \max(F^t_{bc(i)}, F^t_{ba(i)}) \qquad \left|\frac{F^t_{B(max)}}{lb_f}\right| \left|\frac{F^t_{bc(i)}}{lb_f}\right| \left|\frac{F^t_{ba(i)}}{lb_f}\right| \tag{3.10}$$

By considering the comfort of standees, F_{bc} is regulated not to exceed a maximum deceleration rate, denoted as b_{max}. According to Equation 3.8, Equation 3.11 can be derived for F_{bc}, in which the maximum rate of acceleration is replaced by the maximum rate of deceleration. Thus,

$$F^t_{bc(i)} = b_{max} W_i / g \cdot \rho + R^t_i \qquad \left|\frac{F^t_{bc(i)}}{lb_f}\right| \left|\frac{b_{max}}{ft/sec^2}\right| \left|\frac{W_i}{ton}\right| \left|\frac{g}{ft/sec^2}\right| \left|\frac{\rho}{-}\right| \left|\frac{R^t_i}{lb_f}\right| \tag{3.11}$$

Unlike $F_{bc(i)}$, $F_{ba(i)}$ is caused by adhesion from the track and the wheel while braking, which has been discussed in presenting Equation 3.5.

The acceleration rate of a train shall not exceed the maximum acceleration rate, denoted as a_{max}, for both safety and passenger comfort concerns. In this regard, the suggested maximum acceleration and deceleration rates are formulated as Equations 3.12 and 3.13, respectively (Hoberock, 1977):

$$a_{max} \le 0.15 \cdot g \qquad \left|\frac{a_{max}}{ft/sec^2}\right| \left|\frac{g}{ft/sec^2}\right| \tag{3.12}$$

$$b_{max} \ge -0.15 \cdot g \qquad \left|\frac{b_{max}}{ft/sec^2}\right| \left|\frac{g}{ft/sec^2}\right| \tag{3.13}$$

Since the TE in the proposed TPS model is calculated based on a user specified time interval, denoted as Δt, a train car's speed and travel distance can be estimated based on the rate of acceleration or deceleration determined in every interval. The increment of train speed, denoted as Δv^t, from t to t+1 is the product of the acceleration rate and the duration of the time interval (Δt in Equation 3.14). The associated travel distance of the i^{th} car, denoted as Δx_i^t, is formulated as Equation 3.15:

$$v_i^{t+1} = v_i^t + \Delta v_i^t = v_i^t + a_i^t \cdot \Delta t \tag{3.14}$$

$$\left|\frac{v_i^{t+1}}{ft/sec}\right| \left|\frac{v_i^t}{ft/sec}\right| \left|\frac{\Delta v_i^t}{ft/sec}\right| \left|\frac{a_i^t}{ft/sec^2}\right| \left|\frac{\Delta t}{sec}\right|$$

$$x_i^{t+1} = x_i^t + \Delta x_i^t = x_i^t + \left(\frac{v_i^t + v_i^{t+1}}{2}\right) \cdot \Delta t \tag{3.15}$$

$$\left|\frac{x_i^{t+1}}{ft}\right| \left|\frac{x_i^t}{ft}\right| \left|\frac{\Delta x_i^t}{ft}\right| \left|\frac{v_i^t}{ft/sec}\right| \left|\frac{v_i^{t+1}}{ft/sec}\right| \left|\frac{\Delta t}{sec}\right|$$

To move the i^{th} car in a train at speed V_i^t, an equation used to calculate the engine power consumed at t, called P_i^t, is derived based on a function discussed by Hay (1982). Thus,

$$P_i^t = \frac{F_i^t \cdot V_i^t}{375 \cdot \eta} \qquad \left|\frac{P_i^t}{hp}\right| \left|\frac{F_i^t}{lb_f}\right| \left|\frac{V_i^t}{mph}\right| \tag{3.16}$$

The energy consumption rate e_i^t required to either propel or brake during Δt can be derived as

$$e_i^t = P_i^t \cdot \Delta t \cdot \left(0.7457 \times \frac{1}{3600}\right) \qquad \left|\frac{e_i^t}{kWh}\right| \left|\frac{P_i^t}{hp}\right| \left|\frac{\Delta t}{sec}\right| \tag{3.17}$$

Note that the unit engine power (hp) is equal to 0.7457 kilowatts (kW), and the time interval (sec) divided by 3,600 is converted to an hourly base. The total energy consumption, denoted as E, over the route segment can be obtained by integrating the power required over time. Thus,

$$E = \sum_{t=1}^{J} e_i^t \qquad \left|\frac{E}{kWh}\right| \left|\frac{e_i^t}{kWh}\right| \tag{3.18}$$

where J is the number of time steps needed for traveling from one station to another.

3.2 Track Alignment Module (TAM)

A vertical track profile is a combination of segments with different grade percentages and transition sections, which need a sag curve and/or a crest curve for smooth connection. Transition rates in grade in 100 ft, denoted as γ, can be estimated by Equation 3.19, and the recommended transition rates by AREA are 0.05 and 0.1 for sag and crest curves, respectively (Hay, 1982).

$$\gamma = \frac{(G_2 - G_1)}{L} \times 100 \qquad \left|\frac{\gamma}{-}\right| \left|\frac{G_2}{\%}\right| \left|\frac{G_1}{\%}\right| \left|\frac{L}{ft}\right| \tag{3.19}$$

where G_1 and G_2 are two adjacent track grades, and L is the horizontal track length.

TAM converts a given vertical track profile into a series of track grades delivered to TTM for calculating train resistances and the TE, which exchanges data (e.g., track grade and train position) in every simulation time step. TAM also provides information (maximum operating speed, denoted as V_M) to the Train Control Module (TCM) so that a proper track alignment can be referred to determine the regime of motion (e.g.,

acceleration, cruising, coasting, and deceleration, etc.). A step procedure summarized below discusses the interaction between TAM and other modules (e.g., TTM and TCM).

- Step 1: Identify the number of inflection points of track alignment and divide the station spacing (S) into a number of segments based on the inflection points.

$$S = \sum_{j=1}^{q} L_j \qquad \left|\frac{S}{ft}\right|\left|\frac{L_j}{ft}\right| \tag{3.20}$$

where q is the total number of segments and j is the segment number in vertical alignment

- Step 2: Develop equations for representing vertical track alignment for segment I identified in Step 1, denoted as $y_j(x^t)$, where x^t is the traveled distance at time t (ft).
- Step 3: Differentiate $y_j(x^t)$ over distance to obtain track grade G_j^t at segment j.

$$G_j^t = \frac{\partial y_j(x^t)}{\partial x^t} \qquad \left|\frac{G_j^t}{\%}\right|\left|\frac{y_j(x^t)}{ft}\right|\left|\frac{x^t}{ft}\right| \tag{3.21}$$

- Step 4: Input G_j^t to TTM and $y_j(x^t)$ to TCM for calculating train resistance and TE and determining the regimes of motion.
- Step 5: Input G_j^t and V_M data to TTM in every time interval and receive travel distance (Δx^t) data from TTM. Note that $\Delta x^t = x^t - x^{t-1}$.

3.3 Train Control Module (TCM)

The responsibility of the Train Control Module (TCM) is to determine the appropriate motion regime based on TE and track alignment information computed by TTM and TAM. TCM will first generate feasible plans formed by different motion regimes. As shown in Figure 4, a general train control, denoted as TC, consisting of accelerating (M_a), first coasting (M_{c_1}), cruising (M_v), second coasting (M_{c_2}), and braking (M_b) is developed for discussing feasible plans. Note that the relationship between speed and time is not necessarily linear.

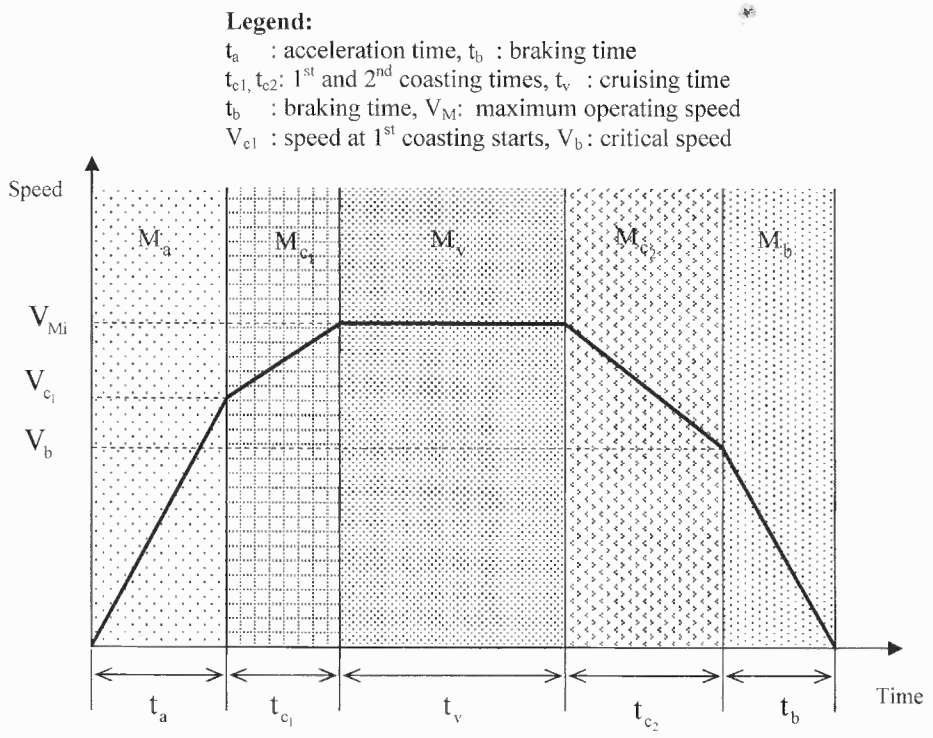

Figure 3.3 Configuration of a speed profile for a general train control on SVA.

While M_a and M_b are always essential for accelerating and decelerating a train departing from and arriving at a station, three other motion regimes (M_{c_1}, M_v, and M_{c_2})

are optional and can be integrated with M_a and M_b. For instance, if the durations for the 1st and 2nd coasting regimes are equal to zero ($t_{c_1} = t_{c_2} = 0$), the resulting train control only consists of accelerating, cruising, and braking regimes. However, if the durations for the 1st coasting and cruising are equal to zero ($t_{c_1} = t_v = 0$), the resulting train control consists of accelerating, coasting, and braking. It is considered that coasting is usually a beneficial motion regime for rail operators because it may save considerable energy; however a longer travel time between stations should be expected.

Considering various track alignments (level, convex, and concave) and applicable motion regimes, the feasible train controls for each alignment are summarized in Table 3.1. It is worth noting that the applied train controls in the developed TPS are not necessarily limited to the train controls below.

- Train Control 1 (TC1): Considering cruising regime (M_v) associated with M_a and M_b
- Train Control 2 (TC2): Considering cruising and both coasting regimes (e.g., M_{c_1} and/or M_{c_2}) associated with M_a and M_b
- Train Control 3 (TC3): Considering coasting regimes (e.g., M_{c_1} and/or M_{c_2}) associated with M_a and M_b

Table 3.1 Feasible Train Controls

Track Alignment	Train Controls and Motion Regimes
Level	(1) $TC_1^L = M_a + M_v + M_b$
	(2) $TC_2^L = M_a + M_v + M_{c_2} + M_b$
	(3) $TC_3^L = M_a + M_{c_2} + M_b$
Convex	(1) $TC_1^U = M_a + M_v + M_b$
	(2) $TC_2^U = M_a + M_{c_1} + M_v + M_{c_2} + M_b$
	(3) $TC_3^U = M_a + M_{c_1} + M_{c_2} + M_b$
Concave	(1) $TC_1^D = M_a + M_v + M_b$
	(2) $TC_2^D = M_a + M_{c_1} + M_v + M_b$
	(3) $TC_3^D = M_a + M_{c_1} + M_b$

While a general train control consists of the five motion regimes as $M_a, M_{c_1}, M_v, M_{c_2}$, and M_b, the station-to-station travel time denoted as T (excluding dwell time at stations) can be formulated as

$$T = t_a + t_{c_1} + t_v + t_{c_2} + t_b \qquad \left|\frac{T}{sec}\right|\left|\frac{t_a}{sec}\right|\left|\frac{t_{c_1}}{sec}\right|\left|\frac{t_v}{sec}\right|\left|\frac{t_{c_2}}{sec}\right|\left|\frac{t_b}{sec}\right| \qquad (3.22)$$

where t_a, t_{c_1}, t_v, t_{c_2}, and t_b represent travel times (sec) for acceleration, the 1st coasting, cruising, the 2nd coasting, and braking, respectively, which can be calculated with Equations 3.23 to 3.27 formulated as

$$t_a = \frac{1.47 \cdot V_{c_1}}{\bar{a}} \qquad \left|\frac{t_a}{sec}\right|\left|\frac{V_{c_1}}{mph}\right|\left|\frac{\bar{a}}{ft/sec^2}\right| \qquad (3.23)$$

$$t_{c_1} = \frac{1.47\left(V_M - V_{c_1}\right)}{\bar{c}_1} \qquad \left|\frac{t_{c_1}}{sec}\right|\left|\frac{V_M}{mph}\right|\left|\frac{V_{c_1}}{mph}\right|\left|\frac{\bar{c}_1}{ft/sec^2}\right| \qquad (3.24)$$

$$t_v = \frac{S_v}{1.47 \cdot V_{M_u}} \qquad \left|\frac{t_v}{\text{sec}}\right|\left|\frac{S_v}{\text{ft}}\right|\left|\frac{V_M}{\text{mph}}\right| \tag{3.25}$$

$$t_{c_2} = \frac{V_M - V_b}{\bar{c}_2} \qquad \left|\frac{t_{c_2}}{\text{sec}}\right|\left|\frac{V_M}{\text{mph}}\right|\left|\frac{V_b}{\text{mph}}\right|\left|\frac{\bar{c}_2}{\text{ft/sec}^2}\right| \tag{3.26}$$

$$t_b = \frac{V_b}{\bar{b}} \qquad \left|\frac{t_b}{\text{sec}}\right|\left|\frac{V_b}{\text{mph}}\right|\left|\frac{\bar{b}}{\text{ft/sec}^2}\right| \tag{3.27}$$

where 1.47 is a parameter to convert the speed from mph to feet per second (ft/sec). Note that $\bar{a}$, $\bar{c}_1$, $\bar{c}_2$, and $\bar{b}$ represent the average speed change rate (ft/sec^2) of acceleration, the 1st coasting acceleration, the 2nd coasting deceleration, and deceleration, while V_{c_1} and V_b are the speed where the 1st coasting begins and critical speed at which where the maximum deceleration must be applied. In Eq. 3.25, S_v represents the distance consumed for vehicle cruising. Thus, the station-to-station travel time can be derived as:

$$T = \frac{1.47V_{c_1}}{\bar{a}} + \frac{1.47\left(V_M - V_{c_1}\right)}{\bar{c}_1} + \frac{S_v}{1.47V_{M_u}} + \frac{1.47\left(V_M - V_b\right)}{\bar{c}_2} + \frac{1.47V_b}{\bar{b}} \tag{3.28}$$

$$\left|\frac{T}{\text{sec}}\right|\left|\frac{V_{c_1}}{\text{mph}}\right|\left|\frac{V_M}{\text{mph}}\right|\left|\frac{V_b}{\text{mph}}\right|\left|\frac{\bar{a}}{\text{ft/sec}^2}\right|\left|\frac{\bar{c}_1}{\text{ft/sec}^2}\right|\left|\frac{\bar{b}}{\text{ft/sec}^2}\right|$$

As the travel time for each regime is known, the station spacing (S) is set equal to the sum of the distances traveled under all motion regimes. Thus,

$$S_a = \frac{1}{2}\bar{a}t_a^2 \qquad \left|\frac{S_a}{\text{ft}}\right|\left|\frac{\bar{a}}{\text{ft/sec}^2}\right|\left|\frac{t_a}{\text{sec}}\right| \tag{3.29}$$

$$S_{c_1} = \frac{1.47}{2}(V_M + V_{c_1})t_{c_1} \qquad \left|\frac{S_{c_1}}{ft}\right|\left|\frac{V_M}{mph}\right|\left|\frac{V_{c_1}}{mph}\right|\left|\frac{t_{c_1}}{sec}\right| \tag{3.30}$$

$$S_v = 1.47 \cdot V_M \cdot t_v \qquad \left|\frac{S_v}{ft}\right|\left|\frac{V_M}{mph}\right|\left|\frac{t_v}{sec}\right| \tag{3.31}$$

$$S_{c_2} = \frac{1.47}{2}(V_M + V_{c_2})t_{c_2} \qquad \left|\frac{S_{c_2}}{ft}\right|\left|\frac{V_M}{mph}\right|\left|\frac{V_{c_2}}{mph}\right|\left|\frac{t_{c_2}}{sec}\right| \tag{3.32}$$

$$S_b = \frac{1}{2}\bar{b}t_b^2 \qquad \left|\frac{S_b}{ft}\right|\left|\frac{\bar{b}}{ft/sec^2}\right|\left|\frac{t_b}{sec}\right| \tag{3.33}$$

where S_a, S_{c_1}, S_{c_2}, and S_b represent the travel distances (ft) for acceleration, the 1st coasting, the 2nd coasting, and deceleration, respectively. Thus, the station spacing denoted as S can be derived as:

$$S = 1.47\left(\frac{V_{c_1}^2}{2\bar{a}} + \frac{V_M^2 - V_{c_1}^2}{2\bar{c_1}} + V_M \cdot t_v + \frac{V_M^2 - V_b^2}{2\bar{c_2}} + \frac{V_b^2}{2\bar{b}}\right) \tag{3.34}$$

$$\left|\frac{V_{c_1}}{mph}\right|\left|\frac{V_M}{mph}\right|\left|\frac{V_b}{mph}\right|\left|\frac{\bar{a}}{ft/s^2}\right|\left|\frac{\bar{c_1}}{ft/s^2}\right|\left|\frac{\bar{c_2}}{ft/s^2}\right|\left|\frac{\bar{b}}{ft/s^2}\right|\left|\frac{t_v}{ft/s^2}\right|$$

To derive the cruising time (t_v), the difference of station spacing and the distances traveled during the regimes of acceleration, the 1st coasting, the 2nd coasting, deceleration is divided by V_{Mi}.

$$t_v = \frac{S - (S_a + S_{c_1} + S_{c_2} + S_b)}{1.47 \cdot V_M} \qquad \left|\frac{t_v}{sec}\right|\left|\frac{S}{ft}\right|\left|\frac{S_a}{ft}\right|\left|\frac{S_{c_1}}{ft}\right|\left|\frac{S_{c_2}}{ft}\right|\left|\frac{S_b}{ft}\right|\left|\frac{V_M}{mph}\right| \tag{3.35}$$

With Equations 3.34 and 3.35, the cruising time can be defined as:

$$t_v = \frac{S}{V_M} - \frac{V_M}{2}\left(\frac{1}{\bar{c}_1} + \frac{1}{\bar{c}_2}\right) - \frac{V_{c_1}^2}{2V_M}\left(\frac{1}{\bar{a}} - \frac{1}{\bar{c}_1}\right) - \frac{V_b^2}{2V_M}\left(\frac{1}{\bar{b}} - \frac{1}{\bar{c}_2}\right) \qquad (3.36)$$

$$\left|\frac{t_v}{sec}\right|\left|\frac{S}{ft}\right|\left|\frac{V_M}{mph}\right|\left|\frac{\bar{c}_1}{ft/s^2}\right|\left|\frac{\bar{c}_2}{ft/s^2}\right|\left|\frac{V_{c_1}}{mph}\right|\left|\frac{\bar{a}}{ft/s^2}\right|\left|\frac{V_b}{mph}\right|\left|\frac{\bar{b}}{ft/s^2}\right|$$

The three modules in the proposed TPS model simulate train movement every second on an iterative basis. A complete cycle of the proposed TPS calculation in each time interval is shown in Figure 3.4, and the step procedure is discussed below.

- Step 1. Start the simulation and feed input data (e.g., motor power, car weight per axle, number of car, number off axle) to TTM and TAM.
- Step 2. Calculate TE, train resistances, and speed at time t with TTM.
- Step 3. Determine train control (e.g., TC_1, TC_2, and TC_3) and check if the 1st coasting (M_{c_1}) can be applied at time t (e.g., $V^t \geq V_{c_1}$) with TCM.
- Step 4. If $V^t \geq V_M$ in TTM, go to Step 6. Otherwise, calculate traveled distance and consumed energy for acceleration, and update simulation clock (i.e., t = t+1), then go to Step 2.
- Step 5. Determine motion regime (e.g., M_v, M_{c_2}, and $M_v + M_{c_2}$) with TCM.
- Step 6. If the remaining distance (RD) is less than the stopping distance (SD), decelerate the train, calculate consumed braking energy in TTM, update the simulation clock, and then go to Step 7. Otherwise, go to Step 2.

- Step 7. If the train arrives at the station, end simulation clock, report consumed travel time and energy, and terminate the simulation. Otherwise, go to Step 6.

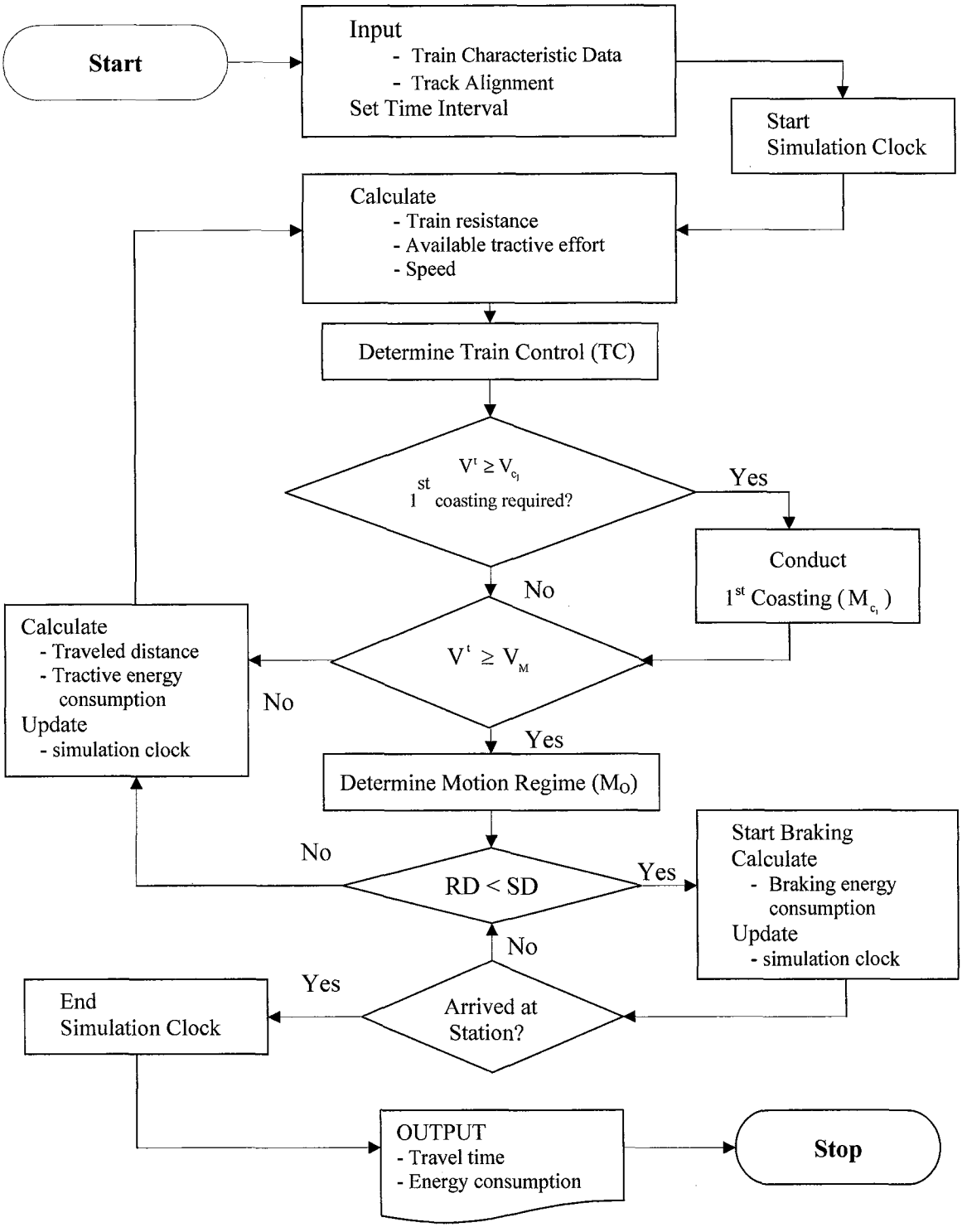

Figure 3.4 Flow chart of the train performance simulation model.

CHAPTER 4

METHODOLOGY

The objective function (i.e., total energy consumption) for the four cases discussed in Chapter 1 is formulated in this chapter. The objective total energy consumption function is affected by various factors such as train control between a pair of stations, the topology of track alignment and schedule adherence. A set of system assumptions is made to formulate the research problem for each case and the associated constraints, which are discussed in Sections 4.1 through 4.4 for Cases I through IV, respectively. The developed models are based on the different vertical track alignments such as single vertical alignment (SVA) and mixed vertical alignment (MVA) associated with fixed and variable maximum operating speed (MOS) over the route. The optimal solutions for the cases are obtained considering the appropriate train control as well as the scheduled travel time.

4.1 Model I - SVA and Constant MOS (Case I)

The model formulated in Case I is designed to optimize train control over a SVA combined with a constant MOS. To formulate the model, system assumptions on the geometry of track (i.e., vertical track alignment), train control (i.e., applied motion regime), and train characteristics (e.g., tractive effort (TE), resistance, acceleration/ deceleration rate, train movement calculation, etc.) are made.

4.1.1 Assumptions

To formulate the research problem discussed in Case I, a list of assumptions is made and discussed below:

1. A generalized vertical rail alignment, which may be symmetric and parabolic, connecting stations A and B as shown in Figure 4.1 can be classified into three types (level, convex, and concave) of track alignments. It is worth noting that the "level" alignment indicates a tangent curve with zero grade. Note that the terms "convex" and "concave" alignments used in this study consist of "crest" and "sag" curves, respectively, with both ascending and descending grades. To obtain a continuous vertical track profile and associated track gradient, a general track alignment which is a function of station spacing (S), inflection points (I_p), and vertical depth/ height (δ) at halfway between two stations is assumed as:

$$y_1(x^t) = -\frac{12\delta}{S^2}(x^t)^2, \qquad G_1^t = \frac{\partial y_1(x^t)}{\partial x} = -\frac{24\delta}{S^2}x^t \qquad \text{for} \quad \Delta_1 \quad (4.1)$$

$$y_2(x^t) = \frac{6\delta}{S^2}(x^t)^2 - \frac{6\delta}{S}(x^t) + \frac{\delta}{2}, \qquad G_2^t = \frac{\partial y_2(x^t)}{\partial x} = \frac{12\delta}{S^2}x^t - \frac{6\delta}{S} \qquad \text{for} \quad \Delta_2 \quad (4.2)$$

$$y_3(x^t) = -\frac{12\delta}{S^2}(x^t)^2 + \frac{24\delta}{S}(x^t) - 12\delta, \qquad G_3^t = \frac{\partial y_3(x^t)}{\partial x} = -\frac{24\delta}{S^2}x^t + \frac{24\delta}{S} \qquad \text{for} \quad \Delta_3 \quad (4.3)$$

where $y_1(x^t)$, $y_2(x^t)$, and $y_3(x^t)$ represent elevations with respect to x^t in feet on different segments, while G_i^t is the gradient at x^t in percent, and Δ_1, Δ_2, and Δ_3 are 1/6, 2/3, and 1/6 of S, respectively, as shown in Figure 4.1.

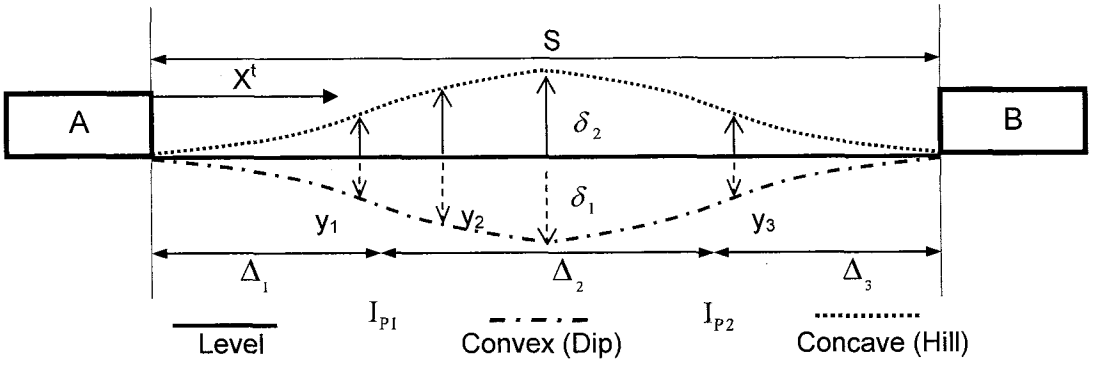

Figure 4.1 Single vertical alignment between stations A and B.

2. The train will use the maximum TE from stand still until it reaches the maximum operating speed (V_M) and the maximum deceleration rate will be used when the remaining distance (RD) is equal to or less than the stopping distance (SD).
3. Four motion regimes are considered, including accelerating, cruising, coasting, and braking. Note that cruising is applied when there is a need.
4. The train movement and its related forces are treated as a string mass on a route. Accordingly, the forces related to train movement, such as TE and resistance, are computed individually for all cars and locomotives.

4.1.2 Model Formulation

The motion of a train can be determined by the difference between the total TE (F_T^t) and resistance (R_T^t), which are directly affected by the train speed and vertical track grade. Thus, F_T^t and R_T^t at time t are functions of speed and vertical track grade represented by f_1 and f_2 respectively , which can be re-formulated as:

$$F_T^t = \sum_{i=1}^{N} F_i^t = f_1(V^t, G^t) \quad \text{for } 1 \le t \le J \qquad \left| \frac{F_T^t}{lb_f} \right| \frac{V^t}{mph} \left| \frac{G^t}{\%} \right| \tag{4.4}$$

$$R_T^t = \sum_{i=1}^{N} R_i^t = f_2(V^t, G^t) \quad \text{for } 1 \le t \le J \qquad \left| \frac{R_T^t}{lb_f} \right| \frac{V^t}{mph} \left| \frac{G^t}{\%} \right| \tag{4.5}$$

where J is the total number of time steps needed for traveling between two stations.

With Equations 4.4 and 4.5, the acceleration rate at time t, denoted as a^t, can be determined by

$$a^t = \frac{f_1(V^t, G^t) - f_2(V^t, G^t)}{\rho \cdot m} \quad \text{for } 1 \le t \le J \qquad \left| \frac{a^t}{ft/sec^2} \right| \frac{V^t}{mph} \left| \frac{G^t}{\%} \right| \left| \frac{\rho}{-} \right| \frac{m}{lb_m} \tag{4.6}$$

where ρ is the coefficient of rotating mass and m is the train mass.

The consumed engine power P^t (also in Equation 3.16) for speed V^t at time step t can be formulated as:

$$P^t = f_1(V^t, G^t) \cdot V^t \quad \text{for } 1 \le t \le J \qquad \left| \frac{P^t}{hp} \right| \left| \frac{V^t}{mph} \right| \left| \frac{G^t}{\%} \right| \tag{4.7}$$

The energy consumption e^t is equal to the product of power used from t to $t+\Delta t$ and the duration of the simulation time step, and can be expressed as:

$$e^t = P^t \cdot \Delta t \cdot \left(0.7457 \times \frac{1}{3600} \right) \quad \text{for } 1 \le t \le J \qquad \left| \frac{e^t}{kWh} \right| \left| \frac{P^t}{hp} \right| \left| \frac{\Delta t}{sec} \right| \tag{4.8}$$

Note that the unit engine power is equal to 0.7457 kilowatts, and the time interval divided by 3,600 is converted to an hourly base. Accordingly, the total consumed energy, denoted as E, for a train movement between stations A and B is the sum of energy used in all time steps:

$$E = \sum_{t=1}^{J} e^t \qquad \left| \frac{E}{kWh} \right| \left| \frac{e^t}{kwh} \right| \tag{4.9}$$

As shown in Equations 4.4 through 4.9, the total energy consumption is directly affected by train speed and vertical track grade. While the track grade is known, the desired train speed can be reached by determining an acceleration rate.

4.1.3 Constraints

The constraints considered in this study include the maximum operating speed, allowable travel time and maximum acceleration/deceleration rates while optimizing train control. The first constraint ensures that the train speed at time t does not exceed the MOS based

on track alignment and operations. Considering a constant maximum operating speed (e.g., fixed MOS) assumed in Case I, Equation 4.10 must hold.

$$V^t \le V_M, \qquad \text{for } 1 \le t \le J \qquad \left|\frac{V^t}{\text{mph}}\right|\left|\frac{V_M}{\text{mph}}\right| \tag{4.10}$$

The second constraint establishes that the range of travel time under optimal train control must be less than or equal to the maximum allowable travel time (e.g., travel time for a train from the upstream station to the downstream station before the scheduled arrival time). The travel time between stations, denoted as T, is ruled by the maximum allowable travel time, denoted as T_M.

$$T \le T_M \qquad \left|\frac{T}{\text{sec}}\right|\left|\frac{T_M}{\text{sec}}\right| \tag{4.11}$$

Note that when a train is already behind schedule, it will use the maximum TE to overtake the scheduled travel time. Three motion regimes including accelerating, cruising, and braking will be used.

The third constraint certifies that the acceleration rate at any time t does not exceed the passenger comfort limit. The maximum acceleration rate, denoted as a_{max}, used in the previous studies (Hoberock, 1977; Martinez et al., 2004; Koo et al., 2006) is $0.15 \cdot g$ (i.e., 4.8 ft/sec^2). Thus,

$$a^t \le \min\left\{a_{max}, \left(\frac{F_T^t - R_T^t}{\rho \cdot m}\right)\right\} \qquad \left|\frac{a^t}{\text{ft/sec}^2}\right|\left|\frac{a_{max}}{\text{ft/sec}^2}\right|\left|\frac{F_T^t}{\text{lb}_f}\right|\left|\frac{R_T^t}{\text{lb}_f}\right|\left|\frac{\rho}{-}\right|\left|\frac{m}{\text{lb}_m}\right| \tag{4.12}$$

4.1.4 Optimization Model

Based on the discussion in Sections 4.1.1 through 4.1.3, the model developed for the research problem in Case I of minimizing total energy consumption considering the effect of train power, track alignment, speed regulation, and schedule adherence is formulated below:

Minimize

$$E = \sum_{t=1}^{J} P^t \cdot \Delta t \qquad \left|\frac{E}{kWh}\right|\left|\frac{P^t}{hp}\right|\left|\frac{\Delta t}{sec}\right|$$

Subject to

$$V^t \le V_M^t, \qquad \text{for } 1 \le t \le J \qquad \left|\frac{V^t}{mph}\right|\left|\frac{V_M^t}{mph}\right|$$

$$T \le T_M \qquad \left|\frac{T}{sec}\right|\left|\frac{T_M}{sec}\right|$$

$$a^t \le \min\left\{a_{max}, \left(\frac{F_T^t - R_T^t}{\rho \cdot m}\right)\right\} \qquad \text{for } 1 \le t \le J \qquad \left|\frac{a^t}{ft/sec^2}\right|\left|\frac{a_{max}}{ft/sec^2}\right|\left|\frac{F_T^t}{lb_f}\right|\left|\frac{R_T^t}{lb_f}\right|\left|\frac{\rho}{-}\right|\left|\frac{m}{lb_m}\right|$$

} Case I

4.2 Model II - SVA and Variable MOS (Case II)

Model II is enhanced from Model I, and minimizes energy consumption considering single vertical alignment (SVA) with a variable MOS. The model assumptions, constraints, and optimization problem for Case II are discussed next.

4.2.1 Assumptions

The assumptions made for formulating the model are the following;

1. The general condition of a single vertical track alignment discussed in Section 4.1.1 is also considered in Case II.
2. The assumption discussed in Section 4.1.1 is also used here. The train uses maximum TE for the initial acceleration until it reaches V_M and maximum deceleration for the final braking to stop at the downstream station.

3. Four motion regimes are considered, including accelerating, cruising, coasting, and braking. Note that the cruising regime is used when there is a need.

4. The movement of the train and its related forces are treated as a string mass on a route. Thus, the forces related to train movement, such as TE and resistance, are computed separately for all cars and locomotives.

The functions for computing train movement and estimating total energy consumption (E) are the same as those used in Case I. The total travel time and acceleration rate constraints considered in Case I can be used in Case II. However, multiple maximum operating speed constraints (i.e., variable MOS) are used in Case II as shown in Figure 4.2, and train speed never exceeds the variable MOS. Thus,

$$V^t \le V^t_{M_u}, \quad u = 1, 2, 3, \ldots, \quad \text{for } 1 \le t \le J, \quad \left| \frac{V^t}{\text{mph}} \right| \left| \frac{V^t_{M_u}}{\text{mph}} \right| \tag{4.13}$$

where u is the index of maximum operating speed used.

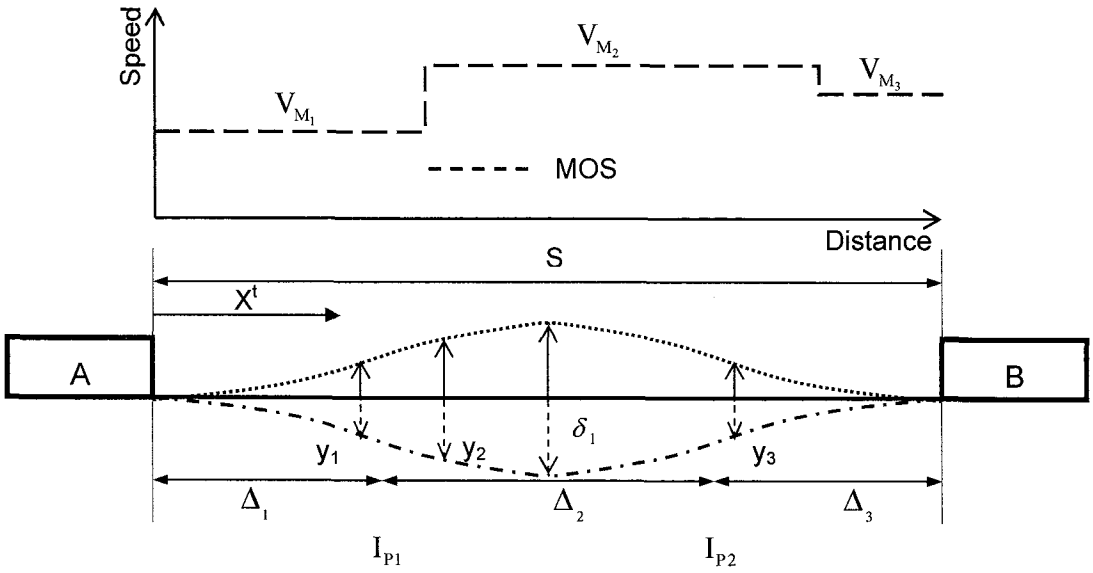

Figure 4.2 Feasible variable MOS profile on SVA in Case II.

4.2.2 Optimization Model

Based on the previous discussion, the studied train control optimization model that minimizes total energy consumption under SVA subject to the variable MOS, the maximum total travel time, and the maximum acceleration rate is the same as discussed in Case I and formulated as follows:

Minimize

$$E = \sum_{t=1}^{J} P^t \cdot \Delta t \qquad \left|\frac{E}{kWh}\right|\left|\frac{P^t}{hp}\right|\left|\frac{\Delta t}{sec}\right|$$

Subject to

$$V^t \le V^t_{M_u}, \quad u=1, 2, 3,.... \quad \text{for } 1 \le t \le J \qquad \left|\frac{V^t}{mph}\right|\left|\frac{V^t_M}{mph}\right|$$

$$T \le T_M \qquad \left|\frac{T}{sec}\right|\left|\frac{T_M}{sec}\right|$$

$$a^t \le \min\left\{a_{max}, \left(\frac{F^t_T - R^t_T}{\rho \cdot m}\right)\right\} \quad \text{for } 1 \le t \le J \qquad \left|\frac{a^t}{ft/sec^2}\right|\left|\frac{a_{max}}{ft/sec^2}\right|\left|\frac{F^t_T}{lb_f}\right|\left|\frac{R^t_T}{lb_f}\right|\left|\frac{\rho}{-}\right|\left|\frac{m}{lb_m}\right|$$

} Case II

4.3 Model III - MVA and Constant MOS (Case III)

The model developed in Case III is enhanced from Model I developed in Case I, and minimizes energy consumption for a train running on a mixed vertical alignment (MVA) with a constant MOS. Other than track alignment, all assumptions made for Case I are used in Case III.

4.3.1 Assumptions

Model III is developed to optimize train control over a mixed vertical curve with constant MOS. The following assumptions are made:

1. A mixed vertical alignment that connects stations A and B is considered in Case III. The alignment may be asymmetric, and may consist of seven types of track curves, including ascending crest, descending crest, ascending sag, descending sag, ascending tangent, descending tangent, and flat tangent as shown in Figure 4.3. A continuous vertical track profile and associated track gradient may be achieved by formulating a general track alignment which is a function of horizontal track segment distance and vertical depth/height at two consecutive inflection points (I_p):

$$y_1(x^t) = 0, \qquad G_1^t = \frac{\partial y_1(x^t)}{\partial x} = 0 \qquad \text{for} \quad \Delta_1 \quad (4.14)$$

$$y_2(x^t) = -\frac{12\delta_1}{S_1^2}(x^t - \Delta_1)^2, \qquad G_2^t = \frac{\partial y_2(x^t)}{\partial x} = -\frac{24\delta_1}{S_1^2}(x^t - \Delta_1) \quad \text{for } \Delta_2 \quad (4.15)$$

$$y_3(x^t) = \frac{6\delta_1}{S_1^2}\left[x^t - \left(\frac{S_1}{2} + \Delta_1\right)\right]^2 - \delta_1, \quad G_3^t = \frac{\partial y_3(x^t)}{\partial x} = \frac{12\delta_1}{S_1^2}\left[x^t - \left(\frac{S_1}{2} + \Delta_1\right)\right] \quad \text{for } \Delta_3 \quad (4.16)$$

$$y_4(x^t) = 0, \qquad G_4^t = \frac{\partial y_4(x^t)}{\partial x} = 0 \qquad \text{for } \Delta_4 \quad (4.17)$$

$$y_5(x^t) = \frac{6\delta_2}{S_2^2}\left[x^t - \sum_{j=1}^{4}\Delta_j\right]^2 - (\delta_2 + 2.5), \quad G_5^t = \frac{\partial y_5(x^t)}{\partial x} = \frac{12\delta_2}{S_2^2}\left[x^t - \sum_{j=1}^{4}\Delta_j\right] \quad \text{for } \Delta_5 \quad (4.18)$$

$$y_6(x^t) = -\frac{12\delta_2}{S_2^2}\left[x^t - \sum_{j=1}^{5}\Delta_j\right]^2 - \delta_2, \quad G_6^t = \frac{\partial y_6(x^t)}{\partial x} = -\frac{24\delta_2}{S_2^2}\left[x^t - \sum_{j=1}^{5}\Delta_j\right] \quad \text{for } \Delta_6 \quad (4.19)$$

$$y_7(x^t) = -\delta_2, \qquad G_7^t = \frac{\partial y_7(x^t)}{\partial x} = 0 \qquad \text{for } \Delta_7 \quad (4.20)$$

where $y_1(x^t)$ through $y_7(x^t)$ represent elevations with respect to x^t in feet on different segments, while G_j^t is the gradient at x^t in percent for Δ_1 through Δ_7. Note that the MVA used for Case III is not necessarily the same as that in Figure 4.3.

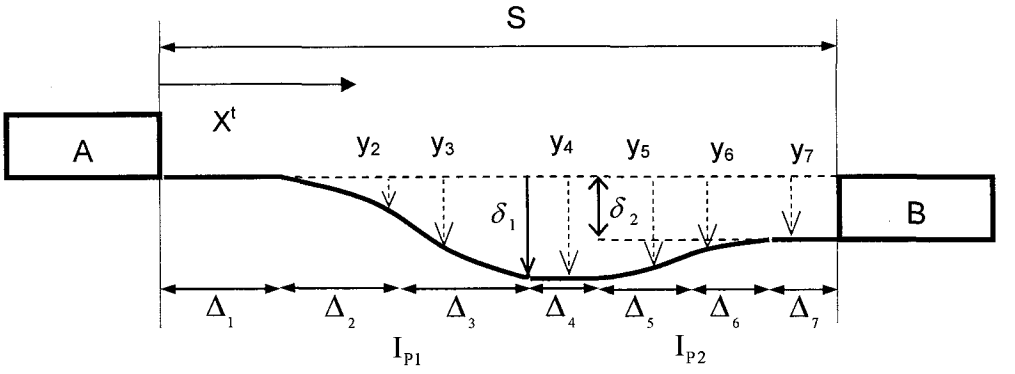

Figure 4.3 Feasible mixed vertical alignment between stations A and B.

2. As discussed in Section 4.1.1, a train uses the maximum TE for the initial acceleration until it reaches V_M and then maximum deceleration is used for the final braking to stop at the downstream station.

3. Four motion regimes are considered, including accelerating, cruising, coasting, and braking. Note that cruising is used when there is a need.

4. The train movement and its related forces are treated as a string mass on a route. Thus, the forces related to train movement, such as TE and resistance, are computed separately for all cars and locomotives.

The functions for estimating train movement and energy consumption (E) are the same as those developed for Cases I and II. The train speed, total travel time, and acceleration rate constraints considered in Case III are the same as those used in Case I.

4.3.2 Optimization Model

Based on the discussion in Section 4.3.1, the studied train control optimization problem that minimized total energy consumption under MVA combined with the constant MOS is formulated as follows:

Minimize

$$E = \sum_{t=1}^{J} P^t \cdot \Delta t \qquad \left|\frac{E}{kWh}\right|\left|\frac{P^t}{hp}\right|\left|\frac{\Delta t}{sec}\right|$$

Subject to

$$V^t \le V_M^t, \qquad \text{for } 1 \le t \le J \qquad \left|\frac{V^t}{mph}\right|\left|\frac{V_M^t}{mph}\right|$$

$$T \le T_M \qquad \left|\frac{T}{sec}\right|\left|\frac{T_M}{sec}\right|$$

$$a^t \le \min\left\{a_{max}, \left(\frac{F_T^t - R_T^t}{\rho \cdot m}\right)\right\} \qquad \text{for } 1 \le t \le J \qquad \left|\frac{a^t}{ft/sec^2}\right|\left|\frac{a_{max}}{ft/sec^2}\right|\left|\frac{F_T^t}{lb_f}\right|\left|\frac{R_T^t}{lb_f}\right|\left|\frac{\rho}{-}\right|\left|\frac{m}{lb_m}\right|$$

} Case III

4.4 MVA and Variable MOS (Case IV)

The model in Case IV considers mixed vertical alignment, which is used in Case III, combined with variable MOS to optimize train control for minimum train energy consumption. The assumptions, constraints, and optimization problem for Case IV are discussed next.

4.4.1 Assumptions

The Case IV model considers mixed vertical alignments with a variable maximum operating speed. The assumptions made for formulating the model are as follows:

1. The track alignment considered in Case IV is the same as discussed in Section 4.3.1.

2. The train acceleration for the initial acceleration and the final braking is the same as discussed in Section 4.1.1.

3. The motion regimes are the same as discussed in Section 4.1.1, including accelerating, cruising, coasting, and braking. Note that cruising is used when there is a need.

4. The train movement and its related forces are treated as a string mass on a route.

The functions for train motion and total energy consumption (E) are the same as those used in Cases I, II, and III. The constraints for the maximum operating speed, total travel time, and the maximum acceleration rate in Case IV are same as those in Case II. Thus, multiple MOS constraints (e.g., variable MOS) as shown in Figure 4.4 are used in Case IV. Note that the used MOS and MVA for Case IV are not necessarily the same as those shown in Figure 4.4.

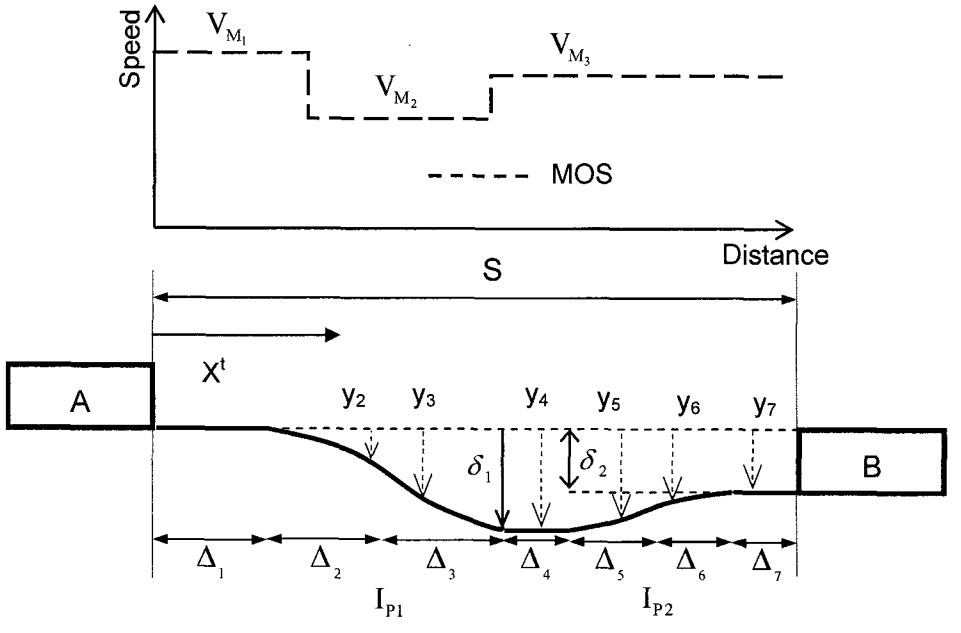

Figure 4.4 Feasible variable MOS profile under MVA in Case IV.

4.4.2 Optimization Model

Based on the discussion from Section 4.4.1, the studied train control optimization model that minimizes total energy consumption under MVA subject to the variable maximum operating speed, the maximum total travel time, and the maximum acceleration rate is formulated as follows:

Minimize

$$E = \sum_{t=1}^{J} P^t \cdot \Delta t \qquad \left|\frac{E}{kWh}\right|\left|\frac{P^t}{hp}\right|\left|\frac{\Delta t}{sec}\right|$$

Subject to

$$V^t \le V^t_{M_u}, \quad u=1, 2, 3,.... \quad \text{for } 1 \le t \le J \qquad \left|\frac{V^t}{mph}\right|\left|\frac{V^t_M}{mph}\right|$$

$$T \le T_M \qquad \left|\frac{T}{sec}\right|\left|\frac{T_M}{sec}\right|$$

$$a^t \le \min\left\{a_{max}, \left(\frac{F^t_T - R^t_T}{\rho \cdot m}\right)\right\} \quad \text{for } 1 \le t \le J \qquad \left|\frac{a^t}{ft/sec^2}\right|\left|\frac{a_{max}}{ft/sec^2}\right|\left|\frac{F^t_T}{lb_f}\right|\left|\frac{R^t_T}{lb_f}\right|\left|\frac{\rho}{-}\right|\left|\frac{m}{lb_m}\right|$$

} Case IV

4.5 Summary

In this chapter, the objective total energy consumption functions and sets of constraints for Case I through IV were formulated. The developed optimization models are based on the assumptions and constraints, which are determined based on the type of track alignments and the number of maximum operating speed. The decision variables used in each model are motion regimes (e.g., acceleration, cruising, coasting, and braking). While considering the given track alignment and speed constraint in Cases I through IV, the optimization model can be solved by using the SA algorithm to minimize total energy consumption.

CHAPTER 5

SOLUTION METHODS

As discussed previously in Chapter 4, the objective of this study is to develop models to optimize train control that minimizes energy consumption under Cases I through IV. The decision variables to be optimized include the timings, durations, and locations of the motion regimes and the rates of acceleration and deceleration.

The train control problem discussed in this study is a combinatorial optimization problem. The timings and locations of motion regimes and acceleration (or deceleration) increase as the complexity of track alignment, the number of feasible motion regimes and speed constraints increase. A meta-heuristic algorithm, called Simulated Annealing Algorithm (SA), is developed and used to search for the optimal solution. Furthermore, a number of train controls are developed and discussed by considering train speed and schedule adherence constraints in Cases I through IV.

5.1 SVA with Constant MOS (Case I)

5.1.1 Train Control

A set of train control profiles consisting of combinations of motion regimes must be established and used to regulate train movement. As discussed in Section 4.1, a single vertical alignment (SVA) associated with a constant maximum operating speed (MOS) is considered in Case I. With these conditions, a general 4-regime train control illustrated in Figure 5.1 is used to minimize energy consumption with SA. The used train control

profile consists of four motion regimes, including acceleration, cruising, coasting, and braking.

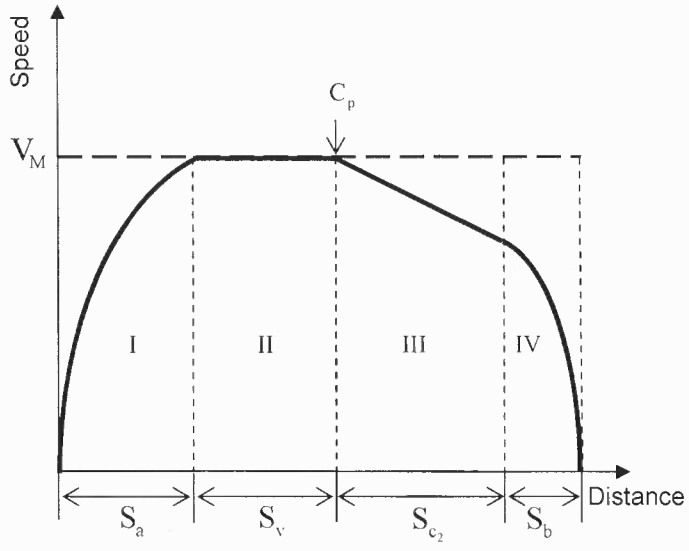

(a) Typical Train Control

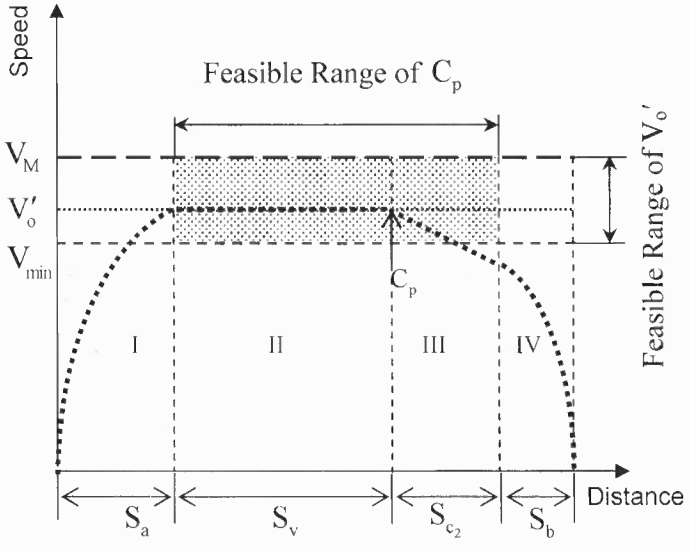

(b) Proposed Train Control

Figure 5.1 Train control with four motion regimes.

The energy consumed in Case I is essentially affected by the timings and durations of individual motion regimes, which will be optimized through the minimization of energy consumption

In general, if the schedule allows and/or a sufficient momentum exists, a coasting regime may be triggered before a train reaches the MOS (see Figure 5.1). As the speed for coasting (or cruising), denoted as V_o' is found, the timing and position to hit V_o' is a reference to change the motion regime from acceleration to coasting (or cruising). Unless the coasting regime is commenced with speed of V_o', a cruising regime is used to maintain the speed V_o'. In case a cruising speed V_o' is used, the timing and location for the coasting must be identified. As shown in Figure 5.1(b), an optimal V_o' is found between V_M and V_{min}. Note that the V_{min} can be determined with the given maximum allowable travel time. In addition, a feasible location for coasting, denoted as C_p, may be found between the times when the regime of acceleration ends and deceleration starts. The feasible ranges for V_o' and C_p are affected by various factors, including station spacing, track alignment, scheduled travel time, acceleration (or deceleration) rate, etc. Note that, if a coasting regime is triggered too early, re-acceleration is needed and more energy will be consumed.

5.1.2 SA for Case I

The energy consumption minimization problem of Case I is a large combinatorial optimization problem where the solution space consists of combinations of multiple decision variables, including the timings, locations, and durations of motion regimes, and the rates of acceleration and deceleration.

As discussed in the literature review, a stochastic computational technique derived from statistical mechanics such as SA can be used to search for near optimum solutions for large optimization problems. It was originally developed by Metropolis et al. (1953) to simulate on a computer the annealing process of crystals. Kirkpatrick et al. (1983) adapted this methodology into an algorithm exploiting the analogy between annealing solids and solving combinatorial optimization problems. The simulated annealing search process attempts to avoid becoming trapped at a local optimum by using a stochastic computational technique, and thus globally or near globally optimal solutions may be found.

The procedure of the proposed SA algorithm can be presented in pseudo-code as shown in Table 5.1. Kirkpatrick et al. (1983) generalized an approach by introducing a multi-temperature approach in which the temperature is lowered slowly in stages. The outer loop (i.e., While^{1}... End^{1}) in Table 5.1 indicates that the temperature (T^{temp}) is lowered by updating T^{temp} in each outer loop until T^{temp} is less than or equal to zero. The inner loop (i.e., While^{2}... End^{2}) indicates that at each temperature the system repeats searching for a lower energy state until the system reaches equilibrium. A system in thermal equilibrium at temperature (T^{temp}) has a probabilistically distributed energy, according to the Boltzmann probability distribution as shown in Equation 5.1.

Table 5.1 Simulated Annealing Algorithm

Begin Anneal
$S' = S'_0$ (Initial solution)
$T^{temp} = T_0^{temp}$ (Initial temperature)
While[1] $T^{temp} > 0$
While[2] (not yet in equilibrium)
S' = random neighboring solution
$\Delta E = E(S'_n) - E(S'_o)$
If $\Delta E \leq 0$, then $S'_\omega = S'_{\omega+1}$
$$P_{\Delta E} = \exp\left(\frac{-\Delta E}{k_B T^{temp}}\right)$$
If random(1,0) $\leq P_{\Delta E}$, then $S'_\omega = S'_{\omega+1}$
End[2]
Update T
End[1]
Output optimal solution
End

Outer Loop — *Inner Loop*

Source: Chen (2003)

$$P_{\Delta E} = \exp\left(\frac{-\Delta E}{k_B T^{temp}}\right) \qquad \left|\frac{\Delta E}{kWh}\right| \left|\frac{T^{temp}}{-}\right| \left|\frac{k_B}{-}\right| \tag{5.1}$$

where k_B is Boltzmann's constant (Metropolis, 1953). At each temperature a neighboring solution (S') is chosen at random and the energy change (total energy consumption), ΔE, is computed, where $\Delta E = E(S'_{\omega+1}) - E(S'_\omega)$. Note that ω is an iteration index in the optimization procedure. Thus, $E(S'_{\omega+1})$ is the energy consumption of the new neighboring solution, and $E(S'_\omega)$ is the energy consumption of the previous solution. If $\Delta E \leq 0$, the new solution is accepted. However, if $\Delta E > 0$, the decision to accept the solution is based on the probability obtained from Equation 5.1. A random number evenly distributed between 0 and 1 is chosen. If the number is smaller than $P_{\Delta E}$, then the new solution is accepted; otherwise, it is discarded, and the old solution is used to generate the next

solution. Note that the simulated annealing procedure allows occasional "uphill moves" that have higher energy (i.e., energy consumption) than the current solution in order to avoid getting trapped at a locally optimal solution. These uphill moves are controlled probabilistically by the temperature (T^{temp}) and become decreasingly likely toward the end of the process as T^{temp} decreases (Press et al., 1988).

Five major components discussed below are necessary to use SA for the energy consumption optimization problem in Case I:

- *State Space*: a suitable domain of decision variables (e.g., feasible boundaries of V_o' and C_p) where the optimum can be sought. In general, state space in SA is often expressed in the form of a constraint equation.
- *Fitness Function (or Objective Function)*: a scalar equation that weighs all of decision variables to provide a measure of the solution goodness at each state. For the minimization problem researched in this study, the solution achieving less energy consumption is identified as a better solution.
- *Perturbation*: a generation rule for new state, which is usually obtained by defining the neighborhood of each state and choosing the next state randomly from the neighborhood of the current one.
- *Acceptance Criteria*: when the new solution provides a better fitness function value, then it is accepted, otherwise it is accepted with a probability in Equation 5.1, or otherwise rejected.
- *Cooling Schedule*: the cooling process in SA starts with an initial control parameter (T_0^{temp}), called temperature. The temperature in SA is cooled with the schedule shown in Equation 5.2.

$$T_0^{temp} \geq T_1^{temp} \ldots \geq T_\omega^{temp} \geq 0 \qquad \left| \frac{T_\omega^{temp}}{-} \right| \qquad (5.2)$$

where ω is the iteration number index in the optimization. Note that if the annealing process is not terminated, the temperature will be decreased to zero. The cooling schedule of the developed SA is discussed in Section 5.1.4.

The implementation of the basic SA algorithm is straightforward as shown in Figure 5.2. The following steps describe the SA algorithm procedure developed for the optimal train control problem.

- Step 0: Set initial parameters: the number of trials at one temperature, initial temperature (T_0^{temp}), temperature change interval, and other parameters. Note that T^{temp} is a control parameter in SA, which should be decreased slowly to ensure that the optimal solution is achieved.
- Step 1: Determine the initial configuration, Set $\omega=0$. Select the starting decision variables [i.e., maximum operating speed (V_0') and coasting position (C_p)] as the initial solution.
- Step 2: Evaluate the energy consumption of the initial solution.
- Step 3: Perturb the initial solution to obtain a new (e.g., neighborhood) solution, Set $\omega=\omega+1$. Update the alternatives of the initial solution.
- Step 4: Evaluate the new solution. Calculate the total energy consumption of the alternatives.
- Step 5: Determine whether to accept the new solution

  Step 5.1: calculate ΔE

Step5.2: if $\Delta E \leq 0$, then accept the new solution, otherwise if $\exp\left(\frac{-\Delta E}{k_B T^{temp}}\right)$>random [0,1), then accept the new solution, if not, go to Step 3

- Step 6: Reduce the system temperature according to the cooling schedule, $T_{\omega}^{temp} = T_0^{temp} \cdot \alpha^{\omega}$ (ω =1,2,3....). Note that α is cooling factor between 0.8 and 0.99.
- Step 7: If $T_{\omega}^{temp} < T_{min}^{temp}$, then terminate the SA process and output the optimized solutions. Otherwise, repeat Step 3 through Step 6 until the stopping criterion is met, or a pre-specified maximum number of iterations is performed.

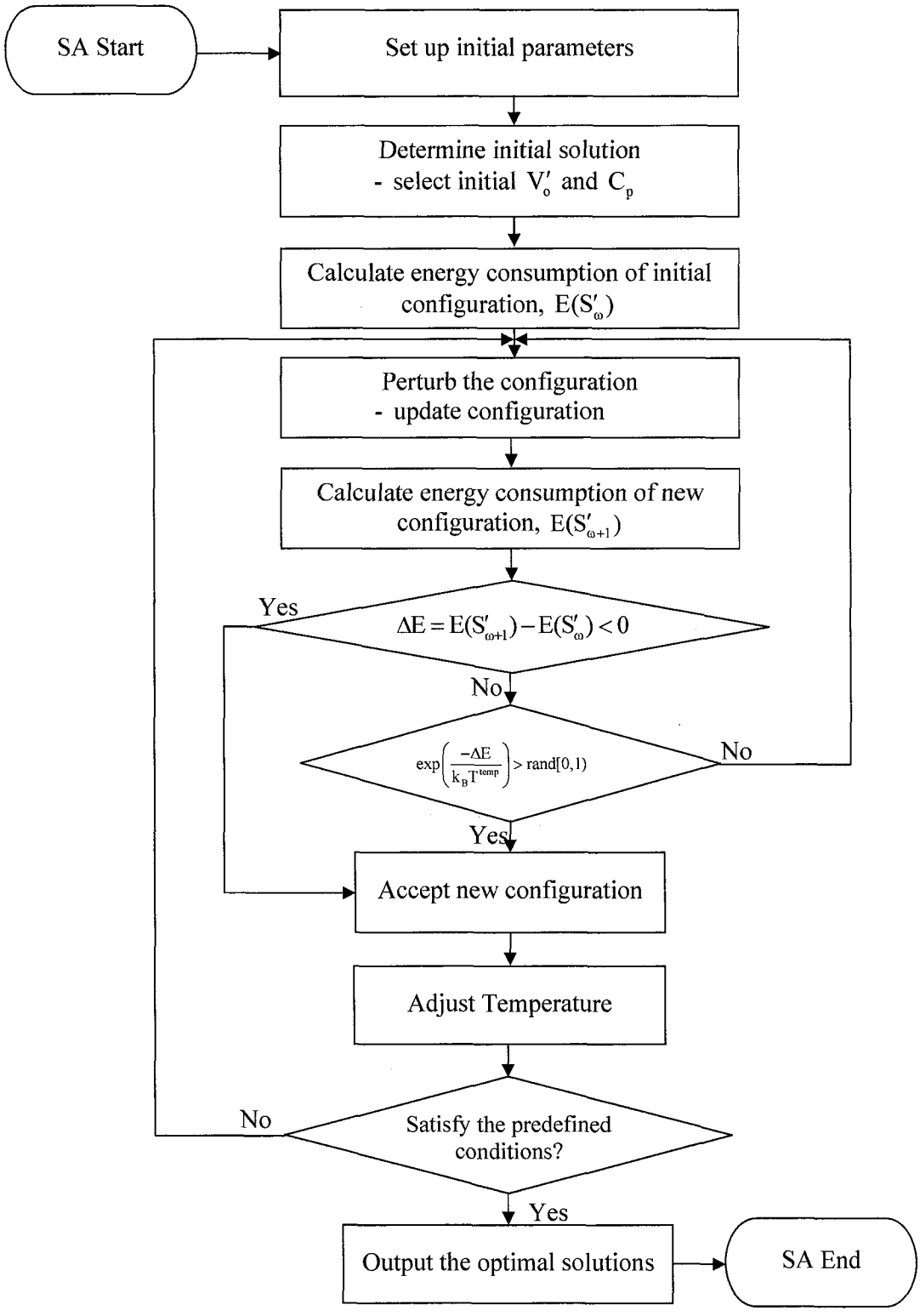

Figure 5.2 Flow chart of the developed Simulated Annealing algorithm.

5.1.3 Fitness Function

As discussed in Chapter 4, three constraints, including the maximum operating speed, maximum allowable travel time, and maximum acceleration (or deceleration) rate, are considered in minimizing the energy consumption problem. The maximum operating speed and acceleration rate are considered to ensure that a train never exceeds the speed limit and always satisfies a passenger comfort level. The train speed and acceleration resulted from the developed SA algorithm is examined and constrained by the developed TPS at any time t.

To deal with the total travel time constraint, a penalty function method is adopted to handle the objective function value when the travel time limit is violated. In general, a constrained optimization problem can be converted into an unconstrained problem with a penalty. A penalty term is added to the objective function of minimizing energy consumption for any violation of the travel time constraint. The penalized objective function, denoted as Z_p, of minimizing total energy consumption can be formulated as:

$$Z_p = Z + \lambda \cdot f_p \qquad \left|\frac{Z_p}{kWh}\right| \left|\frac{Z}{kWh}\right| \left|\frac{\lambda}{-}\right| \left|\frac{f_p}{-}\right| \tag{5.3}$$

where $f_p = \max\left(\frac{T}{T_M} - 1, 0\right)$ is a penalty function, and λ is a penalty factor. The penalty factor used here is a static factor with a sufficiently large value, which prescribes a large amount of energy consumption to rule out infeasible solutions.

5.1.4 Cooling Schedule

An efficient cooling schedule is critical to the performance of SA during search. In general, SA is used to search for the global optimum (i.e., minimum energy consumption) of a broad state space at high temperature. As the temperature decreases, the SA algorithm reduces the searching space to refine the solution found at high temperatures. This search process makes SA superior when the study problem has multiple local optima. It is worth noting that the temperature must go down slowly, which enables SA to search thoroughly at each temperature.

Two typical cooling schedules are considered: linear and exponential. A typical exponential cooling schedule spends little time at high temperatures, and as the temperature decreases more and more time is spent at each temperature to refine the solutions found at high temperatures. On the other hand, linear cooling decreases the temperature linearly as the process time increases, thus, the algorithm spends the same amount of time at each temperature. It is important to note that the temperature must go down slowly to search for feasible solution at each temperature. Thus, an exponential cooling schedule (ECS) is used in the developed SA, which starts with an initial temperature (T_0^{temp}).

$$T_{\omega}^{temp} = T_0^{temp} \cdot \alpha \qquad \left|\frac{T_{\omega}^{temp}}{-}\right| \left|\frac{T_0^{temp}}{-}\right| \left|\frac{\alpha}{-}\right| \tag{5.4}$$

where α is the cooling parameter that has to be tuned between 0 and 1 (e.g., α=0.95). In addition to determining the cooling schedule, the initial temperature and stopping criterion or final temperature must be specified before implementing SA, as discussed below:

Initial Temperature: Given a suitable initial temperature (T_0^{temp}), there is probability that change in the fitness function (ΔE) will be positive and the new solution will be accepted, which can be derived from Equation 5.1 as:

$$T_0^{temp} = \frac{-\Delta E}{k_B \cdot \ln(P_{\Delta E})} \qquad \left|\frac{T_0^{temp}}{-}\right| \left|\frac{\Delta E}{kWh}\right| \left|\frac{k_B}{-}\right| \tag{5.5}$$

Final Temperature (or Stopping Criterion): the final temperature can be determined by fixing the number of temperature values to be used, or the total number of solutions to be generated. Alternatively, the search process can be stopped when the acceptance ratio [i.e., $P_{\Delta E}$] falls below a very small number, or no improved solutions are found at one temperature.

5.2 SVA with Variable MOS (Case II)

The model developed for Case II, which minimize energy consumption, is enhanced from Model I by considering a variable MOS.

5.2.1 Train Control

The train control developed in Section 5.1.1 is enhanced by considering a variable MOS for Case II. As shown in Figures 5.3 and 5.4, the train control is adjusted for two different variable MOS scenarios. Scenario 1 is for the situation shown in Figure 5.3 where the MOS increases (i.e., $V_{M_1} < V_{M_2}$) as the train moves toward to the next station, which affects train acceleration. When the coasting speed (V_o') is greater than V_{M_1}, the train accelerates until it reaches V_{M_1} and then a cruising regime starts immediately. When a

train reaches the beginning of the track segment under V_{M_2}, it continues to accelerate until it reaches V_o'.

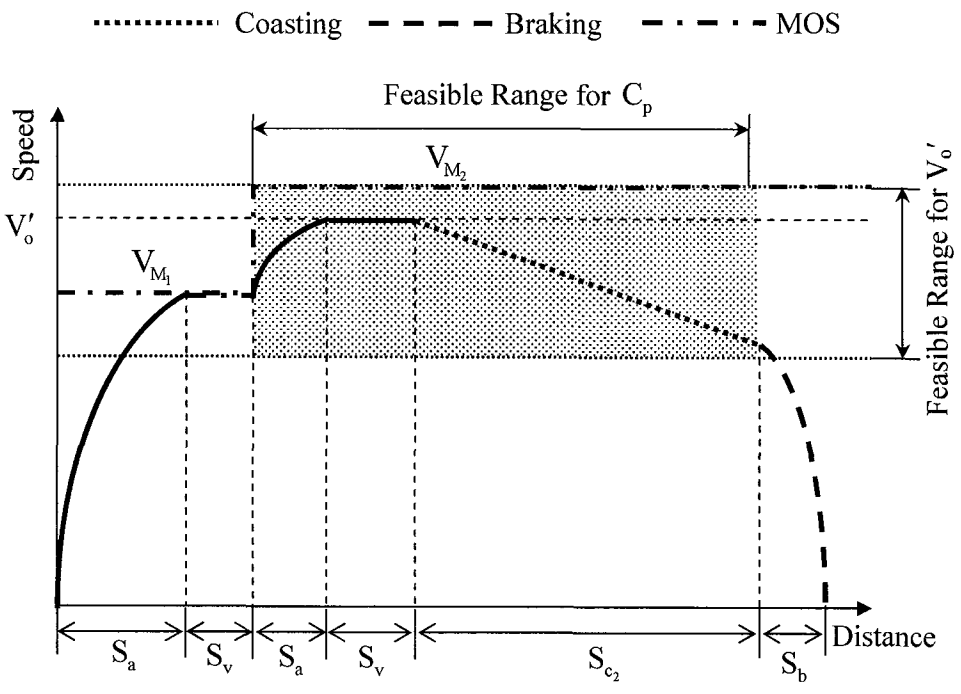

Figure 5.3 Train control under variable MOS Scenario 1 ($V_{M_1} < V_{M_2}$).

Scenario 2, illustrated in Figure 5.4, indicates that the maximum operating speed rapidly decreases (i.e. $V_{M_1} > V_{M_2}$) as train moves to the next station. In this situation, braking must be used effectively enforced to reduce the train speed whenever there is a need.

The SA for Case II is the same as that developed for Case I, and its major parameters, including the fitness function, state space, perturbation, acceptance criteria, and cooling schedule are the same as those used for Case I.

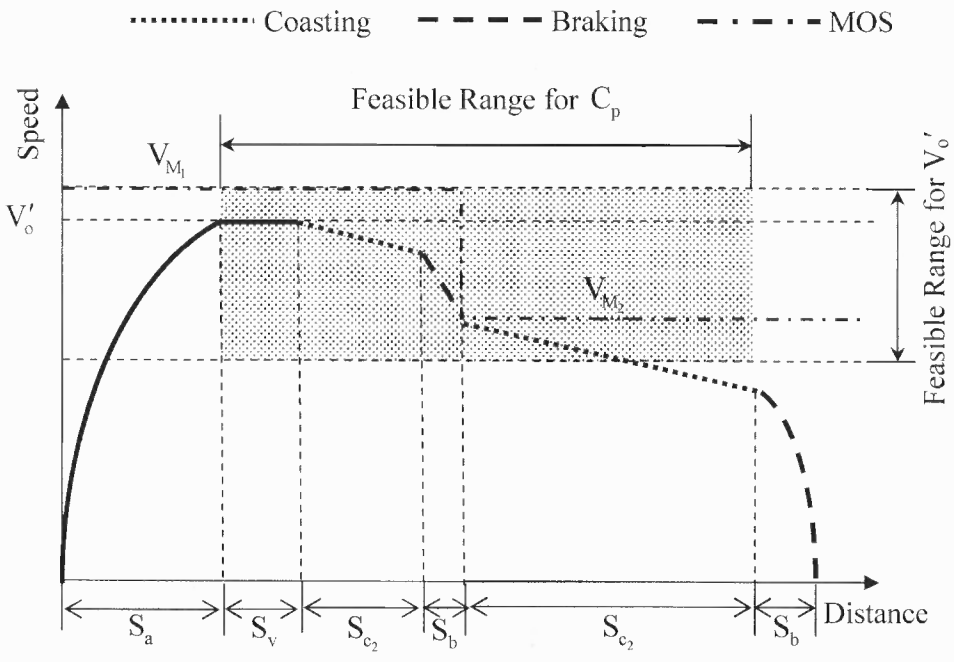

Figure 5.4 Train control under variable MOS Scenario 2 ($V_{M_1} > V_{M_2}$).

5.3 MVA and Constant MOS (Case III)

The objective function of the energy consumption minimization problem formulated in Case III is enhanced from the model developed for Case I, but considers a mixed vertical alignment (MVA) with a constant MOS. The train control profiles, SA, fitness function, and cooling schedule for Case III are the same as those discussed for Case I.

5.4 MVA with Variable MOS (Case IV)

The objective energy consumption function formulated in Case IV is enhanced from the models developed for Cases I, II, and III. By considering a MVA with a variable MOS, Model IV optimizes train control that yields minimum energy consumption. The train

control profiles, the fitness function, and the cooling schedule of SA for Case IV are the same as those discussed in Case II.

5.5 Summary

In this chapter, an SA-based solution method was developed to search for the optimal solution for the research problems discussed in Chapter 4. With SA, Models I through IV were used to explore optimal solutions that minimize energy consumption discussed in Cases I through IV, respectively. While searching for the optimal solution subject to a given travel time constraint, a train control plan (i.e., speed vs. time diagram) may be established to satisfy the maximum operating speed constraint. To demonstrate the applicability of the developed methods, two real-world examples of the New Haven Line of the Metro-North Railroad are analyzed and discussed in Chapter 6.

CHAPTER 6

CASE STUDY

This chapter demonstrates the applicability of the models for Cases I through IV discussed in Chapter 4 and the solution SA algorithm developed in Chapter 5. The optimal results for Cases I and II are discussed in Section 6.1, and two real-world track alignments and operating data of the New Haven Line of the Metro-North Railroad used for Cases III and IV are presented in Section 6.2. The findings and the results comparison are summarized in Section 6.3. Finally, a sensitivity analyses that evaluate the impact of various train operation conditions, such as travel time constraint, speed constraint, coasting position, and vertical dip of convex alignment, is conducted and discussed in Section 6.4.

6.1 Optimal Results for Cases I and II

In this section, the models and the solution SA algorithm developed in Chapters 4 and 5 are used to minimize energy consumption for three single vertical alignments (SVA), including level, convex, and concave alignments, associated with constant and variable maximum operating speed (MOS). The optimal train controls for minimum energy consumption discussed in Cases I and II are presented in Sections 6.1.1 and 6.1.2, respectively.

A 10-car passenger train is considered whose maximum motor power is 10,600 hp (8,000 kW). A constant maximum operating speed (V_M) of 65 mph is used in Case I, and the variable maximum operating speed used in Case II is composed of 40 and 70 mph. The maximum acceleration rate is determined by the tractive effort (TE), which will not

exceed 0.15g (i.e., 4.83 ft/sec^2) for passenger comfort, while the maximum deceleration rate of -0.15g (i.e., -4.83 ft/sec^2) is used to stop the train before reaching the downstream station. The baseline inputs used for Cases I and II, including train characteristics, vertical track alignment, operational constraints, and the options for the SA algorithm, are summarized in Table 6.1.

Table 6.1 Inputs for Cases I and II

	Parameters	**Values**
Train Characteristics	Motor Power	8,000 kW
	Number of Cars per Train	10 cars/train
	Car Mass	140,672 lb
	Car Length	85 ft
	Max. Acceleration (Deceleration) Rate	± 4.83 ft/sec^2
	Spring Constant	68,536.6 lb/ft
	Damping Constant	342.7 lb·sec/ft
Track Alignment	Station Spacing (S)	12,000 ft
	Vertical Dip/Height (δ)	90 ft
	Dip/Height Percentage ($\delta / S \times 100$)	0.75 %
	Ruling Grade	3 %
Operational Constraints	Maximum Speed Limit (V_M) for Case I	65 mph
	Maximum Speed Limit (V_M) for Case II	40 mph, 70 mph
	Feasible Boundary for C_p	2,500 -11,000 ft
	Feasible Boundary for V_o' in Case I	55 -65 mph
	Feasible Boundary for V_o' in Case II	40-70 mph
	Maximum Allowable Travel Time (T_M)	170 sec
Simulated Annealing Options	Initial Temperature	100
	Annealing Function	Boltzmann
	Temperature Update	Metropolis Rule
	Re-annealing Interval	100
	Cooling Schedule	Exponential

6.1.1 SVA with Constant MOS (Case I)

To evaluate the impact of track alignment and the maximum operating speed on the optimal train control that minimizes energy consumption, a number of figures are produced to illustrate the relationship of speed versus distance and time under different track alignments.

Operating the train on a level track alignment, a minimum energy of 77.7 kWh was consumed at a coasting speed (V_o') of 58.8 mph starting at a coasting position (C_p), 3,097 ft from the upstream station as shown in Figure 6.1. To achieve minimum energy operation, the train must accelerate with full motor power from stand still at the upstream station until the speed (V_o') of 58.8 mph is reached at a location of 2,087 ft from the upstream station. The train then maintains this speed with a motor power of 565.7 kW until a coasting regime is commenced at 3,097 ft, and then the brakes must be applied at 11,386 ft so the train can safely arrive at the downstream station. The relationship of speed versus travel time for this situation is illustrated in Figure 6.2.

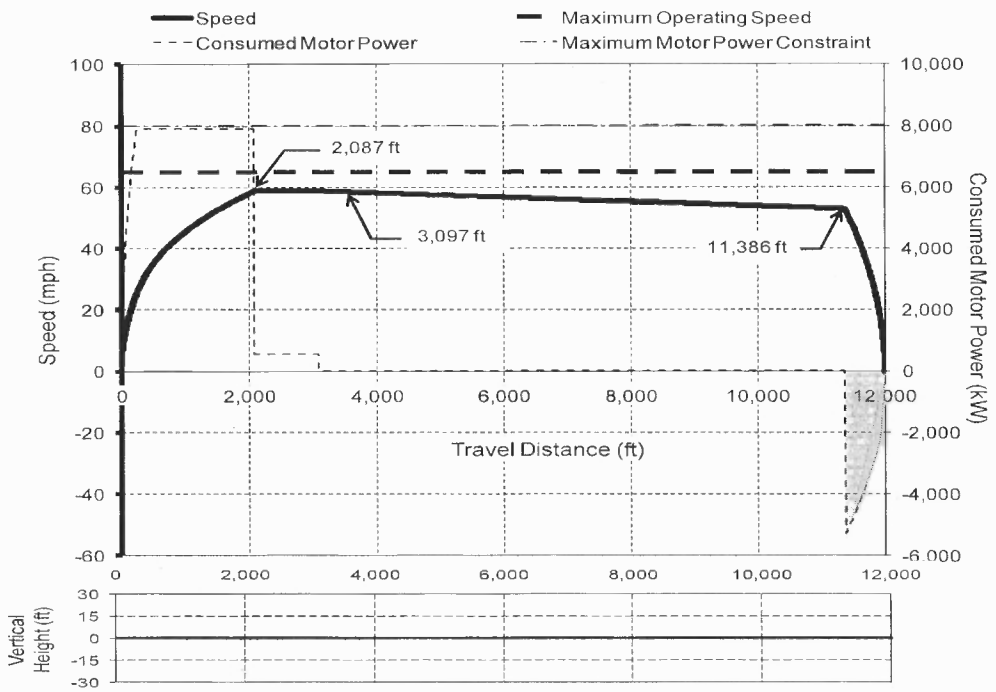

Figure 6.1 Tractive effort and speed vs. distance (Level-Case I).

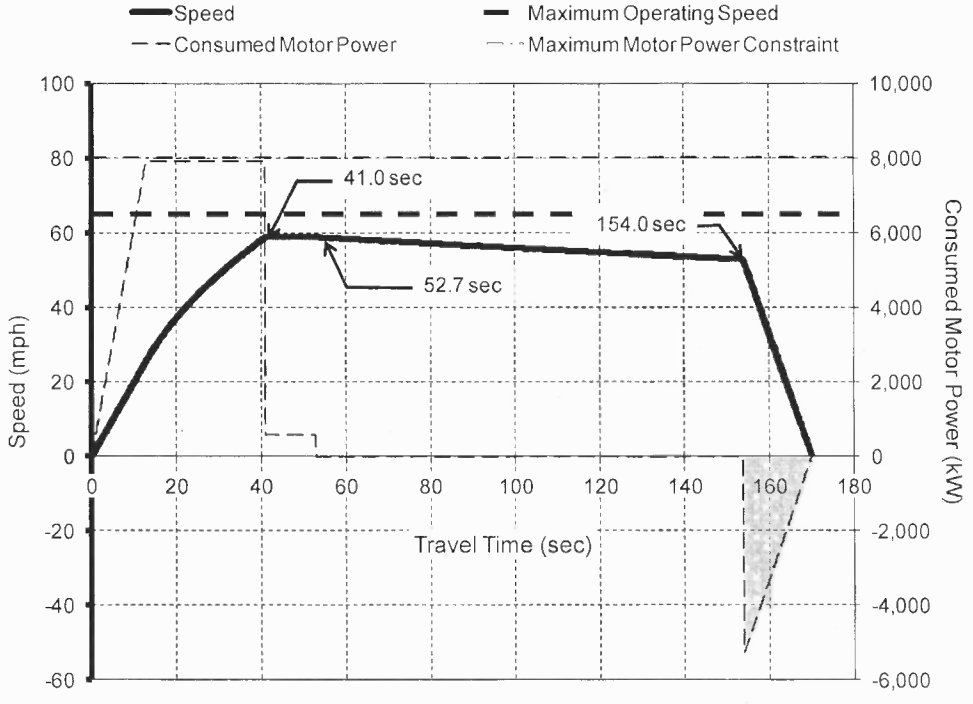

Figure 6.2 Tractive effort and speed vs. time (Level-Case I).

Running the train on a convex alignment, it was found that a minimum energy of 45.7 kWh was consumed at a coasting speed (V_o') of 64.1 mph starting at position (C_p) 5,862 ft from the upstream station. As shown in Figure 6.3, a train accelerates with full TE (i.e., 7,904 kW) from standstill at the upstream station to speed (V_o') of 64.1 mph (2,034 ft from the upstream station). Then, the train maintains this speed with a negative motor power of 684.8 kW (i.e., the shaded area in Figure 6.3) due to the steep down-hill track slope until coasting is triggered at a distance of 5,862 ft, and then the brakes must be used at 11,737 ft from the upstream station. The relationship of speed versus travel time under optimal train control is illustrated in Figure 6.4.

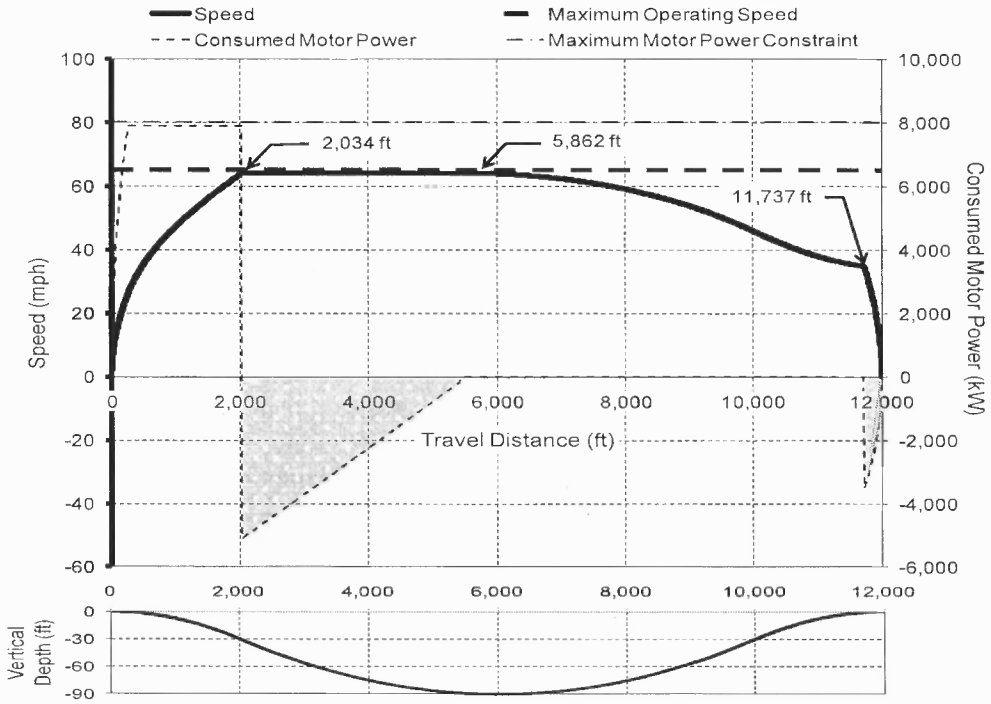

Figure 6.3 Tractive effort and speed vs. distance (Convex-Case I).

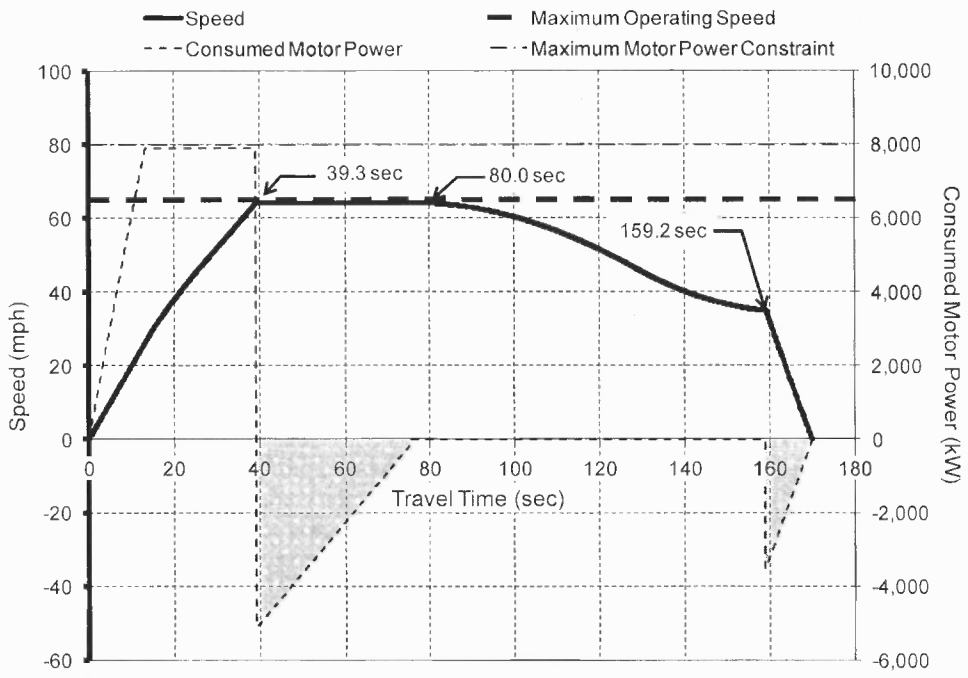

Figure 6.4 Tractive effort and speed vs. time (Convex-Case I).

For a concave alignment in Case I, a minimum energy consumption of 121.9 kWh was yielded when a coasting speed (V_o') of 55.5 mph is used at the position (C_p) of 4,846 ft from the upstream station. To achieve the optimized train control as illustrated in Figure 6.5, the train accelerates with maximum TE to reach V_o' at 2,769 ft from the upstream station. After that, the train cruises with a speed of 55.5 mph until the coasting regime is initiated at 4,846 ft. The train takes the advantage of a down-hill slope to reach the maximum operating speed (V_M) of 65 mph, and then light braking is used for not exceeding V_M until maximum braking must be used at 10,107 ft from the upstream station, as shown in Figure 6.6.

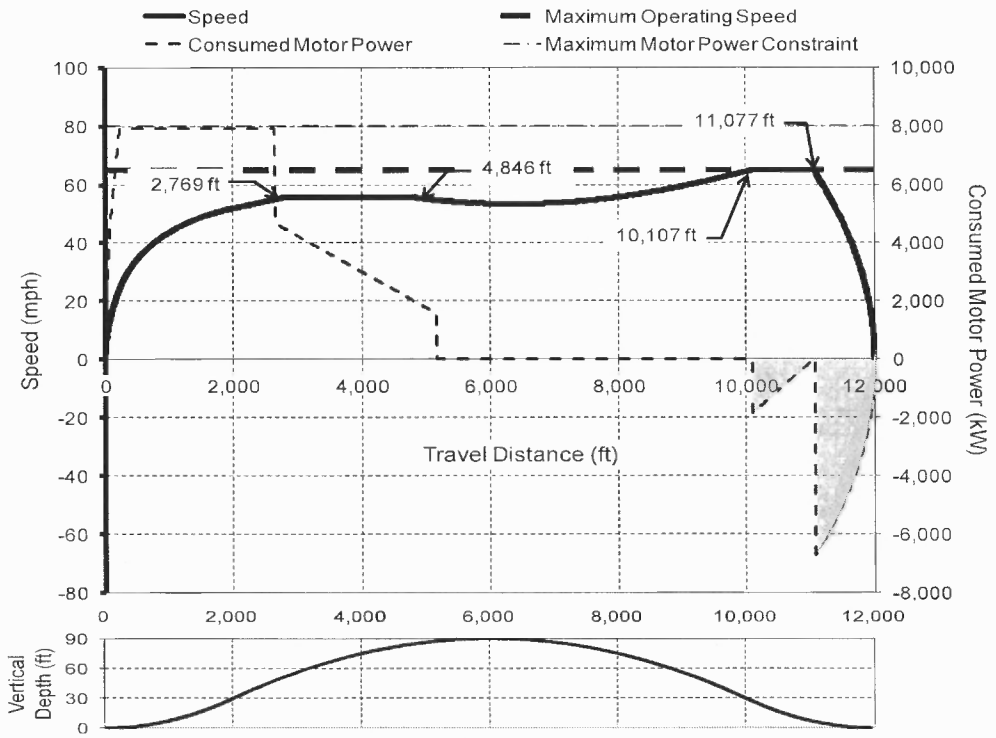

Figure 6.5 Tractive effort and speed vs. distance (Concave-Case I).

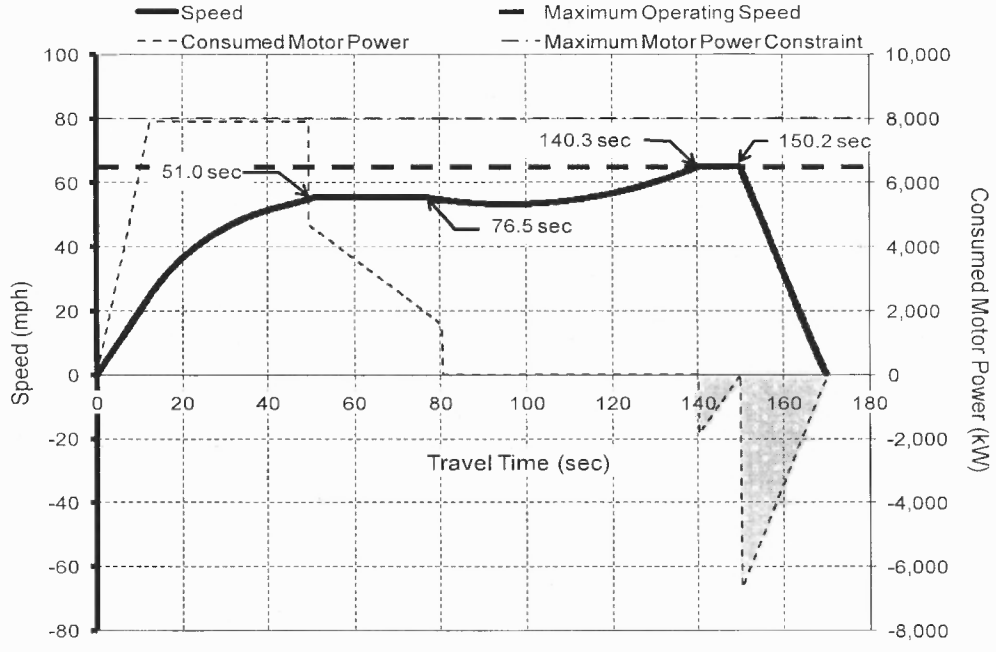

Figure 6.6 Tractive effort and speed vs. time (Concave-Case I).

6.1.2 SVA with Variable MOS (Case II)

The impact of track alignments and a MOS varying between 40 and 70 mph to optimal train control was estimated, and the relationship of speed versus distance and time of the optimized train control are discussed below.

For a level track alignment, a minimum energy consumption of 89.3 kWh was achieved with a coasting speed (V_0') of 63.1 mph associated with a coasting position (C_p) at 3,880 ft from the upstream station. To obtain the minimum energy operation as illustrated in Figure 6.7, the train must accelerate with full TE from stand still at the upstream station until the first maximum operating speed (V_{M_1}) of 40 mph is achieved at 709 ft. The train, then, maintains this speed with a motor power of 332.9 kW until the train accelerates again at 2,004 ft. The coasting regime is commenced at 3,880 ft, and then the brakes must be applied at 11,273 ft. The relationship of speed and travel time is shown in Figure 6.8.

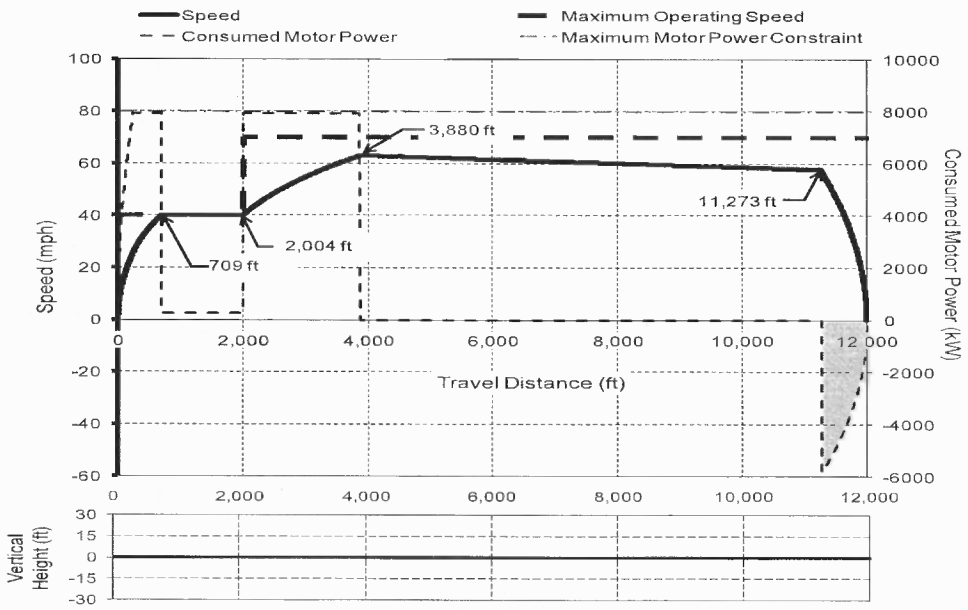

Figure 6.7 Tractive effort and speed vs. distance (Level-Case II).

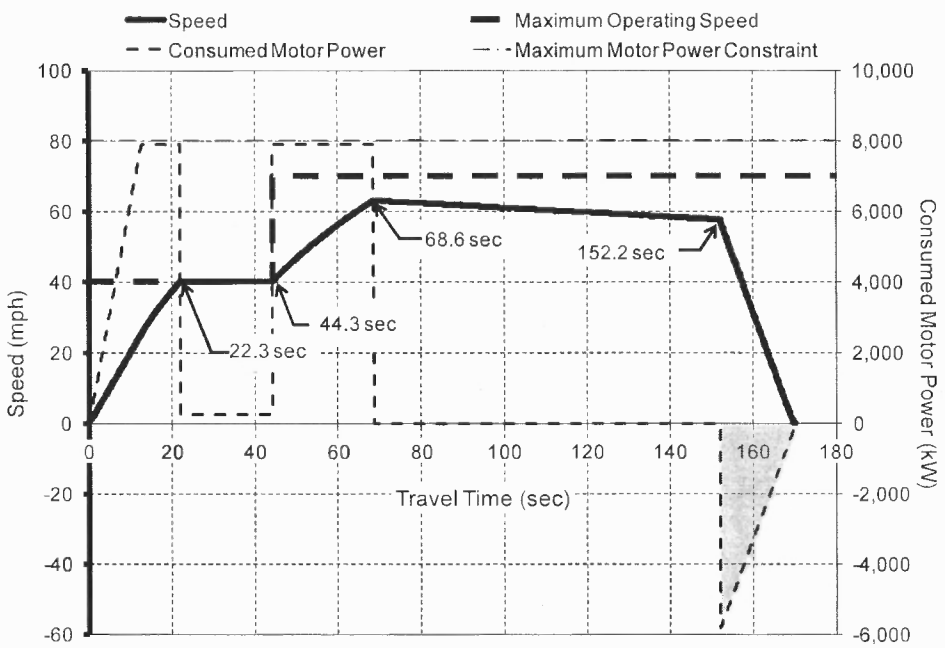

Figure 6.8 Tractive effort and speed vs. time (Level-Case II).

For a convex alignment, it was found that a minimum energy consumption of 82.8 kWh was accomplished at a coasting speed (V_o') of 64.9 mph at the coasting position (C_p) of 3,399 ft from the upstream station. As shown in Figure 6.9, a train accelerates with full TE from stand still at the upstream station until the speed (V_{M_1}) of 40.0 mph is attained at 667 ft from the upstream station. Then the train maintains this speed with negative motor power due to the down-hill track slope until the train accelerates again at a distance of 2,001 ft. Once coasting is triggered at 3,399ft, the speed increases up to 68.4 mph because of the down-hill track slope. Then, braking must be applied at 11,615 ft from the upstream station. The relationship of speed versus travel time is illustrated in Figure 6.10.

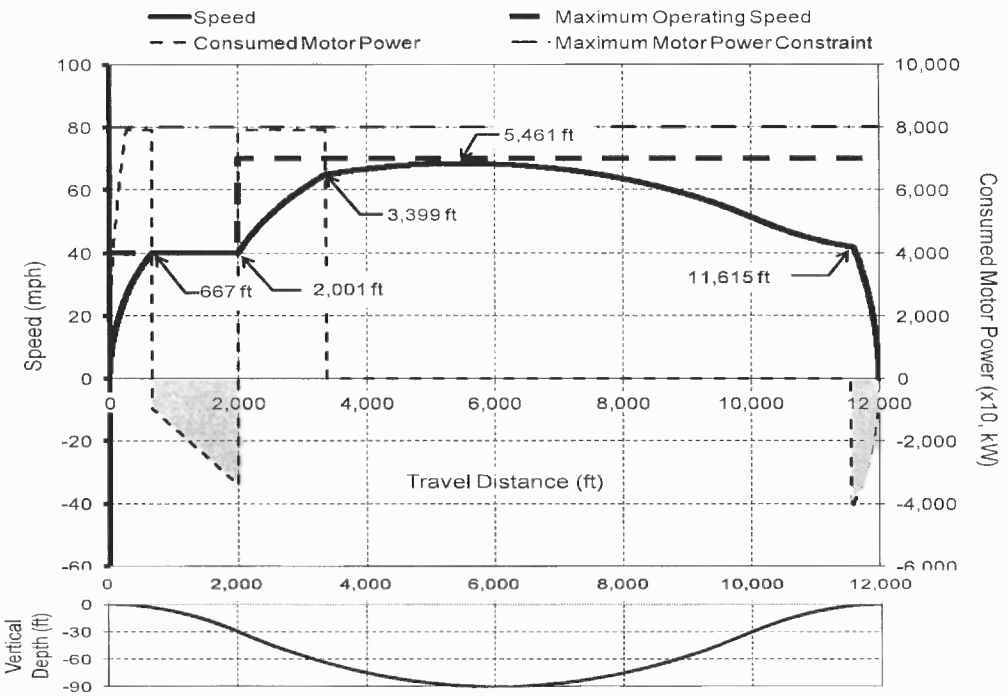

Figure 6.9 Tractive effort and speed vs. distance (Convex-Case II).

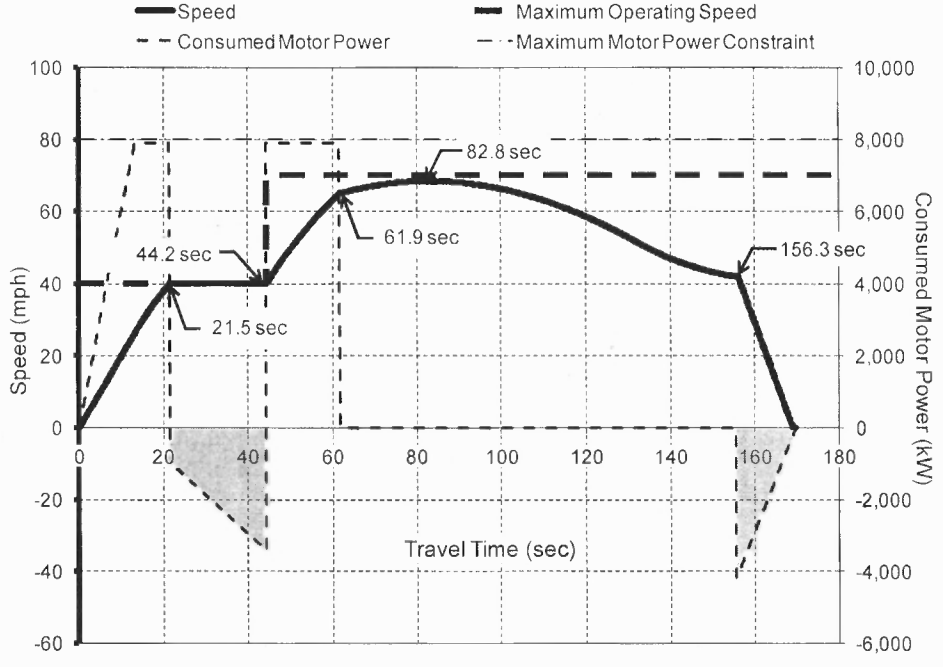

Figure 6.10 Tractive effort and speed vs. time (Convex-Case II).

For a concave alignment in Case II, the minimum energy consumption of 133.5 kWh was yielded when the coasting speed (V_o') of 60.0 mph is applied at position (C_p) 5,007 ft from the upstream station. To achieve the optimized train control shown in Figure 6.11, the train accelerates with full TE to reach V_{M_1} at 761 ft from the upstream station. Then, the train accelerates again at 2,001 ft to reach V_o' at 4,576 ft from the upstream station. After that, the train cruises with a speed of 60.0 mph until the coasting regime is initiated at 5,007 ft. Due to the advantage of a down-hill slope, the train reaches the second maximum operating speed (V_{M_2}) of 70.0 mph, and then a light braking is applied not to exceed V_{M_2} until the braking regime must be used at 10,904 ft from the upstream station. The relationship of speed and travel time generated by optimal train control is shown in Figure 6.12.

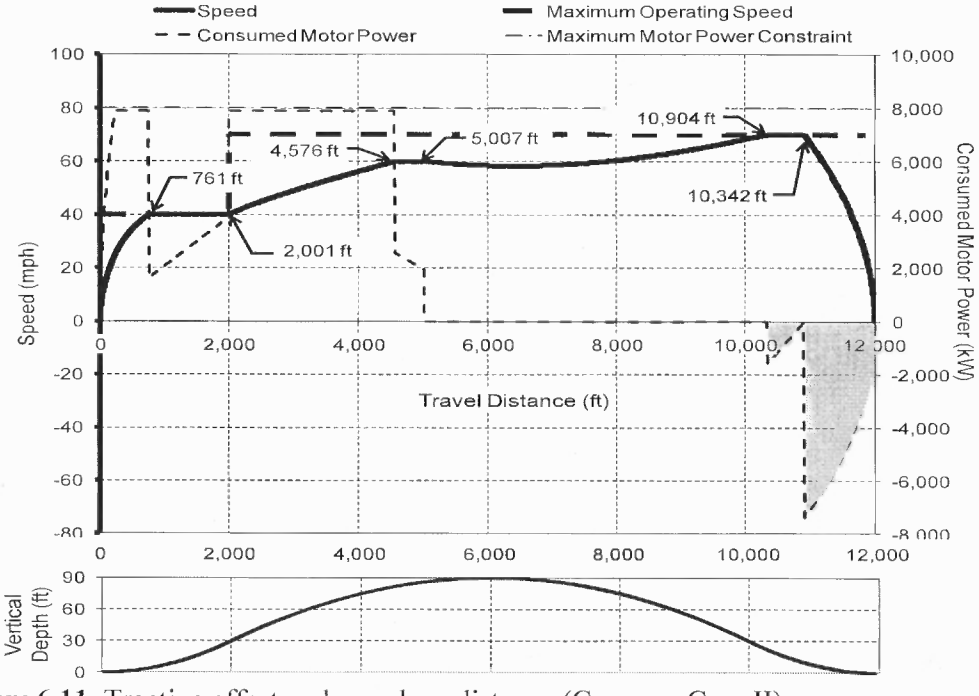

Figure 6.11 Tractive effort and speed vs. distance (Concave-Case II).

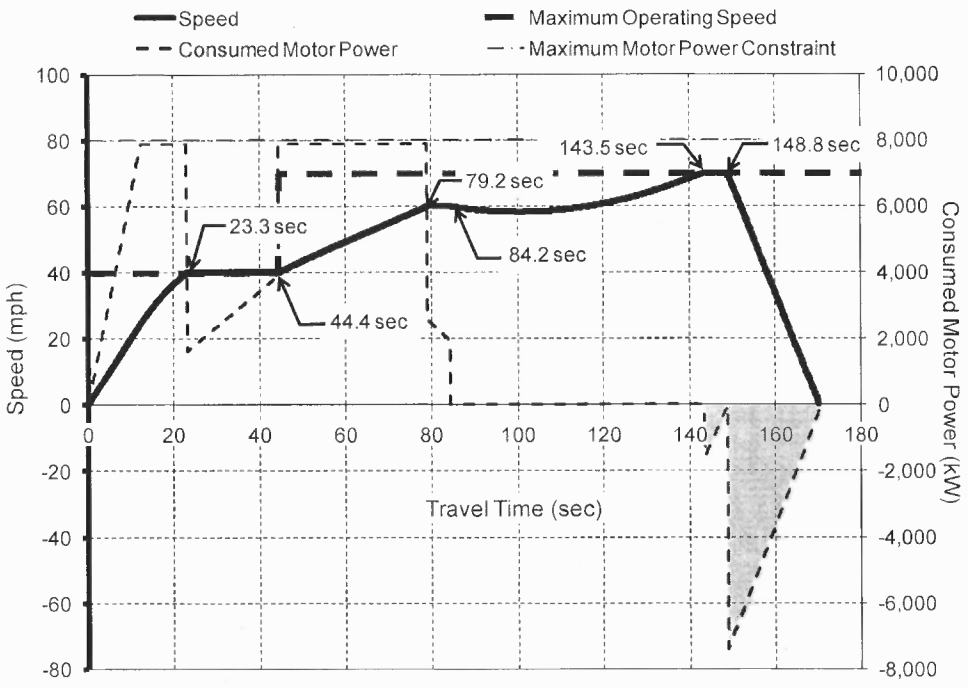

Figure 6.12 Tractive effort and speed vs. time (Concave-Case II).

6.2 Optimal Results for Cases III and IV

In this section, Models III and IV are used to two real-world commuter rail segments with constant and variable maximum operating speed for Cases III and IV, respectively. According to the segment configuration and operational data discussed in Section 6.2.1, the impact of the optimized train control to the consumed energy is estimated in Sections 6.2.2 and 6.2.3. The baseline values of input parameters employed for Cases III and IV are summarized in Table 6.2. The information of the track profile (i.e., track length and vertical grade) and the associated maximum operating speed is shown in Table 6.3.

Table 6.2 Inputs for Cases III and IV

	Parameters	**Values**
Train Characteristics	Motor Power	8,000 kW
	Number of Cars per Train	10 cars/train
	Car Mass	140,672 lb
	Car Length	85 ft
	Max. Acceleration (Deceleration) Rate	2.93 (-4.83) ft/sec^2
	Spring Constant	68,536.6 lb/ft
	Damping Constant	342.7 lb·sec/ft
Track Alignment	Station Spacing (S) for Case III	11,087 ft
	Station Spacing (S) for Case IV	11,616 ft
	Ruling Grade for Case III	-0.322%
	Ruling Grade for Case IV	0.708%
Operational Constraints	Maximum Speed Limit (V_M) for Case III	70 mph
	Maximum Speed Limit (V_M) for Case IV	75 mph, 40 mph
	Feasible Boundary for C_p	2,500 -10,000 ft
	Feasible Boundary for V_o' in Case III	60 -70 mph
	Feasible Boundary for V_o' in Case IV	65-75 mph
	Maximum Allowable Travel Time (T_{max})	150 sec
Simulated Annealing Options	Initial Temperature	100
	Annealing Function	Boltzmann
	Temperature Update	Metropolis Rule
	Re-annealing Interval	100
	Cooling Schedule	Exponential

Table 6.3 Track Alignment Geometry and Speed Limit

Case III	Length (ft)*	0-982	982-2,512	2,512-5,405	5,405-6,988	6,988-9,333	9,333-11,087
	Grade (%)	0.00	-0.243	-0.322	-0.098	0.122	0.023
	V_M (mph)	70	70	70	70	70	70
Case IV	Length (ft)**	0-1,011	1,011-2,324	2,324-6,016	6,016-8,194	8,194-11,616	-
	Grade (%)	0.033	0.567	0.708	-0.256	-0.057	-
	V_M (mph)	75	75	75	75	40	-

*: from Harrison to Rye Station
**: from East Norwalk to Westport Station

6.2.1 Metro-North Railroad (New Haven Line)

The Metro-North Railroad's New Haven line is a 74-mile long rail line serving 30 stations combined in 3 branch lines, which run from Woodlawn, New York to New Haven, Connecticut. The service interval of the studied rail line varies over time and station due to the pattern of local and express services. The headway range is between 13 and 33 minutes. The rolling stock servicing in the studied line consists of Electric Multiple Units (EMU), and the characteristics of M8 (i.e., EMU car model manufactured by Kawasaki Rail Car, Inc.) was used in the developed TPS model. As shown in Figure 6.13, the segment between Harrison and Rye was selected and studied for Case III, and the segment between East Norwalk and Westport was used for Case IV.

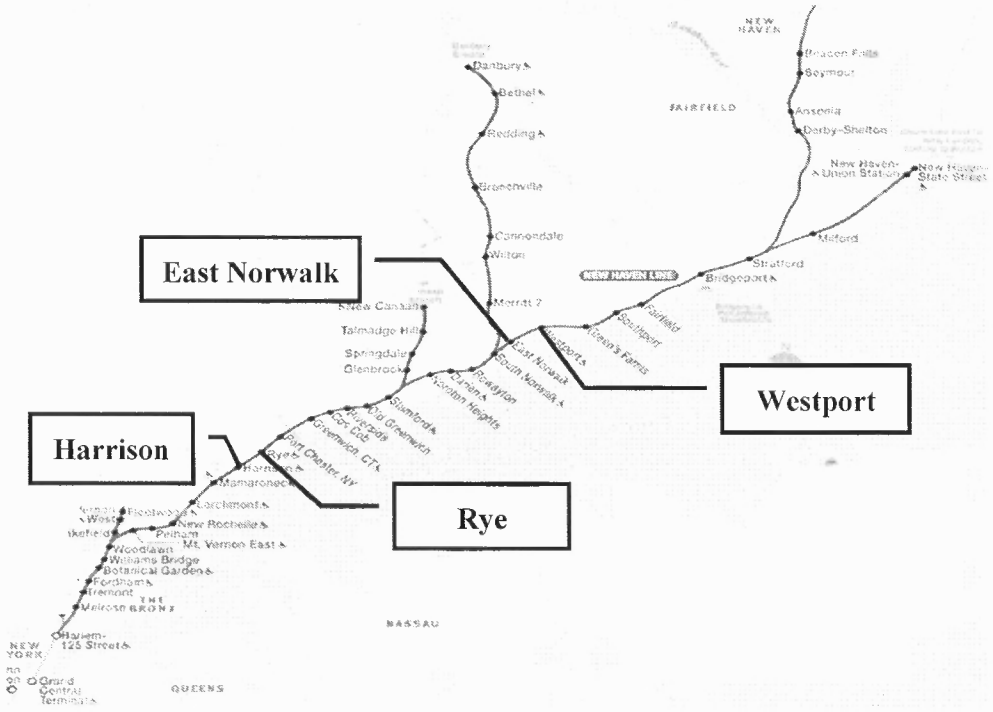

Figure 6.13 Configuration of Metro North - The New Haven Line.

Source: http://www.mta.info/mnr/html/mnrmap.htm

6.2.2 MVA with Constant MOS (Case III)

Similar to the analysis discussed in Cases I and II, the impact of the optimized train control to the consumed motor power and speed is developed and shown in Figure 6.14.

The minimum energy consumption of 82.4 kWh was yielded when the optimal coasting speed (V_o') of 64.0 mph begins at the position (C_p) of 4,414 ft away from the Harrison Station. It was found that the train accelerates with full motor power (i.e., 7,904 kW) from standstill to speed (V_o') of 64.0 mph (2,528 ft from Harrison Station). Then, the train keeps this speed with negative motor power until the coasting regime is triggered at 4,414 ft. After that, braking at 10,348 ft must be used to arrive at the Rye Station.

If a train is equipped with a Regenerative Braking System (RBS), the applied light braking (i.e., the shaded area in Figure 6.14) can be stored as energy in a battery or condenser bank for later use. The relationship of speed versus travel time under optimal train control is illustrated in Figure 6.15.

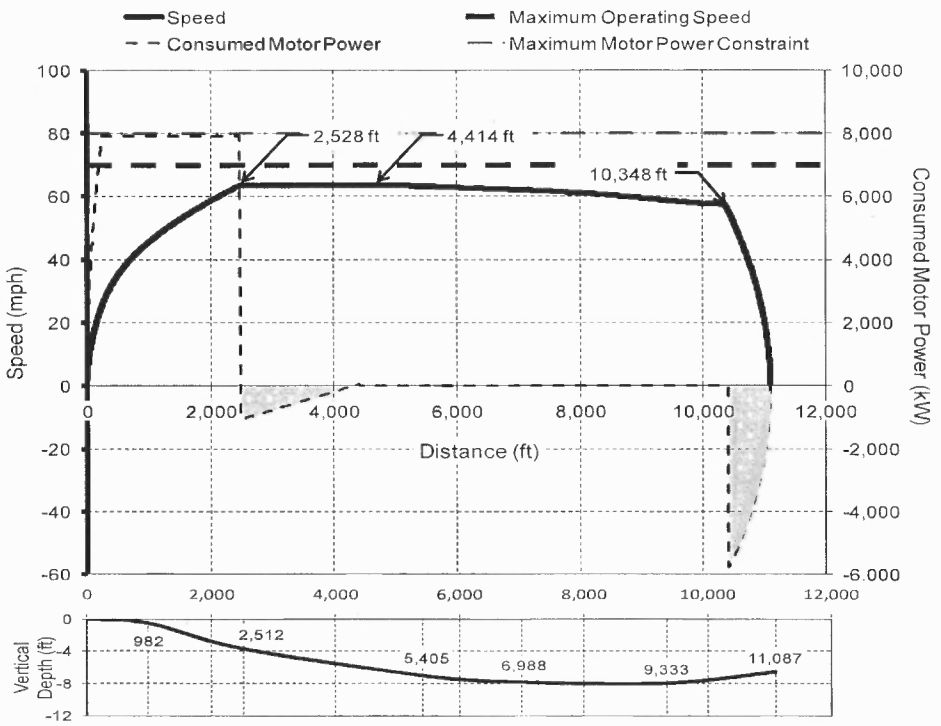

Figure 6.14 Tractive effort, speed, and vertical track profile vs. distance (Case III).

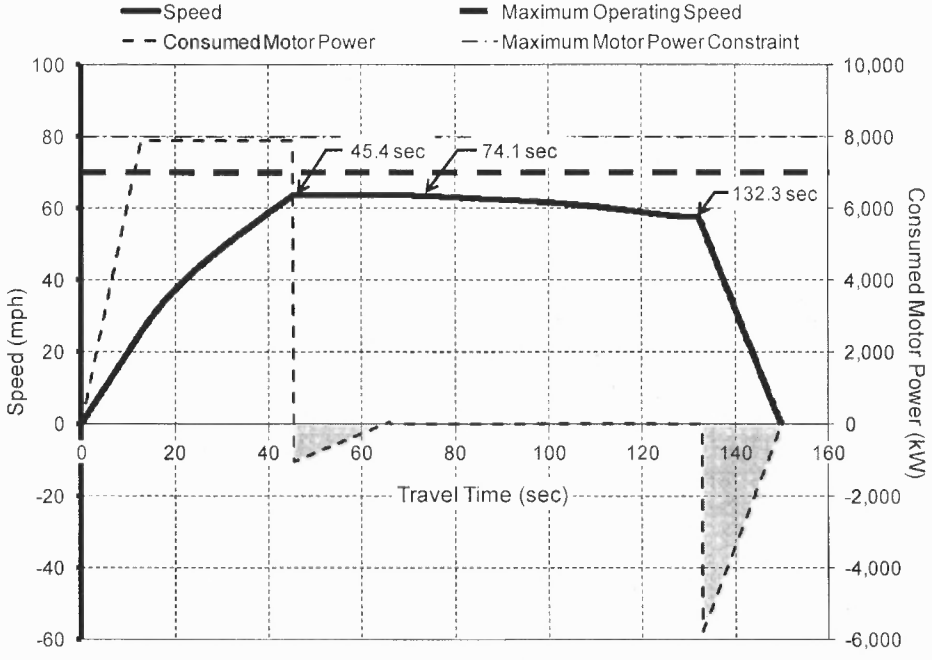

Figure 6.15 Tractive effort and speed vs. time (Case III).

6.2.3 MVA with Variable MOS

To evaluate the impact of track alignments and variable maximum operating speed to the optimal train control that minimizes energy consumption, figures demonstrating the relationship of speed versus distance and time of the optimized train control are developed and discussed next.

The minimum energy consumption of 96.7 kWh was obtained when the coasting speed (V_o') of 72.0 mph starts at position (C_p), 4,607 ft from the East Norwalk Station. To accomplish the minimum energy operation as shown in Figure 6.16, a train must accelerate with the maximum TE to reach V_o' at 3,909 ft from the East Norwalk Station. After that, the train cruises with the speed of 72.0 mph until the coasting regime is commenced at 4,607. Then, brakes must be applied at 7,537 ft to reduce the speed to the second maximum operating speed (V_{M_2}) of 40 mph, and the coasting regime repeats at 8,194 ft until final braking must be applied at 10,199 ft. The resulting relationship between speed and travel time due to the application of optimal train control is illustrated in Figure 6.17.

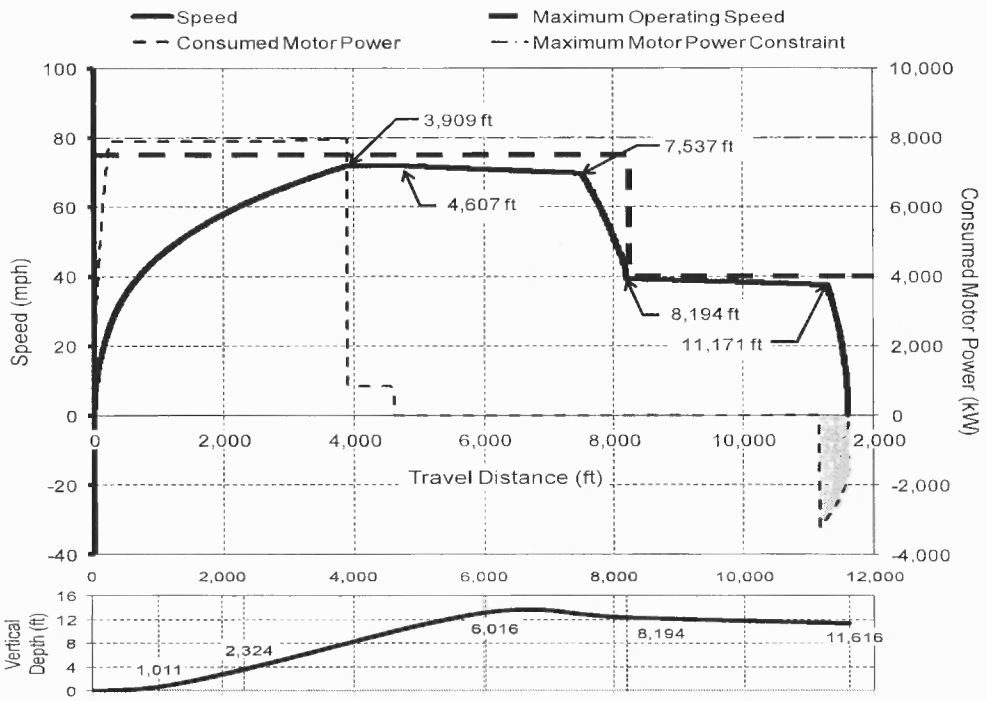

Figure 6.16 Tractive effort, speed, and vertical track profile vs. distance (Case IV).

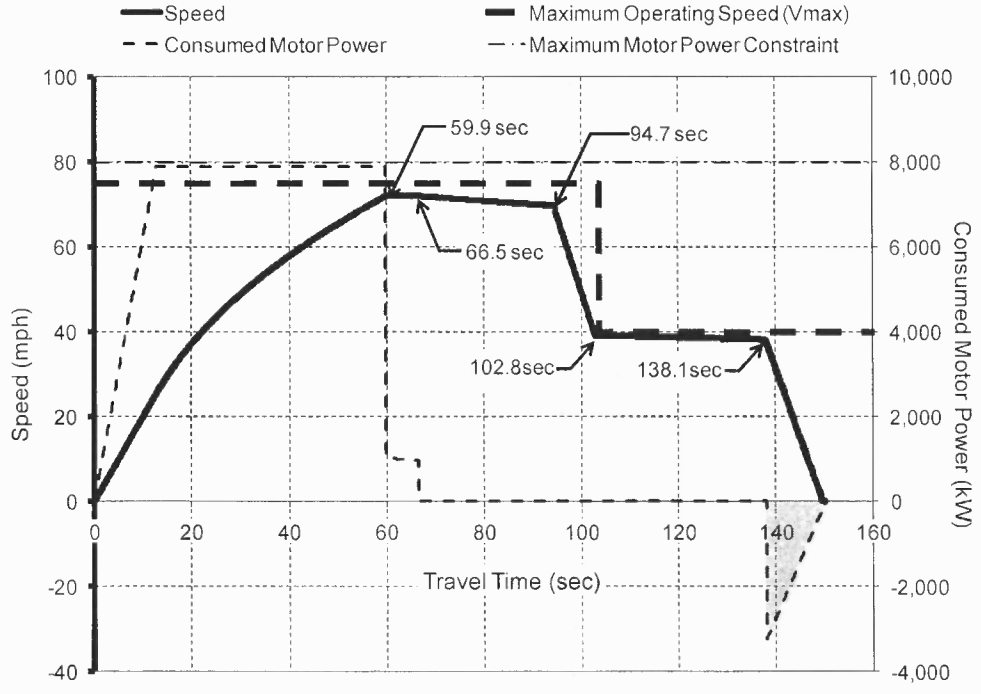

Figure 6.17 Tractive effort and speed vs. time (Case IV).

6.3 Results Comparison

The energy consumption under various travel times for various settings defined in Cases I through IV were evaluated and discussed in previous sections. As summarized in Table 6.4, the studied three track alignments (i.e., level, convex, and concave) in Cases I and II are symmetric and parabolic with vertical dips of 0 ft, -90 ft, and 90 ft, respectively and the station spacing is 12,000 ft. While a constant MOS (V_M) of 65 mph is used for Case I, a variable MOS of 40 mph and 70 mph is considered for Case II.

The results of optimal train control under Cases I and II are summarized in Table 6.4. It was found that the energy consumption is notably sensitive to the track alignment in Cases I and II. Particularly in Case I, the minimized energy consumption for a 10-car train on a convex alignment is about 62.5% less than that when operating on a concave alignment. However, considering the MOS varying between 40 and 70 mph in Case II, the energy consumption difference by a train running between a level and a convex alignment seems small. Since the first MOS of 40 mph increases the duration of the acceleration regime, the timing and position to begin the coasting regime are affected. As a result, the benefits of a dipped track alignment that reduces energy consumption are diminished.

The resulting energy consumption for running a train on the studied alignments in Cases I and II ranges between 45.7 and 121.9 kilowatt-hour and 82.8 and 133.5 kilowatt-hour, respectively. It was found that the convex alignment is the most energy efficient one among the three alignments discussed in Cases I and II.

Table 6.4 Results under Optimal Control in Cases I and II

Cases / Operation Conditions & Optimal Results		Case I			Case II		
		Constant MOS (65 mph)			Variable MOS (40, 70 mph)		
		Level	Convex	Concave	Level	Convex	Concave
Station Spacing (ft)		12,000	12,000	12,000	12,000	12,000	12,000
Vertical Dip/Height (ft)		0	-90	90	0	-90	90
Dip/Station Spacing (%)		0%	0.75%	0.75%	0%	0.75%	0.75%
Ruling Grade (%)		3	3	3	3	3	3
V_M (mph)		65	65	65	40,70	40,70	40,70
T_{max} (sec)		170	170	170	170	170	170
Energy Consumption (kWh)		77.7	45.7	121.9	89.3	82.8	133.5
Coasting Speed (mph)		58.8	64.1	55.5	63.1	64.9	60.0
Maximum Speed (mph)		58.8	64.1	65.0	63.1	68.4	70.0
Coasting Position (ft)		3,097	5,862	4,846	3,880	3,399	5,007
Cruising*	Timing (sec)	-	-	-	22.3	21.5	44.4
	Position (ft)	-	-	-	709	667	761
Cruising**	Timing (sec)	41.0	39.3	51.0	-	-	79.2
	Position (ft)	2,087	2,034	2,769	-	-	4,576
Coasting	Timing (sec)	52.7	80.0	76.5	68.6	61.9	84.2
	Position (ft)	3,097	5,862	4,846	3,880	3,399	5,007
Braking	Timing (sec)	154.0	159.2	150.2	152.2	156.3	148.8
	Position (ft)	11,386	11,737	11,077	11,273	11,615	10,904

*: Cruising under V_{M_1} (40 mph) in Case II

**: Cruising under V_M (65 mph) and V_{M_2} (70 mph) in Case II

Considering different track alignments and related operational conditions, the minimum energy consumption, coasting speed, and positions and timings of motion regimes of Cases III and IV are summarized in Tables 6.5 and 6.6, respectively.

Table 6.5 Results of Optimal Control in Case III

Case III						
Track Alignment & Operational Condition				**Optimal Results**		
Station Spacing (ft)		11,087		Energy Consumption (kWh)		82.4
Track Characteristics		V_M (mph)	Grade (%)	Coasting Speed (mph)		64.0
Segment Length (ft)	0-982	70	0.0	Maximum Speed (mph)		64.0
	982-2,512	70	-0.243	Coasting Position (ft)		4,414
	2,512-5,405	70	-0.322	Cruising	Timing (sec)	45.4
	5,405-6,988	70	-0.098		Position (ft)	2,528
	6,988-9,333	70	0.122	Coasting	Timing (sec)	74.1
	9,333-11,087	70	0.023		Position (ft)	4,414
Ruling Grade (%)		-0.322%		Braking	Timing (sec)	132.3
T_{max} (sec)		150			Position (ft)	10,348

Table 6.6 Results of Optimal Control in Case IV

Case IV						
Track Alignment & Operational Condition				**Optimal Results**		
Station Spacing (ft)		11,616		Energy Consumption (kWh)		96.7
Track Characteristics		V_M (mph)	Grade (%)	Coasting Speed (mph)		72.0
Segment Length (ft)	0-1,011	75	0.033	Maximum Speed (mph)		72.0
	1,011-2,324	75	0.567	Coasting Position (ft)		4,607
	2,324-6,016	75	0.708	Cruising	Timing (sec)	59.9
	6,016-8,194	75	-0.256		Position (ft)	3,909
	8,194-11,616	40	-0.057	Coasting	Timing (sec)	66.5
	-	-	-		Position (ft)	4,607
Ruling Grade (%)		0.708%		Braking	Timing (sec)	138.1
T_{max} (sec)		150			Position (ft)	10,199

The energy consumption and travel time under the optimal run and the flat-out run (shortest travel time) are compared. For Case I, the optimal train control decreases energy consumption by 32.8 kWh (29.6%), 42.0 kWh (47.9%), and 67.7 kWh (35.7%), while increases travel time by 12.7 seconds (9.3%), 14.5 seconds (8.5%), and 10.1 seconds (6.3%) for a level, convex, and concave alignment, respectively (See Figure 6.18). Note that the number in the parentheses represents the percentage increase (or decrease) in either energy consumption or travel time.

The travel time difference between optimal and flat-out runs on convex alignment is greater than that on the level and concave alignments. Meanwhile, the greatest energy consumption difference between the optimal and flat-out runs is found under the concave alignment. Thus, the consumed energy can be easily reduced with a train control found from a wider range of feasible coasting speeds and positions under the condition that the resulting travel time is less than 170 seconds.

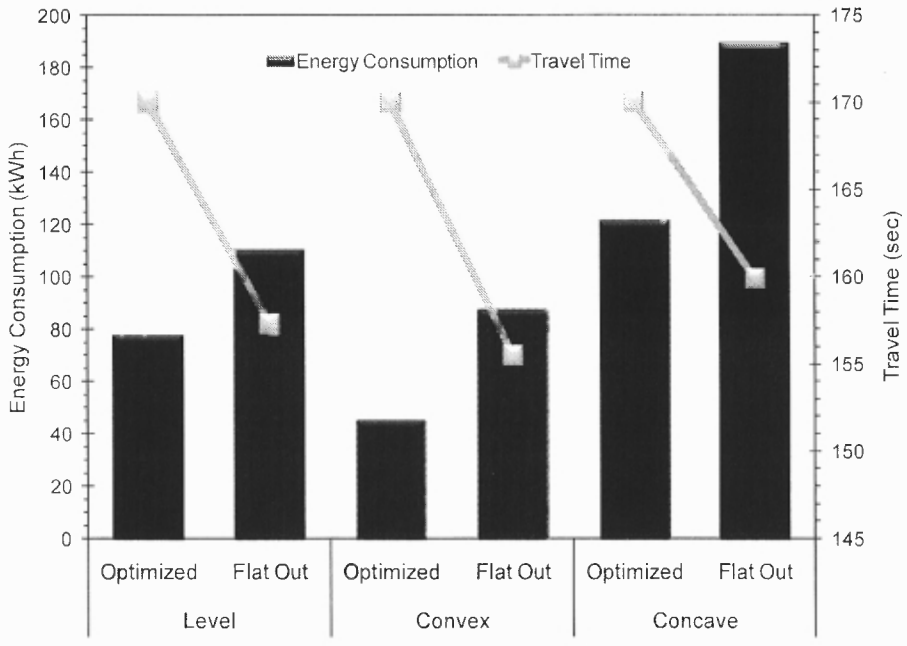

Figure6.18 Energy consumption and travel time vs. track alignment and control (Case I).

For Case II, the amount of saved energy is 46.4 kWh (36%), 35.7 kWh (28.6%), and 67.4 kWh (33.6%), while travel time increases by 13.3 seconds (8.5%), 9.3 seconds (5.8%), and 5.9 seconds (3.6%) for level, convex, and concave alignments, respectively (See Figure 6.19). In Case II, the greatest travel time difference between the optimal and flat-out runs is observed on level alignment, while the biggest energy consumption saved was found by running a train on the concave alignment.

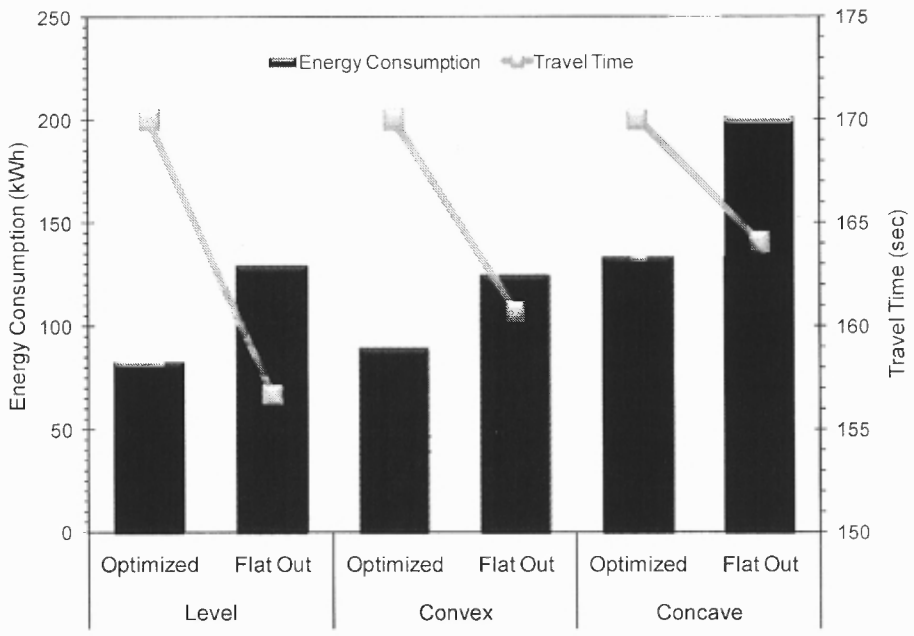

Figure 6.19 Energy consumption and travel time vs. track alignment and control (Case II).

Alternatively for Case III, the reduced energy consumption by using optimal train control is 26.1 kWh (24.1%) with a 9.6 second (5.9%) travel time increase. For Case IV, the saved energy is 17.1 kWh (15.0%), while travel time increases by 7.3 seconds (4.7%). The observed time and energy consumption difference between the optimal and flat-out runs in Cases III and IV are comparatively less than those in Cases I and II, which may result from the track alignment, MOS, and applied motion regimes.

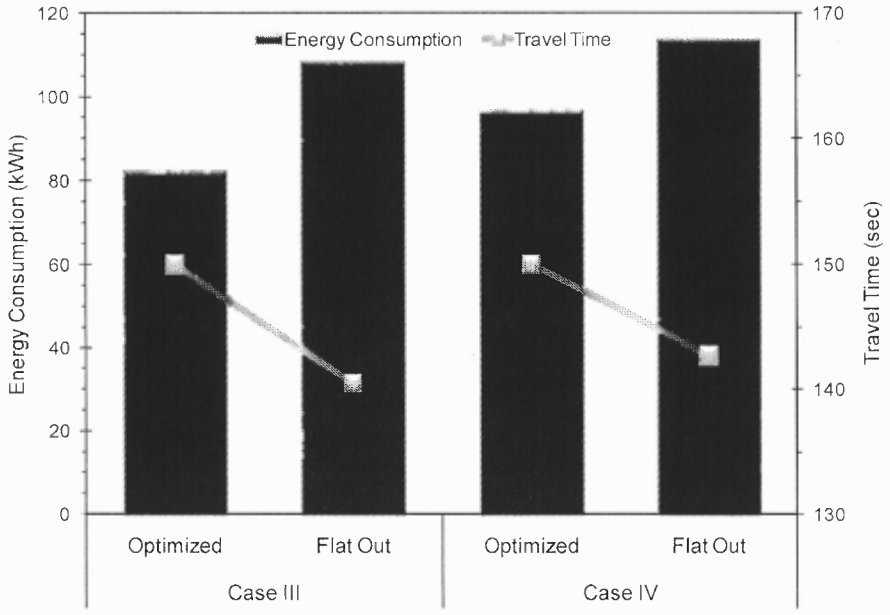

Figure 6.20 Energy consumption and travel time vs. track alignment and control (Case III and IV).

In summary, it was found that the optimal runs achieved in Cases I through IV can save considerable energy in comparison with the flat-out runs by considering any track alignment associated with constant or variable MOS.

6.4 Sensitivity Analysis

Previous sections of this chapter discussed optimized train control under various track alignments considering constant and variable MOS. To investigate the impact of model parameters (i.e., coasting position, travel time constraint, maximum operating speed, vertical depth, and train weight) on train control and energy consumption, a sensitivity analysis is conducted and discussed in this section.

The impact of coasting position and travel time constraint to energy consumption is evaluated by varying the coasting position by 1,000 ft with the coasting speed (V_o')

kept constant. The resulting energy consumption and travel time at various coasting positions on level, convex, and concave alignments in Case I are illustrated in Figures 6.21 through 6.23, respectively. It was found that the earlier the coasting started, less energy was consumed and the travel time increased.

For a level track alignment, the impact of the coasting position on energy consumption and travel time are illustrated in Figure 6.21. The energy consumption and travel time vary with the coasting position commencing at 2,097 ft. Considering the travel time constraint (170 seconds), coasting must be triggered at 3,097 ft or farther from the upstream station; otherwise, the train will be late at the next station. Note that if the coasting is triggered too early (i.e., any location before 3,097 ft), a lower coasting speed (V_o') is prescribed, which results in a considerably increased travel time and will not be a feasible solution.

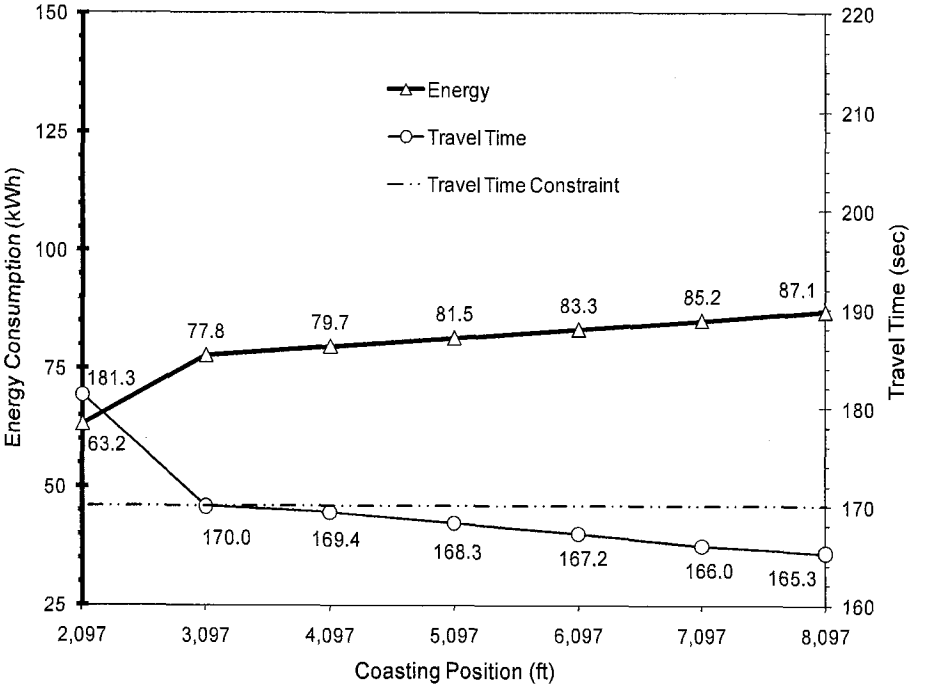

Figure 6.21 Energy consumption and travel time vs. coasting position (Level-Case I).

For a convex alignment, the impact of the coasting position on energy consumption and travel time is shown in Figure 6.22. The energy consumption and travel time nonlinearly vary with the coasting position, which is a result of the track alignment slope. To ensure that the travel time is less than 170 seconds, coasting must be commenced at 5,862 ft or later to satisfy the travel time constraint.

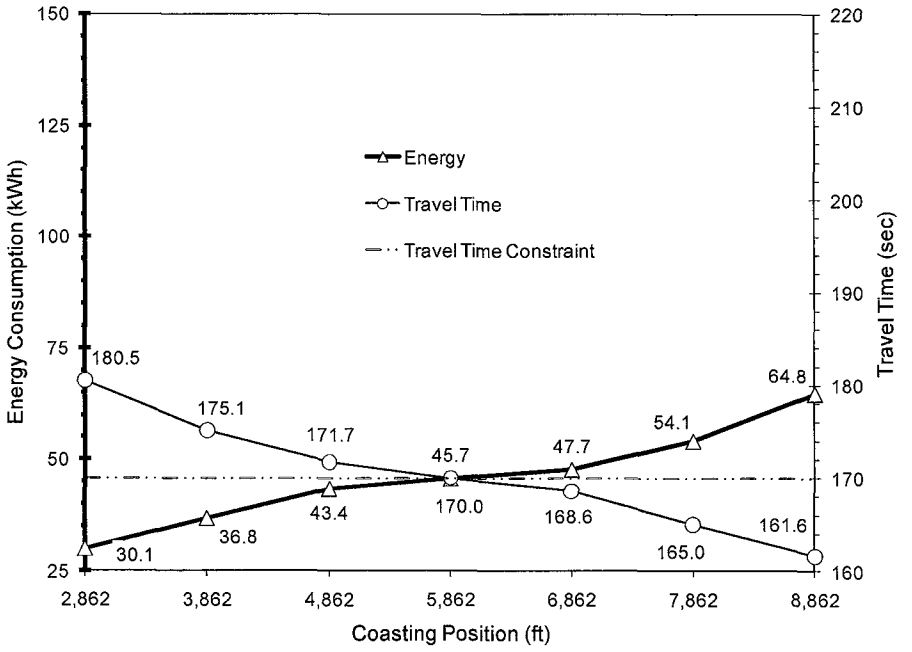

Figure 6.22 Energy consumption and travel time vs. coasting position (Convex-Case I).

Considering a concave alignment, the impact of varying the coasting position on energy consumption and travel time can be observed from Figure 6.23. The energy consumption and travel time vary significantly with the coasting position especially between 1,846 ft and 4,846 ft from the upstream station. If the allowable travel time is 170 seconds, coasting must be triggered at 4,846 ft or later from the upstream station.

Energy consumption and travel time are more sensitive on convex and concave alignments than they are on a level alignment, which is result of the grade. Note that the least attainable energy and travel time are associated with the convex alignment.

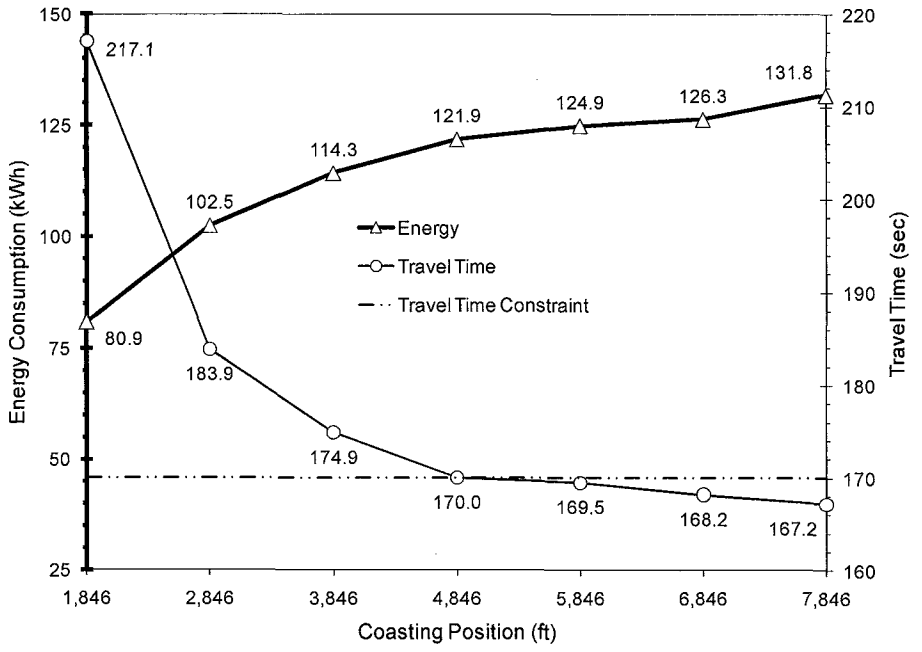

Figure 6.23 Energy consumption and travel time vs. coasting position (Concave-Case I).

The impact of the coasting position and travel time constraint to energy consumption is assessed for Case II, and the resulting energy consumption and travel time at various coasting positions on level, convex, and concave alignments are shown in Figures 6.24 through 6.26, respectively.

For a level track alignment, the impact of coasting on energy consumption and travel time is analyzed by varying the coasting position from 2,880 to 8,880 ft as shown in Figure 6.24. Considering the travel time constraint (170 seconds), coasting must commence at 3,880 ft from the upstream station or later. It was found that the resulting energy consumption with different coasting positions ranged between 63.7 and 120.3 kWh as the coasting position increase, while the corresponding travel times ranged between 188.6 and 159.8 seconds.

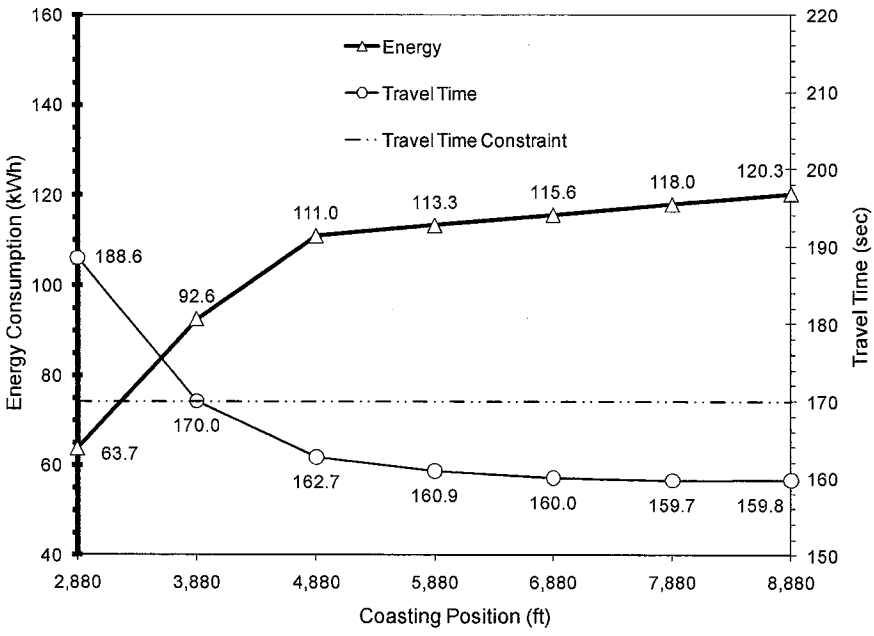

Figure 6.24 Energy consumption and travel time vs. coasting position (Level-Case II).

For a convex alignment, the impact of the coasting position on energy consumption and travel time can be observed in Figure 6.25. To reach the downstream station within the travel time constraint, coasting should be initiated at 3,399 ft or later from the upstream station. It was found that the consumed energy varies from 56.9 kWh to 111.3 kWh, while the corresponding travel time changes from 178.9 seconds to 158.1.

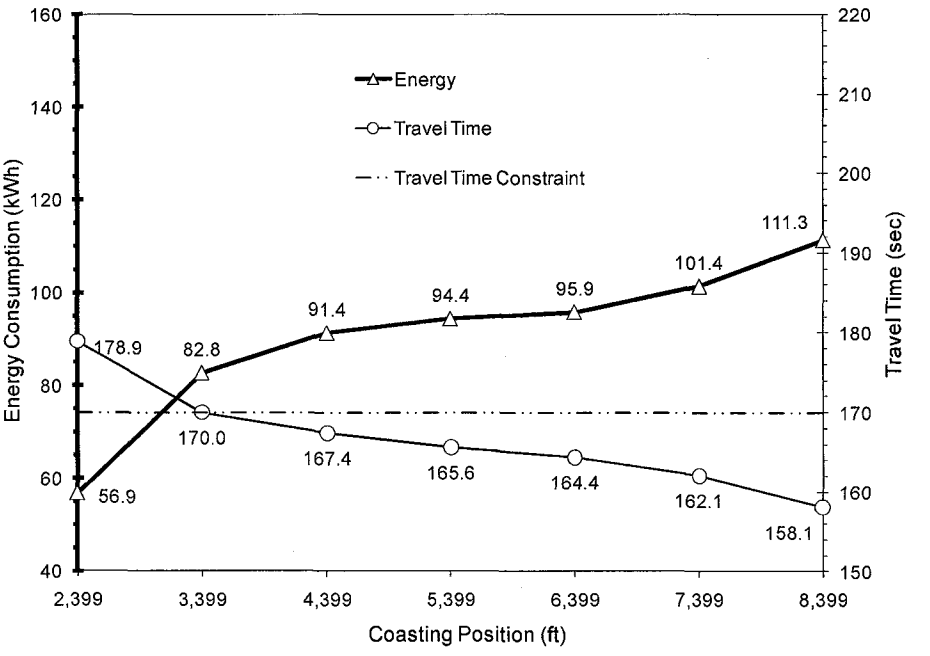

Figure 6.25 Energy consumption and travel time vs. coasting position (Convex-Case II).

For a concave alignment, the impact of coasting on energy consumption and travel time is evaluated and shown in Figure 6.26. The energy consumption and travel time are considerably changed when compared with those on level and convex alignments. To reach the downstream station before the travel time constraint (170 seconds), the train must trigger coasting at 5,007 ft. Note that the train cannot reach the coasting speed (i.e., 60.0 mph) when the coasting regime is triggered at 3,007 ft, which results in a significantly increased travel time.

On the whole, the sensitivity of various coasting positions to energy consumption and travel time in Case II is similar to that observed in Case I. However, the amount of consumed energy and travel time is considerably larger than that observed in Case I because variable MOS (V_{M_1}) makes the train reach V_o' later, which results in an increase of energy consumption and travel time.

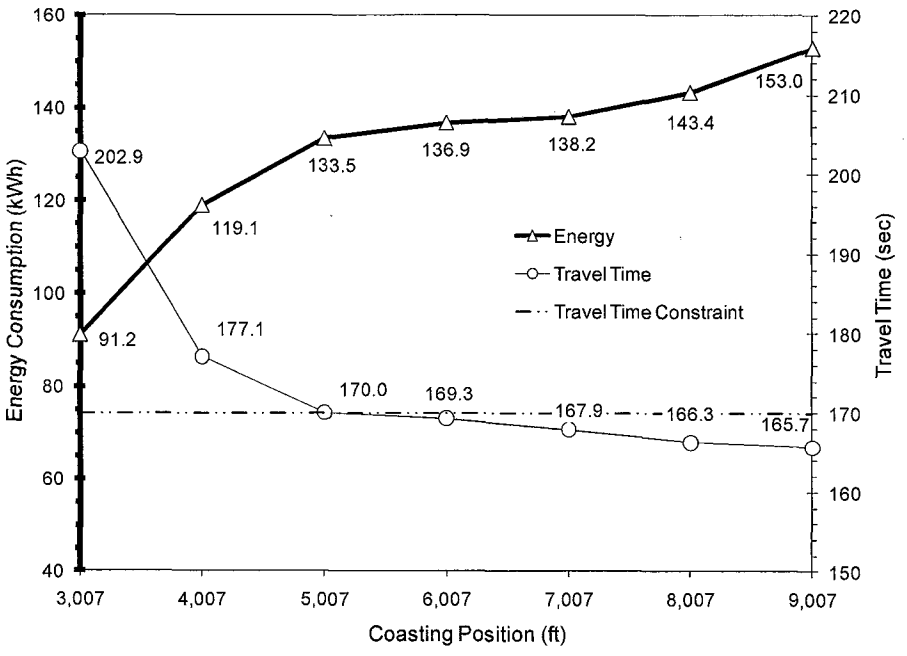

Figure6.26 Energy consumption and travel time vs. coasting position (Concave-Case II).

Figure 6.27 shows the impact of the coasting position on energy consumption and travel time in Case III by varying the coasting position. It was found that the variations of energy consumption and travel time observed in Figure 6.27 are less sensitive than those observed in Cases I and II, which might result from the track alignment, MOS used, and coasting speed. Note that the dashed line indicates the maximum allowable travel time.

Figure 6.28 indicates the resulting energy consumption and travel time at various coasting positions in Case IV. It was found that the energy consumption and travel time are very sensitive to the coasting position, which results from the vertical alignment, similar to an asymmetric shallow concave alignment, and the variable MOS.

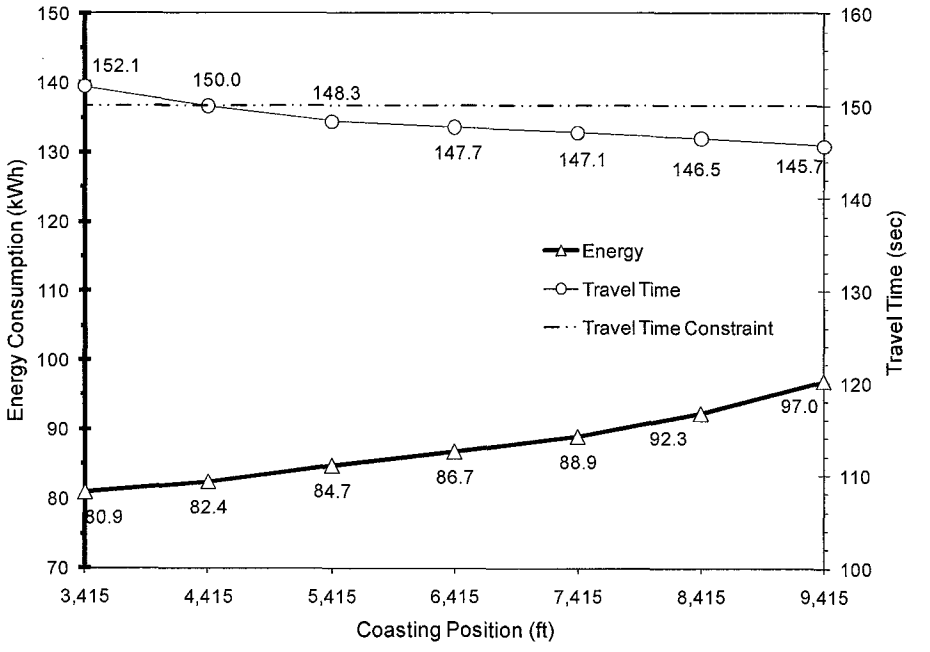

Figure 6.27 Energy consumption and travel time vs. coasting position (Case III).

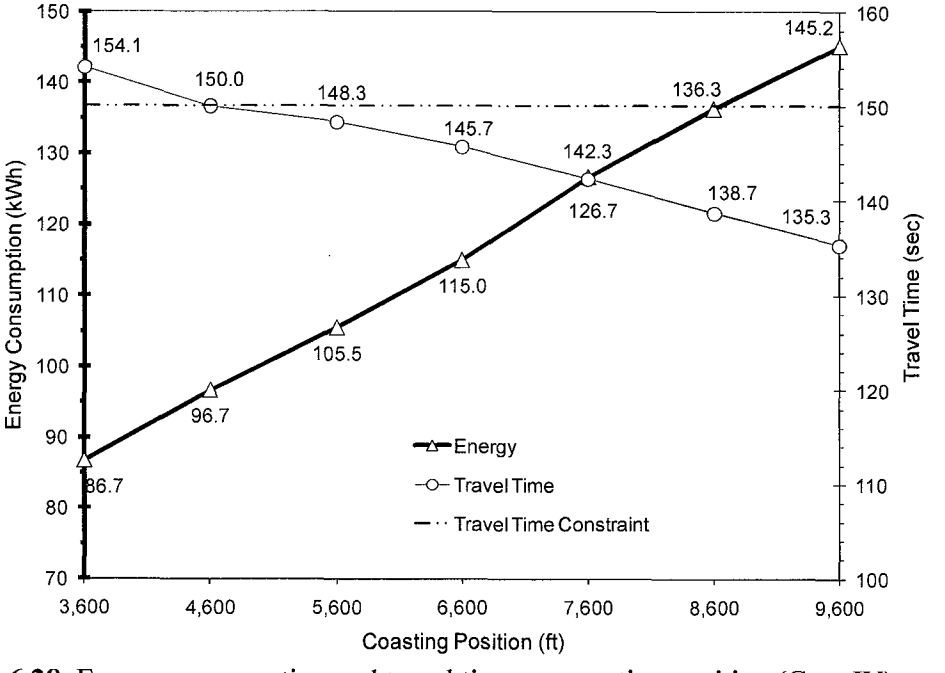

Figure 6.28 Energy consumption and travel time vs. coasting position (Case IV).

Considering the various travel time constraints, the optimal coasting positions which affect energy consumption for level, convex, and concave alignments in Cases I and II are found and illustrated in Figures 6.29 and 6.30, respectively.

In Figures 6.29 and 6.30, the impact of the travel time constraint on coasting position and energy consumption is assessed and illustrated. When the travel time constraint increases (e.g., due to an early arrival of a train at the upstream station), the optimized coasting position is moving towards to the downstream station to further reduce energy consumption. However, if the scheduled travel time is fairly long (e.g., greater than 180 seconds), coasting may be triggered before reaching V_0'. On the other hand, if the travel time constraint is short (e.g., shorter than 160 seconds), the coasting regime should not be used and maximum energy will be consumed, yet the train arrival delay can be reduced. It was found that the optimized coasting positions for the scheduled travel times (e.g., from 160 to 180 seconds) are sensitive to the track alignment and MOS. For example, the energy consumption and coasting position on level alignment are linearly changing by the travel time constraint, while those on convex and concave alignments are changing irregularly. Note that the dashed lines in Figure 6.30 indicate that the coasting speed is out of the feasible speed region.

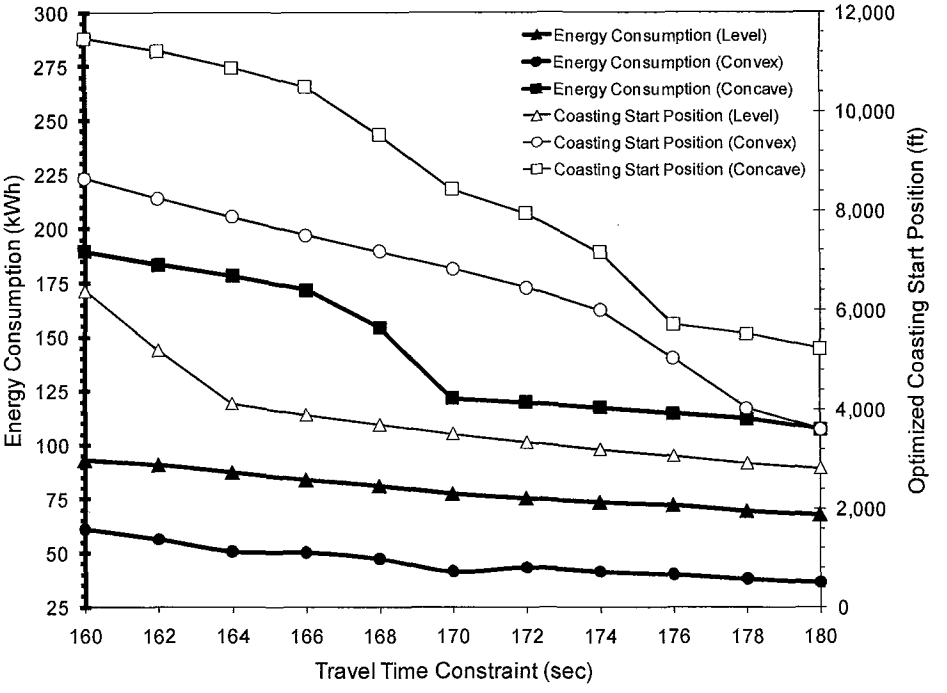

Figure 6.29 Coasting position and energy consumption vs. travel time (Case I).

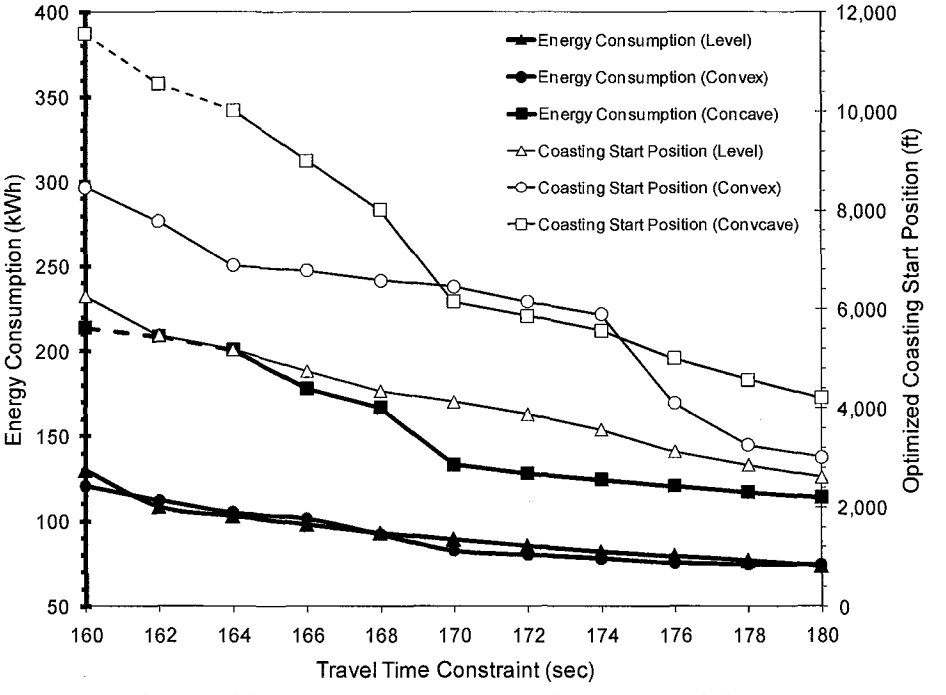

Figure 6.30 Coasting position and energy consumption vs. travel time (Case II).

By varying the allowable travel time, the optimal coasting positions that yield minimum energy consumption for Cases III and IV are shown in Figures 6.31 and 6.32, respectively. It was found that the amount of saved energy is 52.8 kWh, when the travel time constraint increases from that of the flat-out run (i.e., 140.4 seconds) to 160 seconds. Note that the results shown in Figure 6.31 can be utilized to determine an appropriate travel time schedule that can reduce energy consumption by considering the rail transit customers' tolerance.

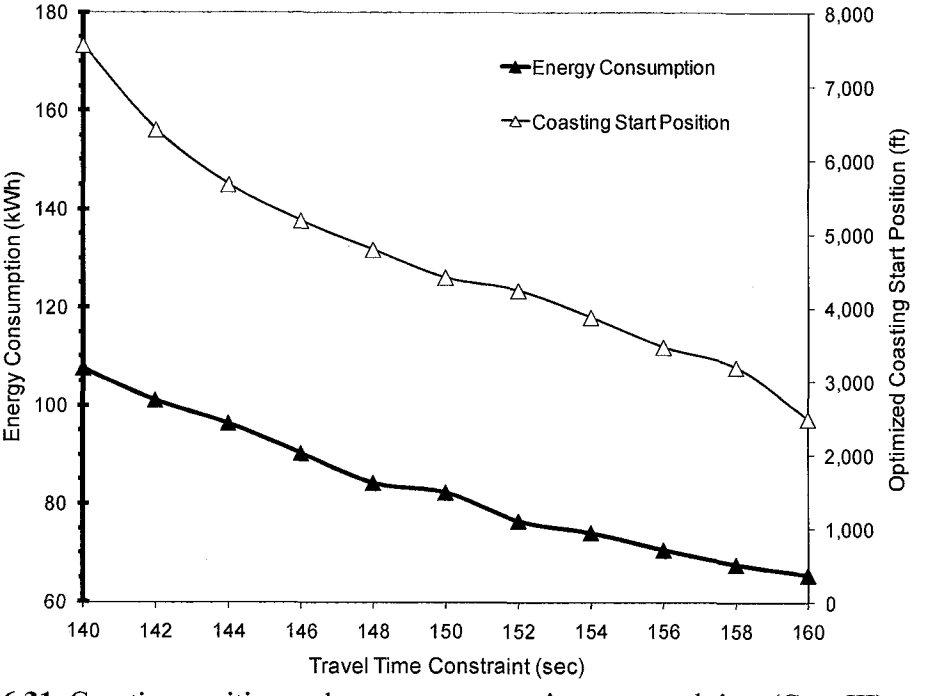

Figure 6.31 Coasting position and energy consumption vs. travel time (Case III).

In Case IV, the amount of saved energy is 85.3 kWh, when the travel time constraint increases from that of the flat-out run (142.7 seconds) to 160 seconds. Note that the dashed line in Case IV indicates that the used coasting speed is greater than V_M (i.e., 75 mph).

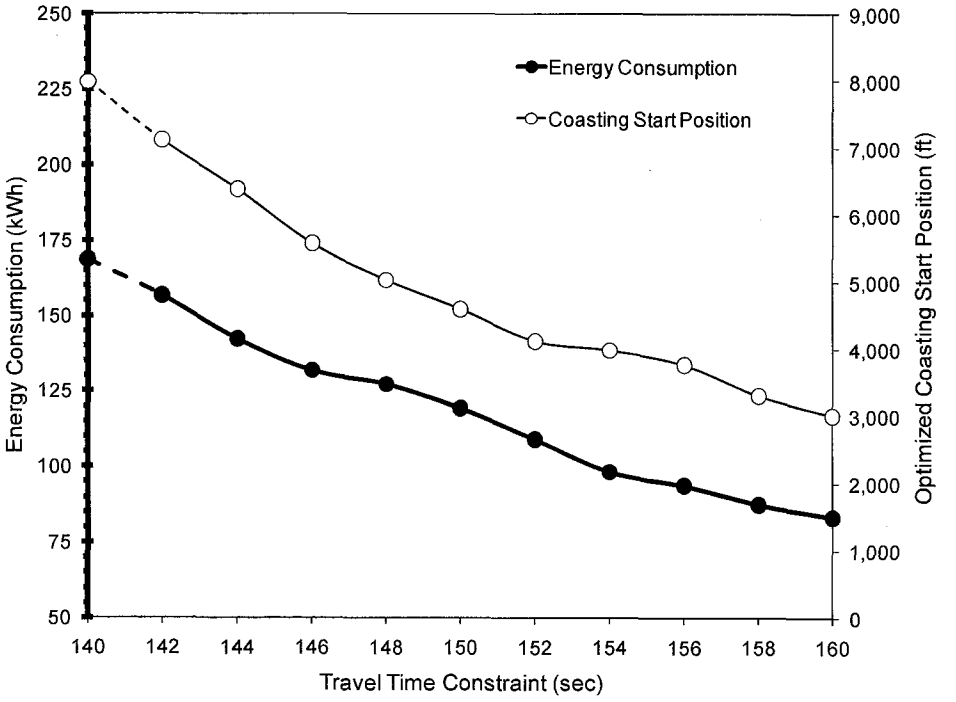

Figure 6.32 Coasting position and energy consumption vs. travel time (Case IV).

In Figure 6.33, the optimal train speed profiles associated with coasting speed (V_o') and position (C_p) for the various maximum allowable travel times (between 140 and 180 seconds) are illustrated for Case III. It was found that while the maximum travel time increases, V_o' increases non-linearly and C_p changes irregularly, which is the direct impact of the vertical track alignment. Note that the results shown in Figure 6.33 can be utilized to determine the optimal coasting speed and position for the various allowable travel times, which are significantly impacted by the downstream traffic condition.

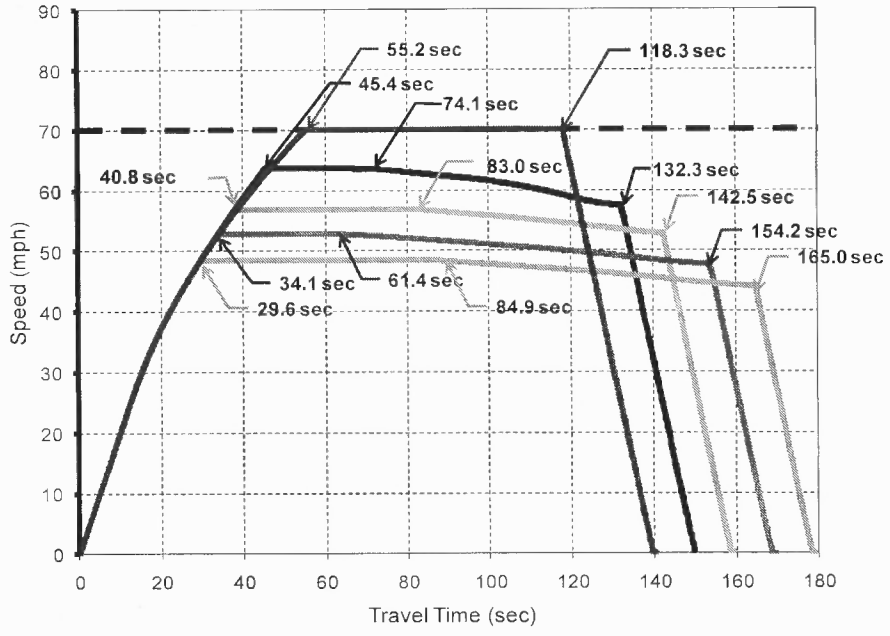

Figure 6.33 Optimal speed profiles vs. maximum allowable travel time.

A sensitivity analysis of the maximum operating speed (i.e., speed limit) with respect to energy consumption and travel time was also conducted. The impact of a maximum operating speed constraint on energy consumption and travel time is evaluated by varying the maximum operating speed by 5 mph. The results of energy consumption and travel time associated with various speed limits on level, convex, and concave alignments in Cases I and II are shown in Figures 6.34 and 6.35, respectively.

It was found that energy consumption on level and concave alignments is more sensitive to the speed limits than that on the concave alignment. In addition, if the speed limit is 83 mph or greater under a given track alignment, energy consumption on the convex alignment is less than that of the level alignment. This result can be utilized to determine the maximum operating speed between level and convex alignments.

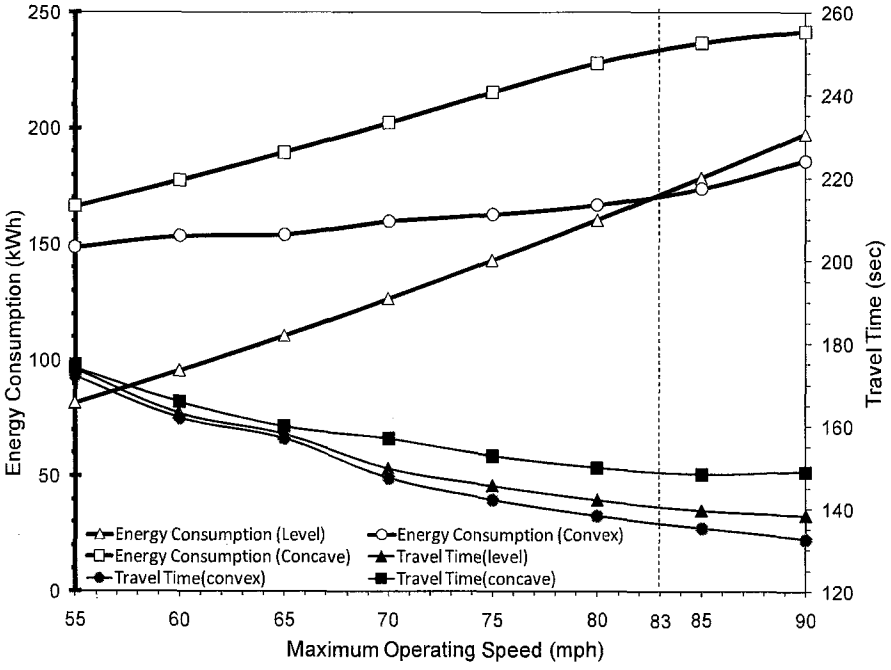

Figure 6.34 Travel time and energy consumption vs. MOS (Case I).

Similarly, the impact of MOS on energy consumption and travel time on level, convex, and concave alignments in Case II is assessed and the results are shown in Figure 6.35. While in Case I with a convex alignment, the energy and travel time are less than those with a level alignment as V_M increases, this result is not valid for Case II, which results from the first MOS (V_{M_1}) that delayed the timing of reaching V_{M_2} (i.e., 70 mph).

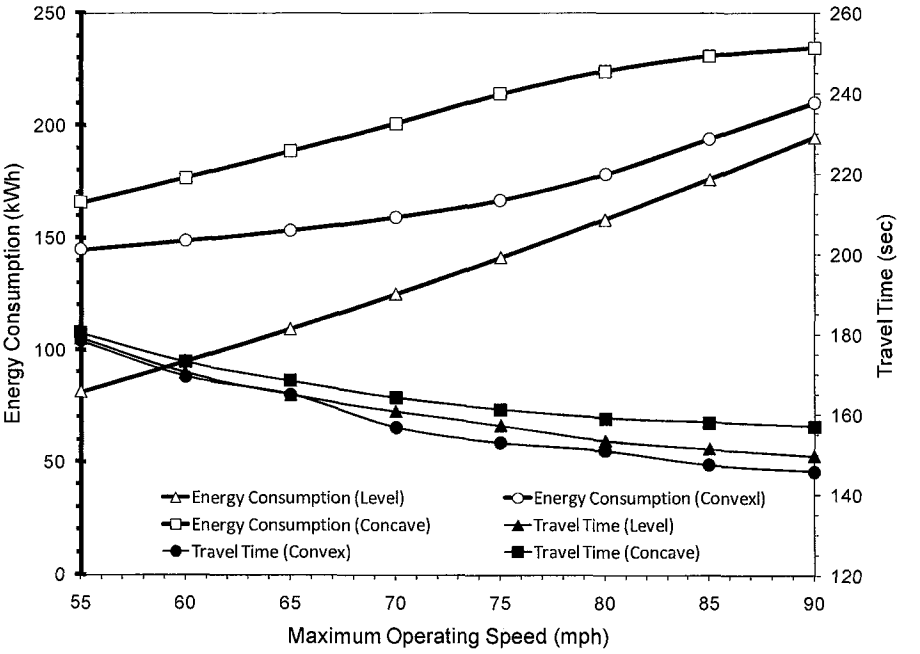

Figure 6.35 Travel time and energy consumption vs. MOS (Case II).

The impact of the vertical dip associated with various maximum operating speeds to energy consumption is investigated by varying the convex alignment depth from 0 ft to 150 ft given a fixed station spacing. The resulting energy consumption distributions with MOS between 55mph and 95 mph are illustrated in Figures 6.36 and 6.37.

Considering the same station spacing and operational conditions as discussed in the previous section, the energy consumption with a convex alignment could be less than that of a level alignment depending on the maximum operating speed. In Figure 6.35, the vertical dip impact of a 12,000-ft convex alignment on energy consumption in Case I is illustrated. It was found that, for example, as the vertical dip increases, the energy consumption decreases with a MOS of 85 mph. However, as the dip exceeds 60 ft, the energy consumption increases. Note that the dip with 0 ft represents a level alignment.

If the used MOS is 55 or 65 mph, the minimum energy consumption is achieved by a level alignment, and the energy consumption increases as the dip increases. It is

recommended that an MOS appropriate for the track alignments should be used to reduce energy consumption. Note that the energy consumption with various maximum operating speeds converges as the vertical dip reaches 150 ft indicating ruling grade of 4.99 %.

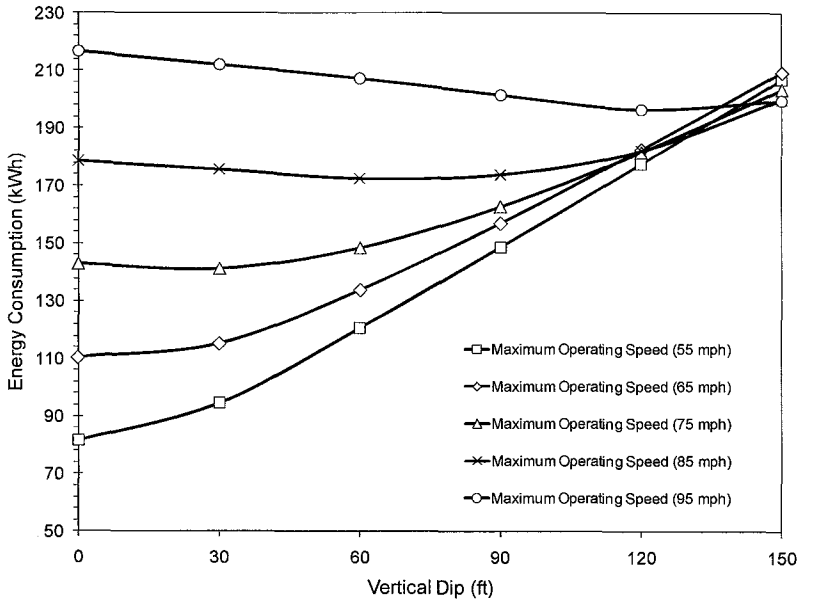

Figure 6.36 Energy consumption vs. vertical dip with various MOS (Case I).

In Figure 6.37, the vertical dip impact with a 12,000-ft convex alignment on energy consumption in Case II is illustrated. It was found that as the vertical dip increases, the energy consumption increases with V_{M_2} varying between 55 and 95 mph. As the first MOS (V_{M_1}) of 40 mph is used from the upstream station to 2,000 ft, the timing of reaching the second MOS (V_{M_2}) is delayed due to the increased acceleration interval for reaching V_o'. As a result, energy consumption increases as the dip increases in Case II.

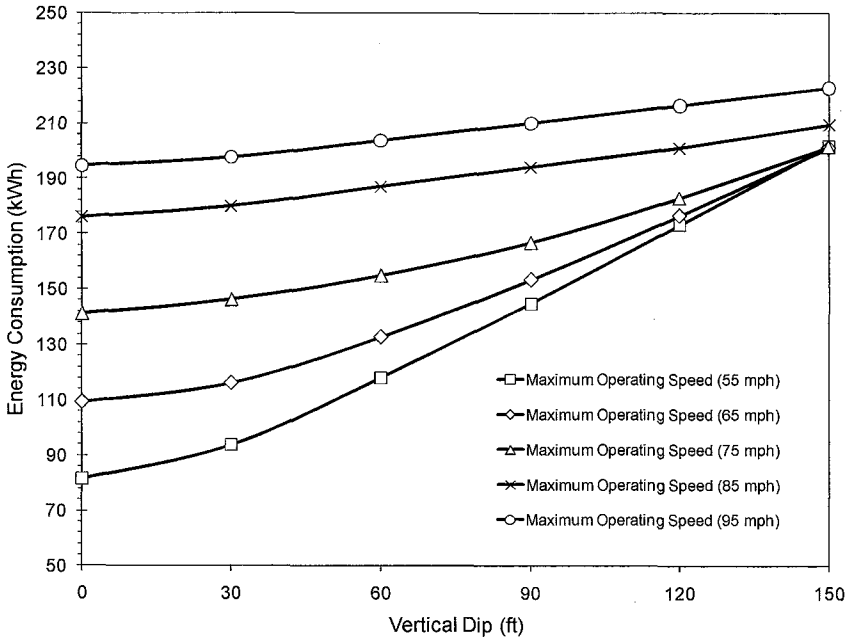

Figure 6.37 Energy consumption vs. vertical dip with various MOS (Case II)

Considering the result of the vertical dip impact on energy consumption for Case I, the most energy efficient MOS for the vertical dip between 0 and 150 ft is identified, and the threshold MOS that energy consumption decreases as the vertical dip increase is found in Figure 6.38. The least energy is consumed with a MOS of 55 mph when the vertical dip is less than 130 ft. As the vertical dip exceeds 130 ft, the track alignment with a MOS of 85 mph should be designed for an energy saving operation. Note that the thick line in Figure 6.38 represents the least energy consumption. In addition, the threshold designed MOS is found to be 71.7 mph, below which the designed vertical dip is recommend to be less than 150 ft subject to a station spacing of 12,000 ft. The results shown in Figure 6.38 can be a reference to determine the energy efficient MOS and dip on a convex alignment.

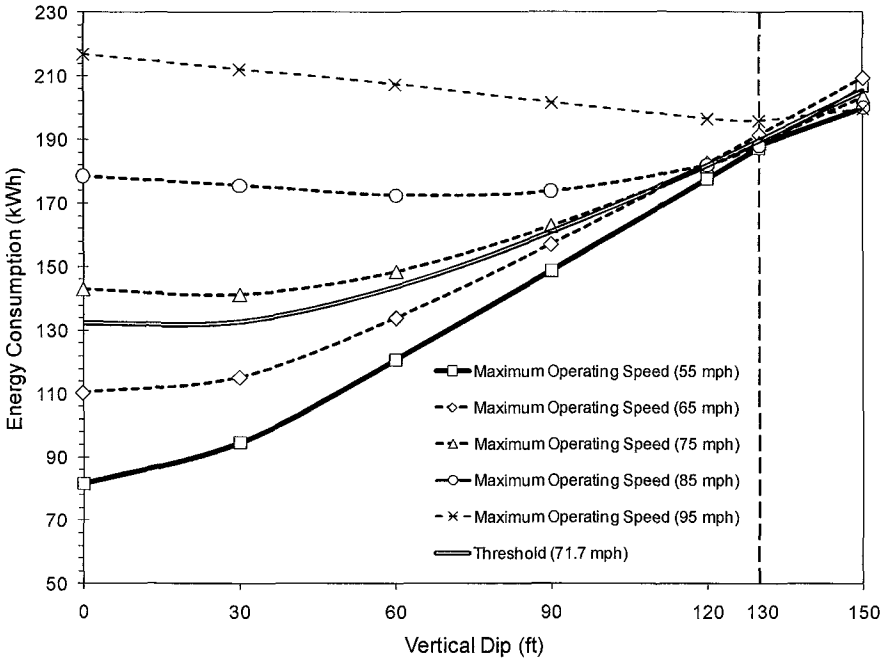

Figure 6.38 Energy consumption vs. vertical dip with threshold MOS (Case I)

The effect of train weight on energy consumption is investigated. As the number of cars per train increases with a fixed motor power, the energy consumption also increases. It was found that a less heavy train equipped with the same power motor must be more energy efficient in the studied example of Cases III and IV. The effect of energy savings by using optimal control is presented in Table 6.7 and increases as the number of cars per train decreases. Note that the train weight does not include passenger load.

Table 6.7 Effect of Train Weight on Energy Consumption (Cases III and IV)

	Number of Cars (cars/train)	Train Weight (lb)	Coasting Speed (mph)	Coasting Position (ft)	Energy Consumption (kWh)
Case III	8	1,004,800	62.4	5,023	63.9
	9	1,130,400	62.9	4,100	72.8
	10*	1,256,000	64.0	4,414	82.4
	11	1,381,600	64.2	4,330	92.4
	12	1,507,200	64.1	4,806	92.5
Case IV	8	1,004,800	69.8	4,987	76.3
	9	1,130,400	70.8	5,003	85.7
	10*	1,256,000	72.0	4,607	96.7
	11	1,381,600	72.6	4,344	104.5
	12	1,507,200	73.4	4,097	113.2

*:baseline values

The results of the optimization model in Cases III and IV are generated based on the train weight without considering the effect of passenger load. Therefore, the impact of passenger load and occupancy rates to energy consumption is evaluated. By assuming that the average passenger weight is 190 pounds (FAA, 2005) and the occupancy rate varies from 0.4 to 1.6 with standees, the energy consumption for Cases III and IV is calculated and illustrated in Table 6.8. It was found that the effect of passenger load on optimal energy consumption is small, but it is increases as the occupancy rate increases. Note that the empty train weight is 1,256,000 pounds.

Table 6.8 The Impact of Passenger Load on Energy Consumption (Cases III and IV)

	Occupancy Rate	Passenger Load (lb)	Coasting Speed (mph)	Coasting Position (ft)	Energy Consumption (kWh)
Case III	0.4	102,600	63.3	4,765	95.1
	0.6	123,120	63.2	4,968	97.2
	0.8	164,160	63.4	4,479	99.4
	1.0*	205,200	63.4	4,967	102.5
	1.2	246,240	63.4	4,692	104.4
	1.4	287,280	63.1	5,198	106.5
	1.6	307,800	63.2	5,261	108.9
Case IV	0.4	102,600	68.6	5,047	107.9
	0.6	123,120	69.8	5,003	109.2
	0.8	164,160	69.8	5,097	110.9
	1.0*	205,200	70.1	5,134	112.3
	1.2	246,240	70.1	5,145	114.2
	1.4	287,280	69.9	5,067	116.5
	1.6	307,800	70.0	5,102	118.3

*:baseline values

The effects of coasting speed and position on energy consumption and travel time for Case III are illustrated in Figure 6.39. It was found that among feasible train controls, more energy is consumed as the coasting regime is triggered later. In particular, if coasting begins at 6,250 ft with a speed between 40 and 52 mph, energy may be saved if the operable travel time is less than the scheduled allowable travel time (T_{max}). The resulting travel times for different coasting speeds and positions are illustrated in Figure 6.40. It was found that, for example, if coasting is triggered after 6,000 ft from the Harrison Station, travel time is less than 150 seconds regardless of the used coasting speed.

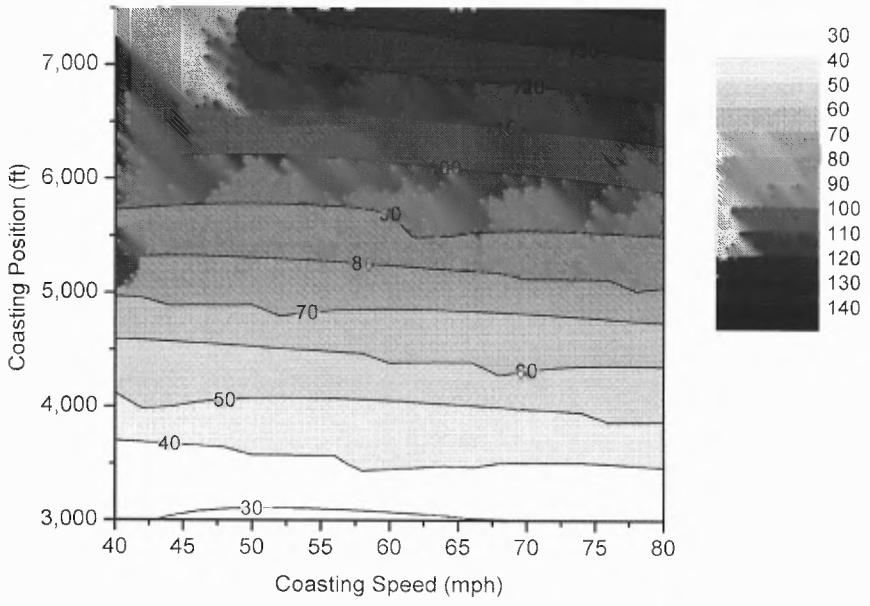

Figure 6.39 Energy consumption vs. coasting speed and position (Case III).

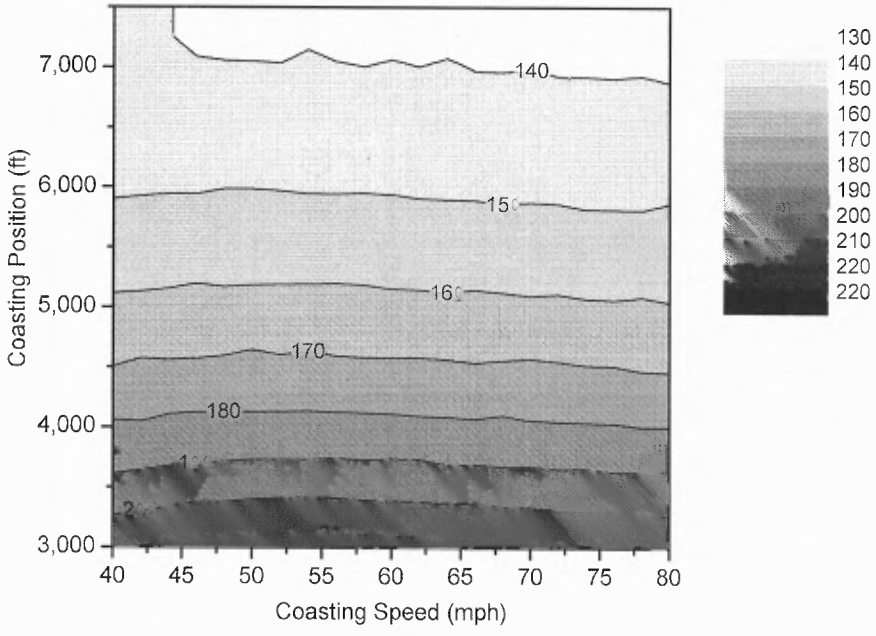

Figure 6.40 Travel time vs. coasting speed and position (Case III).

Similar to Figure 6.39 the impact of coasting speed and position on energy consumption and travel time are investigated and illustrated for Case IV in Figures 6.41 and 6.42, respectively. It was found that more energy is consumed as the coasting regime is triggered later at a higher coasting speed. Especially, the variation of energy consumption is mainly affected by coasting position rather than coasting speed before 6,000 ft when the coasting speed between 40 and 80 mph. However, if the coasting regime is commenced after 6,000 ft, the consumed energy is influenced by both coasting position and speed when the coasting speed is between 40 and 50 mph. For example, the coasting triggered at 7,000 ft with V_0' at 45 mph consumed less energy (approximately 20 kWh) than the coasting triggered at 7,000 ft with V_0' at 80 mph. The resulting travel times for different coasting speeds and positions are illustrated in Figure 6.42.

Note that if the allowable travel time is known, the results of energy consumption and travel time shown in Figures 6.39 through 6.42 can be utilized to determine the appropriate coasting speed and position for the run with minimum energy consumption.

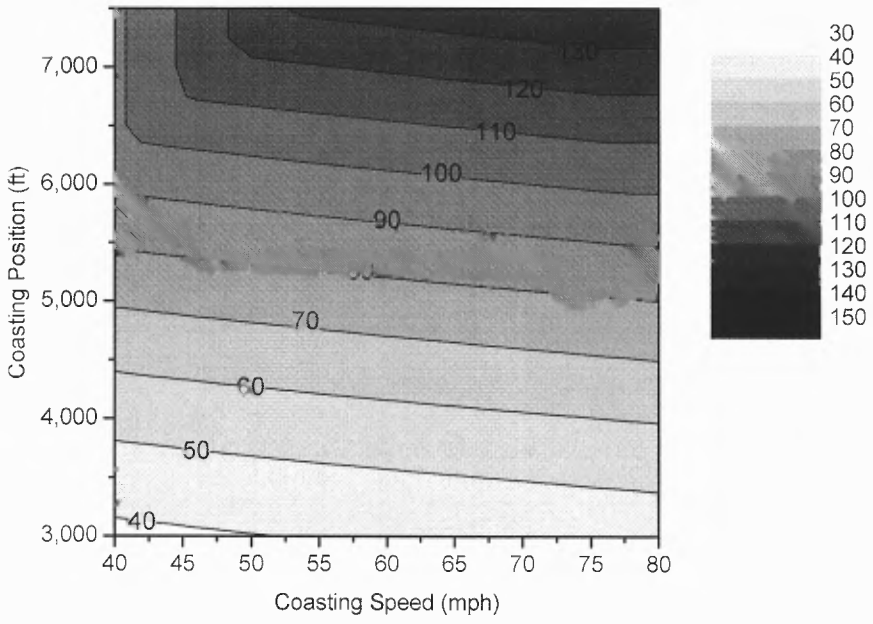

Figure 6.41 Energy consumption vs. coasting speed and position (Case IV).

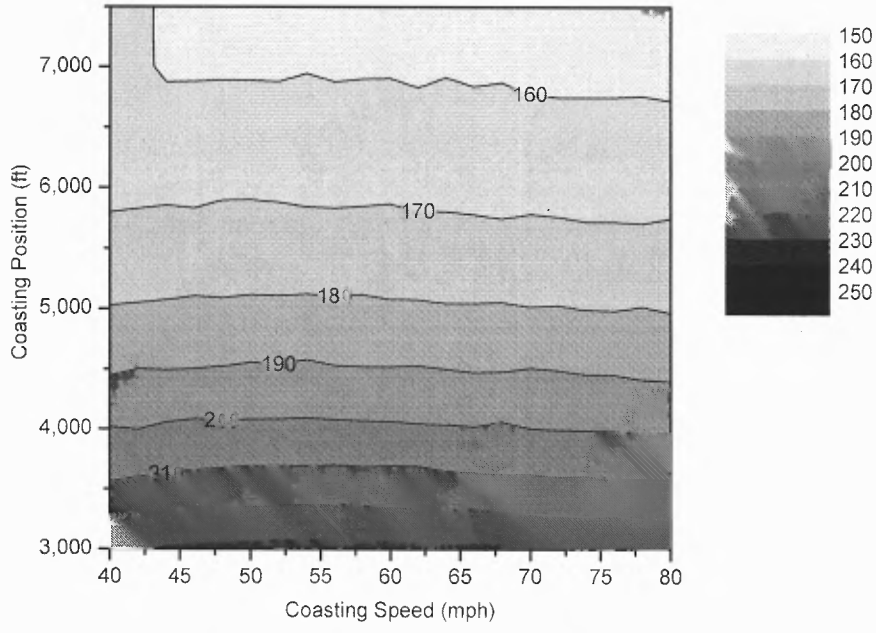

Figure 6.42 Travel time vs. coasting speed and position (Case IV).

CHAPTER 7

CONCLUSIONS AND FUTURE RESEARCH

An optimal train control for minimizing energy consumption of passenger train operations subject to a travel time constraint was developed by exploring combinations of motion regimes as well as the timing and duration of the applied motion regimes. The objective total energy consumption function and sets of model constraints were developed for Cases I through IV, while a Train Performance Simulation (TPS) model that simulates train movement, calculates energy consumption, and estimates travel time was developed, and a meta-heuristic, Simulated Annealing algorithm (SA) was used to search for the optimal solution.

A real world example of the Metro-North Railroad's New Haven Line was introduced to demonstrate the applicability of the developed models and solution algorithm to optimize the studied problem. The scheduled maximum allowable travel time, maximum operating speed, and maximum acceleration/deceleration rate were of concern in the models developed to optimize total energy consumption. Sensitivity analyses were conducted for investigating the relationship among important decision variables and model parameters.

7.1 Conclusions

Subject to a maximum operating speed which varies by track alignments and operating condition as well as the maximum allowable travel time and maximum acceleration (or deceleration) rate, the optimal train control that minimizes energy consumption can be

found through the SA algorithm. The major findings and conclusions are the as following:

(1) Developed model and solution algorithm

- The developed time-driven TPS model can be used to effectively simulate train movement, calculate energy consumption, and estimate travel time, considering various vertical track alignments and control regimes. In addition, the intermediate results of acceleration (or deceleration) rate, speed, energy consumption rate, and travel distance can be generated according to the user specified time interval.

- Given specific train characteristics, track alignment, and travel time schedule, the developed models found the optimal coasting (or cruising) speed and position that yield minimum energy consumption.

- The developed SA algorithm is a suitable searching approach for the optimal solution of the studied energy minimization problem. The parameters of SA, including perturbation, acceptance schedule, cooling schedule, and fitness function, were calibrated using the benchmark solution solved by Simulated Annealing (Chen, 2003). In this study, the exponential cooling schedule was used for the developed SA, and it achieved more satisfactorily optimized solutions after multiple iterations than the linear cooling schedule.

- The developed models can be utilized to optimize the energy consumption of a passenger rail transit, if the track vertical alignment, allowable travel time, maximum operating speed, and train characteristics are available. In particular, the developed model and results of this study could be considered by modern train control systems (e.g., ATC, ATO, PTC, etc) for energy efficient train scheduling and operation subject to travel time and speed constraints.

- A dipped track alignments provides considerable savings of energy and time although it may cost more to construct. However, construction cost can be redeemed by the reduced energy and travel time.

(2) Optimal result and sensitivity analysis

- The results (See Figure 6.18) of energy consumption on the single vertical alignments (level, convex, and concave) in Case I indicated that a convex track alignment [e.g., 90 ft dip and 0.75 % dip ($100\delta / S$)] brought considerable benefits including a 42 kWh (47.9%) reduction of energy consumption and a travel time increase of 14.5 seconds (8.5%), which satisfies the maximum operating speed constraint and allows sufficient momentum to perform coasting. However, the results of energy consumption in Case II shows that the benefit of track alignment (e.g., same as the Case I) on energy consumption might be considerably reduced if the maximum operating speed is low.

- The impact of the coasting position and travel time constraint to energy consumption is evaluated by varying the coasting position with a fixed coasting speed. The resulting energy consumption and travel time at various coasting positions on level, convex, and concave alignments as well as real world track alignments in Cases I through IV are illustrated (See Figure 6.19 through 26). Given a set of energy consumption and travel time results based on various coasting positions, it is viable to save energy under any operational event (e.g., earlier arrival or delay) that causes deviations from the scheduled travel time

- When the allowable travel time increases (e.g., due to an early arrived train at the upstream station), the optimal coasting position is shifting towards the downstream station. However, if the allowable travel time is long enough, coasting may be triggered before reaching the maximum operating speed (See Figures 6.29 through 6.32). On the other hand, if the allowable travel time is shorter than the minimum travel time, the coasting regime will not be used.

- The impact of the maximum operating speed on energy consumption and travel time in Case I (See Figure 6.33) indicated that the energy consumption incurred with the level and concave alignments is more sensitive than that incurred with the convex alignment. In addition, if the maximum operating speed is 83 mph or greater, the consumed energy incurred on the convex alignment is less than that on the level alignment.

- The impact of vertical dip associated with maximum operating speed to energy consumption is investigated by varying the dip of the convex alignment. It was found (Figure 6.35) that energy consumption is very sensitive to the vertical dip as well as the applied maximum operating speed (V_M). In addition, the resulting energy consumption at various dips can be employed to search for the most energy efficient vertical dip and maximum operating speeds (Figure 6.37).

- The impact of passenger load on energy consumption for Cases III and IV was investigated by assuming that the average passenger weight is 190 pounds (FAA, 2005) and the occupancy rate varies from 0.4 to 1.6 considering standees. It was found that the energy consumption increases slightly as the occupancy rate increases (See Table 6.8) since the train mass is the major contributor to the weight of a train.

- The results of the sensitivity analyses (See Figures 6.21 through 6.40 and Tables 6.7 and 6.8) that produce the relationship between energy consumption and travel time versus various operation conditions can be utilized to generate guidelines for energy-efficient train control

- The optimal results can be a reference to design a new train schedule when the value of customer's tolerance and energy saving are known.

7.2 Future Research

Future research areas related to the energy minimization problem are listed below:

- The modified Davis equation used in the TPS was developed based on a surface railroad system, which may not perfectly fit an underground system (i.e., subway) because the wind effects on train movement are different. Thus, the train resistance equation needs to be enhanced to handle the wind effect while the train is running in a tunnel.

- The developed SA algorithm can be enhanced by incorporating the Genetic Algorithm to reduce the gap between the final and optimal solution. With population-based state transition, the efficiency in the algorithm can achieve a gap between the final and optimal solution of less than 3 % and reduce the computation time. (Lin et al., 1993).

- An immediate extension of this study is to enhance the developed model by considering various station spacings (e.g., ≥ 2 miles) and maximum operating speed (i.e. speed limit). To achieve optimal train control for longer station spacing, there may be a need to trigger multiple coasting regimes.

- Some factors that may affect energy-saving operations (e.g., including coasting, train weight, scheduled travel time, etc.) were identified. Other factors, such as customers' needs and tolerance, the value of saved energy, etc. may be of concern when balancing the impact of travel time/schedules and energy savings.

- The impact of the length of a car to the variation of track slope as well as the effect of the number of cars per train on optimal control can be investigated in a future study. The number of cars per train may be limited subject to the track alignment, tractive effort, maximum operating speeds, and service frequency needed to accommodate passenger demand.

- The coasting used in this research allows the train speed to deviate from the maximum speed when triggered. However, a different type of coasting, whereby a train traction system locks the train into a narrow speed range (i.e. constant speed command) may be considered while optimizing train control in a future study. In addition, the conditions (e.g., station spacing, service frequency, operational constraint, and rolling stock characteristics, etc.) for two different coasting can be compared.

- While the model described helps to find the right balance of power consumption and travel time, its usefulness may be limited. Operator driven rail vehicles will hardly adhere to the given acceleration and speed scheme unless a sophisticated train control system (ATC, ATO, PTC, etc.) is in place. This also would require a short distance block layout and frequent for speed.

- The optimal train speed profile derived in this study can be considered for the planning and operation of signals for controlling train speed over a line. According to the study by Dongen and Schuit (1989), energy efficient train control can be implemented with educated train drivers. Although the actual train speed operated by drivers may not be the same as suggested, energy may still be saved.

- The impact of light braking on energy consumption will be estimated by enhancing the train model to include a regenerative braking system (RBS) that stores braking energy into a battery or condenser bank for later use.

REFERENCES

Albrecht, T. 2004. *Improvements of Energy Efficiency of Urban Rapid Rail Systems*: 573-582, WIT Press.

American Public Transportation Association. 2003. Average New Rail Vehicle Costs, http://www.apta.com/research/stats/rail/railcost.cfm [accessed November18, 2007].

American Railway Engineering Association (AREA). (1984). *Manual for Railway Engineering,* Washington, D.C.

Baselga, S. 2007. Global Robust Estimation and Its Application to GPS Positioning, *Computers and Mathematics with Applications*, 56 (3): 709-714.

Bernsteen, S. A., Uher, R. A., and Romualdi, J P. 1983. Interpretation of Train Rolling Resistance From Fundamental Mechanics. *IEEE Tractions on Industry Applications*, IA-1 (5): 802-817.

Black, J.A., Paez, A., and Suthanaya, P. A. 2002. Sustainable Urban Transportation: Performance Indicators and Some Analytical Approaches, *Journal of Urban Planning and Development*, 128 (4): 184-209.

Bocharnikov, Y.V., Tobias, A.M., Roberts, C., Hillmansen, S., and Goodman, C.J. 2007. Optimal Driving Strategy for Traction Energy Saving on DC Suburban Railways, *IET Electrical Power Applcation*, 1 (5): 675-682.

Busetti, F. 2003. Simulated Annealing Overview, geocities.com/francorbusetti [accessed December 10, 2008]

Chang, C.S., Chua, C.S., Quek, H.B., Xu, X.Y., and Ho, S.L. 1998. Development of Train Movement Simulator for Analysis and Optimization of Railway Signaling Systems, *International Conference on Developments in Mass Transit Systems* 543: 20-23

Chang, C. S., and Sim, S. S. 1997. Optimizing train movements through coast control using genetic algorithms. *IEE Proceedings: Electric Power Applications* 144 (1): 65-72

Chen, C. H. 2003. Integrated Management of Highway Maintenance and Traffic. Ph.D. Dissertation, University of Maryland, College Park.

Danziger, N. H. 1975. Energy Optimization for Rail Public Transit Systems, *Transportation Research Record*, 552: 31-39.

Davis Jr., W.J. 1926. Tractive resistance of electric locomotives and cars. *General Electric Review* 29: 685-708.

Davis, S. C and Diegel, S. W., and Boundy, R. G. 2008. Transportation Energy Data Book: Edition 27. Oak Ridge National Laboratory; Department of Energy.

Dongen, L. A. M., and Schuit, J. H. 1989. Energy-efficient driving patterns in electric railway traction. *IEE Conference Publication* (312): 154-158

Durate, M. A. and Sotomayor, A. X. 1999. Minimum energy trajectories for subway systems, *Optimal Control Applications and Methods* 20 (6): 283-286.

Energy Information Administration. Average Revenue per Kilowatt-hour from Retail Sales to Ultimate Consumers - Estimated by Sector, by State. http://www.eia.doe.gov/cneaf/electricity/epm/table5_6_a.html. (accessed August 18, 2007).

Federal Aviation Administration. 2005. Advisory Calculator – Aircraft Weight and Balance Control. Flight Standard Service, Washington D. C.

Filipovic, Z. 1995. Elektrische Bahnen, Springer-Verlag, Berlin-Haidelberg-New York: 23-27

Fleischer, Mark. 1995. Simulated Annealing: Past, Present, and Future.Proceedings of the 1995 Winter Simulation Conference, Department of Engineering Management, Old Dominion University, Norfolk, VA

Franke, R., Terwiesch, P., Meyer, M. 2000. An algorithm for the optimal control of the driving of trains, *Proceedings of the 39th IEEE Conference on Decision and Control*, 3: 2123-2128

Golovitcher, I.M. 2001. Energy Efficient Control of Rail Vehicles. Systems, Man, and Cybernetics, *IEEE International Conference*, 1: 658-663.

Gordon, S.P. and Lehrer, D.G. 1998. Coordinated train control and energy management control strategies. *Railroad Conference. Proceedings of the 1998 ASME/IEEE Joint*: 165-176

Han, S., Byen, Y., An, T., Lee, S., and Park, H. 1999. An optimal automatic train operation (ATO) control using genetic algorithms (GA). *Proceedings of the IEEE Region 10 Conference*, 1: 360-362.

Hay, W. W. 1982. *Railroad Engineering, 2nd Ed.* John Wiley & Sons, Inc., New York, N.Y

Hiraguri, S., Y. Hirao, I. Watanabe, N. Tomii, and S. Hase. 2004. Advanced train and traffic control based on prediction of train movement. *JSME International Journal, Series C: Mechanical Systems, Machine Elements and Manufacturing* 47, (2): 523-528

Hoberock, L.L. 1977. A Survey of Longitudinal Acceleration Comfort Studies in Ground Transportation Vehicles. *ASME Transactions, Journal of Dynamic Systems, Measurement and Control*, 99 (2): 76-84

Hopkins, J. B. 1975. Railroads and the environment—estimation of fuel consumption in rail transportation Volume I: Analytical model." *Final Rep. No. FRA-OR&D-75-74.I to U.S. Federal Railroad Administration, Rep. No. PB-244150*, National Technical Information Service, Springfield, VA.

Horn, P. 1971. Uber die Anwendung des Maximum-Prinzips von Pontrjagin zur Ermittlung von Algorithmenfur eine energieoptimale Zugsteuerung Was*senschaftliche Zeitschrift der Hochschule fur Verkehrswesen "Fhedrich List" in Dresden,* 18(4).

Howard, S.M., Linda, C.G., and Wong, P.J. 1983. Review and Assessment of Train Performance Simulation Models, *Transportation Research Record* 917: 1-6.

Howlett, P. G., and Pudney P. J. 1995. Energy-efficient train control, Series in advances in industrial control, Springer, London.

Hoyt, E. V. and Levary, R.R. 1990. Assessing the Effects of Several Variables on Freight Train Fuel Consumption and Performance Using a Train Performance Simulator. *Transportation Research Part A*. 24A (2): 99-112.

Hwang, H. S. 1998. Control strategy for optimal compromise between trip time and energy consumption in a high-speed railway. *IEEE Transactions on Systems, Man, and Cybernetics Part A:Systems and Humans.* 28, (6): 791-802.

Isaev, I. P. and Golubenko,A. L.1989. Improving experimental research into adhesion of the locomotive wheel with the rail. *Rail Int.*, 20(8-9): 3-10.

Jeon, C M and Amekudzi, A. 2005. Addressing Sustainability in Transportation Systems: Definitions, Indicators, And Metrics. *American Society of Civil Engineers.*

Jong, J.C. and Chang,S. 2005. Algorithms for Generating Train Speed Profiles. *Journal of the Eastern Asia Society for Transportation Studies*, 6: 356-371.

Kenworthy, J and Laube, F. 1999. *The Significance of Rail In Building Competitive And Effective Urban Public Transport Systems: An International Perspective.* World Markets Research Centre

Khmelnitsky, E. 2000. On an optimal control problem of train operation. *IEEE Transactions on Automatic Control* 45 (7): 1257-1266.

Kikuchi, S. A. 1991. Simulation Model of Train Travel on a Rail Transit Line. *Journal of Advanced Transportation*, 25(2) (1991): 211-224.

Kim, D. N. and Schonfeld, P. M. 1997. Benefits of Dipped Vertical Alignments for Rail Transit Routes, *Journal of Transportation Engineering* 123: 20-27.

Kim, K. and Chien, S. 2009. Simulation Analysis of Energy Consumption for Various Train Control and Track Alignment, *Transportation Research Board.*

Kim, K. and Chien, S. 2010. Optimal Train Operation for Minimum Energy Consumption Considering Schedule Adherence, *Transportation Research Board.* (forthcoming)

Kirkpatrick, S., Gelatt, C.D., and Vecchi, M.P. 1983. Optimization by Simulated Annealing, *Science* 220: 671-680.

Koo, S. L, Tan, H. S., and Tomizuka, M. 2006. Analysis of vehicle longitudinal dynamics for longitudinal ride comfort. *American Society of Mechanical Engineers, Dynamic Systems and Control Division*

Lin, F.T., Kao, C.Y., and Hsu, C.C. 1993. Applying the genetic approach to simulated annealing in solving some NP-hard problems. *IEEE Transaction on System, Men, and Cybernectics.* 23 (6): 1752-1767.

Lipetz, A. I. 1935. Diesel Engine in Rail Transportation, *Engineering Bulletin Research Series 49*, Purdue University, Lafayette, Indiana.

Lukaszewicz, P. 2000. Driving Techniques and Strategies for Freight Trains: 1065-1073, WIT Press.

Lukaszewicz, P. 2002. *Driving Describing Parameters, Energy Consumption and Running Time: Results and Conclusions from Measurements and Simulations.* WIT Press.

Lukaszewicz, P. (2004) *Energy Saving Driving Methods for Freight Trains*, pp. 901-909, WIT Press.

Lukaszewicz, P. 2006. *Impact of Train Model Variables on Simulated Energy Usage and Journey Time*: 723-731,WIT Press.

Lukaszewicz, P. 2007. Running Resistance - Results and Analysis of Full-Scale Tests with Passenger and Freight Trains in Sweden. *Institution of Mechanical Engineers.*

Luethi, M., Weidmann, U. A., Laube, F. B., and Medeossi, G. 2007. Rescheduling and Train Control: A New Framework for Railroad Traffic Control in Heavily Used Networks. *Transportation Research Board*

Martin, P. 1999. Train Performance and Simulation, Proceedings of the 31st conference on Winter simulation: Simulation-a bridge to the future, 2: 1287-1294.

Martinez, J. J., and Canudas-De-Wit, C. 2004. Model reference control approach for safe longitudinal control. *Proceedings of the American Control Conference*, 3: 2757-2762

Mellitt, B. 1987. Energy Minimization Using an Expert System for Dynamic Coast Control in Rapid Transit Trains, *Institution of Engineers Australia.*

Metropolis, N., Rosenbluth, A. W., Rosenbluth, M., Teller, A. H., and Teller, E. 1953. Equation of State Calculations by Fast Computing Machines." *Journal of Chemical Physics.* 21: 1087-1092.

Minciardi, R., Savio S., and Sciutto G. 1994. Models and Tools for Simulation and Analysis of Metrorail Transit Systems, *Computers in Railways IV*, 1: 391-402.

Muhlenberg, J.D. 1978. Resistance of a Freight Train to Forward Motion - Volume 1: Methodology and Evaluation. Metrek Division, Mitre Corporation, McLean, VA, Report PT-280 969

Nash, Andrew Butler and Weidmann, Ulrich and Bollinger, Stephan and Luethi, Marco and Buchmueller, Stefan. 2006. *Increasing Schedule Reliability on the S-Bahn in Zurich, Switzerland: Computer Analysis and Simulation. Transportation Research Board.*

Nouvion, F. 1968. The French High Speed Motor Units, *French Railway Techniques*, 11 (2): 79-95.

Ohyama, T. 1989. Some basic studies on the influence of surface contamination on adhesion force between wheel and rail at high speed. *Q. Rep. Railway. Tech. Res. Inst.*, 30(3): 127-135.

Ohyama, T. and Shirai, S. 1982. Adhesion at Higher Speeds and Its Control. *RTRI (Japan) Quarterly Reports*, 23(3): 97-104.

O'Toole, Randal. 2008. *Does Rail Transit Save Energy or Reduce Greenhouse Gas Emissions?*, CATO Institute.

Peckham, Christian. 2007. Improving the Efficiency of Traction Energy Use: Summary Report. *Rail Safety and Standards Board.*

Press, W. H., Flannery B. P., Teukolsky S. A. and Vetterling W. T. 1988. *Numerical Recipes (Fortran Version)*, Cambridge University Press, New York, NY

Profillidis, V. A. 1995. *Railway Engineering*, Ashgate Publishing Company, Brookfield, VT.

Richardson, B. 2000. Role of Motor-Vehicle Industry in a Sustainable Transportation System, *Transportation Research Record* 1702: 21–27

Schwarzkopf, A. B., and Leipnik, R. B. 1977. Control of highway vehicles for minimum fuel consumption over varying terrain. *Transportation Research Board*, 279-286: 11- 46.

Schmidt, E. C. 1935. Freight Train Resistance and Its Relation to Average Car Weight, *University of Illinois Engineering Experiments Station Bulletin*, 31 (48), Urbana, Illinois

Schultz, G and Tong, I and Kefauver, K and Ishibashi, J. 2005. *Steering and Handling Testing Using Roadway Simulator Technology*. Inderscience Enterprises Limited.

Sinha, K. C. 2003. Sustainability, Public Transportation and Technological Innovations. *Journal of Transportation Engineering, American Society of Civil Engineers*, 129 (4): 459-482.

Shirai, S. 1977. Adhesion phenomena at high-speed range and performance of an improved slip-detector. *Q. Rep. Railway .Tech. Res. Inst.*, 18(4): 189-190.

Sjokvist, E. H. 1988. Worldwide Development of Propulsion Systems For High-Speed Trains. *Transportation Research Record* 1177: 54-83.

Ting, C. J. and Chen, C. 2008. A Combination of Multiple Ant Colony System and Simulated Annealing for the Multi-Depot Vehicle Routing Problem with Time Windows. *Transportation Research Record* 2089: 85-92.

Uher, R. A. and Disk, D. R. 1987. *A Train Operations Computer Model*, Computational Mechanics Publications

Uher, R. A., and Sathi, N. 1983. Reduction of Peak-Power Demand for Electric Rail Transit System, *National Cooperative Transit Research and Development Program Report 3, Transportation Research Board*, Washington, D.C.

Uher, Sathi, and Sathi. 1984. Traction Energy Cost Reduction of the WMATA Metrorail System, *IEEE Transactions on Industry Applications*, Vol. IA 20 (3): 472-483.

United Nations Report of the World. 1987. *Commission on Environmental and Development. Our Common Future*. Oxford University Press, Oxford, England.

Vuchic, V. R. 2007. *Urban Transit System and Technology*, John Wiley & Sons, Inc., New York, N.Y.

Wong, K. K. and Ho, T. K. 2004. Coast Control for Mass Rapid Transit Railways with Searching Methods, *Institution of Electrical Engineers*, 151 (3): 356-376.

Wright, P. H. and Ashford, N. J. 1997. *Transportation Engineering*, John Wiley & Sons, Inc., New York, N.Y.

Yasukawa, S., Fujita, S., Hasebe, T., Sato, K. 1987. Development of an On-Board Energy Saving Train Operation System for the Shinkansen Electric Railcars. *Quarterly Report of RTRI*, 28: 2-4.

Zhao, F. and Zeng, X. 2006. *Simulated Annealing-Genetic Algorithm for Transit Network Optimization.* Journal of Computing in Civil Engineering, 20 (1): 57-68.

Zou, Y., Oghanna, W., Hoffmann, K. 1999. A Simulation Model of Energy Efficient Automatic Train Control (ATC), Queensland University of Technology.